CZECH TECHNICAL UNIVERSITY IN PRAGUE

FACULTY OF MECHANICAL ENGINEERING

Department of Production Machines and Equipment

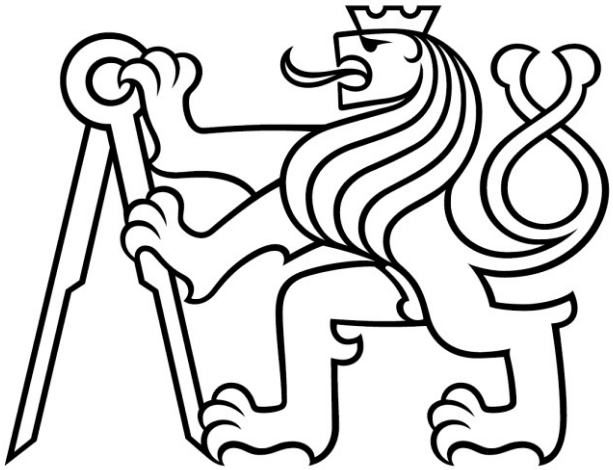

Master's thesis

Optimization of feed rates in NC programs based on tool load

Bc. Jan Uhlíř

2023 1836

MASTER‘S THESIS ASSIGNMENT

I. Personal and study details

Student's name: **Uhlíř Jan** Personal ID number: **482404**

Faculty / Institute: **Faculty of Mechanical Engineering**

Department / Institute: **Department of Production Machines and Equipment**

Study program: **Robotics and Production Machines**

Specialisation: **Production Machines**

II. Master’s thesis details

Master’s thesis title in English:

Optimization of feed rates in NC programs based on tool load

Master’s thesis title in Czech:

Optimalizace posuvových rychlostí v NC programech na základě zatížení nástroje

Guidelines:

During roughing operations, there is variable removal of material and, as a result, different force loads on individual movement axes of the machine. The goal of the work will be to design a strategy for optimizing the feed rate in NC programs according to the defined limits of the directional force load of the tool. Outline of work: 1. Research of approaches and methods to optimize feed rates during milling and the use of process digital dual parts; 2. Design of a roughing operation with variable directional force loading of the tool; 3. Virtual machining simulation and tool force load analysis; 4. Algorithmization proposal for optimization of feed rates in NC code; 5. Verification and evaluation of the results on the test components in relation to the load on the movement axes of the machine. Scope of the graphic part: Necessary figures and tables. Scope of the text part: approx. 60 – 80 pages.

Bibliography / sources:

[1] LAŠOVÁ, V. Základy stavby obráběcích strojů. Západočeská univerzita v Plzni, Plzeň, 2012
[2] ALTINTAS, Y. Manufacturing automation: metal cutting mechanics, machine tool vibrations, and CNC design. 2nd. New York: Cambridge University Press, 2012
[3] ALTINTAS, Y., KERSTING, P., BIERMANN, D., BUDAK, E., DENKENA, B., & LAZOGLU, I. Virtual process systems for part machining operations. CIRP Annals, 63(2), 585–605, 2014.
[4] ARMENDIA, M., et al. Twin-Control. A Digital Twin Approach to Improve Machine Tools Lifecycle. Springer, 2019.

Name and workplace of master’s thesis supervisor:

Ing. Matěj Sulitka, Ph.D. Department of Production Machines and Equipment FME

Name and workplace of second master’s thesis supervisor or consultant:

Ing. Michal Stejskal Department of Production Machines and Equipment FME

Date of master’s thesis assignment: **13.10.2023** Deadline for master's thesis submission: **02.01.2024**

Assignment valid until: **15.09.2024**

Ing. Matěj Sulitka, Ph.D.	doc. Ing. Petr Kolář, Ph.D.	doc. Ing. Miroslav Španiel, CSc.
Supervisor’s signature	Head of department’s signature	Dean’s signature

III. Assignment receipt

The student acknowledges that the master’s thesis is an individual work. The student must produce his thesis without the assistance of others, with the exception of provided consultations. Within the master’s thesis, the author must state the names of consultants and include a list of references.

. _____
Date of assignment receipt

_____
Student’s signature

Acknowledgements

Firstly, I would like to express my honest gratitude to my supervisor, Ing. Matěj Sulitka, Ph.D., for his guidance and valuable insights throughout the work on this thesis. I am also thankful to my consultant, Ing. Michal Stejskal, for his technical advice during our consultations. I extend my appreciation to Mgr. Jiří Falta and Ing. Jakub Ullrich for their insightful discussions on the topic of modeling cutting forces, to Ing. Jan Moravec, Ph.D., for conducting virtual machine simulations, and to Ing. Petr Mašek, Ph.D., for his assistance with the experiment. Finally, I want to express my heartfelt thanks to everyone who has been part of my academic journey, and to my family and girlfriend for their support throughout all my studies.

Declaration

I hereby declare that the presented thesis is my own work and that I have cited all sources of information in accordance with the Guideline for adhering to ethical principles when elaborating an academic final thesis.

I acknowledge that my thesis is subject to the rights and obligations stipulated by the Act No. 121/2000 Coll., the Copyright Act, as amended. I further declare that I have concluded a license agreement with the Czech Technical University in Prague on the utilization of this thesis as school work under the provisions of Article 60(1) of the Act. This fact shall not affect the provisions of Article 47b of the Act No. 111/1998 Coll., the Higher Education Act, as amended.

In Prague on December 31, 2023 .....

Annotation

Author:	Bc. Jan Uhlíř
Title:	Optimization of feed rates in NC programs based on tool load
Extent:	132 p., 104 fig., 12 tab.
Academic year:	2023/2024
University:	Czech Technical University in Prague, Faculty of Mechanical Engineering
Department:	12135 Department of Production Machines and Equipment
Supervisor:	Ing. Matěj Sulitka, Ph.D.
Consultant:	Ing. Michal Stejskal
Submitter:	Czech Technical University in Prague, Faculty of Mechanical Engineering
Application:	feed rate adjustment, tool load reduction
Key words:	milling, feed rate, cutting forces, directional tool load, NC code, virtual machining
Abstract:	This thesis focuses on the design of a continuous control of feed rate based on the tool load. The research section covers theoretical foundations for tool load calculations, and the current state of the art of adjusting feed rates according to the tool load is presented. In the practical part, an algorithm for a feed rate adjustment in an NC code based on the directional tool load is introduced. The proposed algorithm has been verified by simulation and experiment.

Anotace

Autor:	Bc. Jan Uhlíř
Název práce:	Optimalizace posuvových rychlostí v NC programech na základě zatížení nástroje
Rozsah práce:	132 str., 104 obr., 12 tab.
Akademický rok:	2023/2024
Škola:	České vysoké učení technické v Praze, Fakulta strojní
Ústav:	12135 Ústav výrobních strojů a zařízení
Vedoucí práce:	Ing. Matěj Sulitka, Ph.D.
Konzultant:	Ing. Michal Stejskal
Zadavatel:	České vysoké učení technické v Praze, Fakulta strojní
Využití:	úprava posuvové rychlosti, snížení zatížení nástroje
Klíčová slova:	frézování, posuvová rychlost, řezné síly, směrové zatížení nástroje, NC kód, virtuální obrábění
Abstrakt:	Tato práce se zabývá návrhem spojitého řízení posuvové rychlosti podle zatížení nástroje. Práce ve své rešeršní části představuje teoretické základy nutné pro výpočty zatížení nástroje a současný stav řešení úlohy úpravy posuvové rychlosti podle zatížení nástroje. V praktické části je pak představen navržený algoritmus na úpravu posuvové rychlosti v NC kódu podle směrového zatížení nástroje. Navržený algoritmus byl simulačně i experimentálně ověřen.

Contents

Chapter 1

Introduction

The emergence of CAD/CAM technology has enabled the production of complex-shaped parts. Nowadays, the prior objective of CAM development is to enhance the efficiency and precision of the machining and production processes. To achieve these goals, numerous optimization methods and algorithms have been developed. When it comes to milling, one option is to optimize the feed rate. However, this task is complicated by the constantly changing cutting conditions and the geometry of the cut. Freeform milling, sculpture surface milling, or pocket roughing, for example, all involve setting the feed rate to a constant value based on the worst-case cutting geometry along the entire toolpath. The inefficiency of this method stems from the fact that the tool load is not constant. The tool experiences varying loads along the toolpath, allowing for the possibility of increasing the feed rate in sections with lower loads.

One practical application where optimizing the feed rate based on directional load limits is crucial is during roughing on a machine with a pivot spindle head. In such cases, roughing is typically indexed, meaning the head is fixed in one position, and it does not change during roughing. If the spindle head lacks a mechanical position lock and the head position is held only electronically, there is a risk of overloading the servo, which could potentially lead to damage to the tool or workpiece. This can occur especially when machining hard-to-cut materials and the tool has a large overhang. An example of machining using the pivot spindle head with A-axis is the TOS Varnsdorf HPFL 50 spindle head shown in Figure 1.1. However, the picture does not show roughing, but finishing or semi-finishing.

This thesis deals with the optimization of feed rates in NC programs based on tool load. The goal is to design a strategy for optimizing the feed rate in NC programs according to the defined limits of the directional force load of the tool.

Chapter 2 deals with the description of milling technology, its kinematics, the description of technological parameters, and the description of cutting forces. Chapter 3 contains the basics of the cutting process dynamics, namely forced and self-excited vibrations and machining stability. Chapter 4 is dedicated to the phenomenon of digital twins and specifically to one of the fundamental issues for building a virtual model of the machining process, which is the description of bodies in virtual space. Another fundamental issue in building a virtual model of the machining process is the description of cutting forces. Due to the scope and importance of this issue, Chapter 5 is devoted to the description, modeling, and measurement of cutting forces. The last chapter of the theoretical part (Chapter 6) of the thesis is a research of the current state of the art and existing approaches to feed rate optimization. The review describes not only scientific research activities but also existing commercial software. In the following practical part (Chapter 7), the proposed strategy for modifying the feed rate in the NC code, its inputs, adjustable parameters, outputs, functionality, and algorithmization are presented. The assumptions on which the strategy is based are also explained. The chapter also includes a case study section where the functionality of the algorithm is demonstrated by simulation. The following part of the thesis (Chapter 9) is devoted to the experiment conducted to verify the algorithm. The design of the experiment, its realization, and its results are presented. The last section (Chapter 10) is devoted to the discussion of the proposed algorithm for feed rate adjustment in NC code, the findings acquired during the work on this thesis, and the results of the experiment.

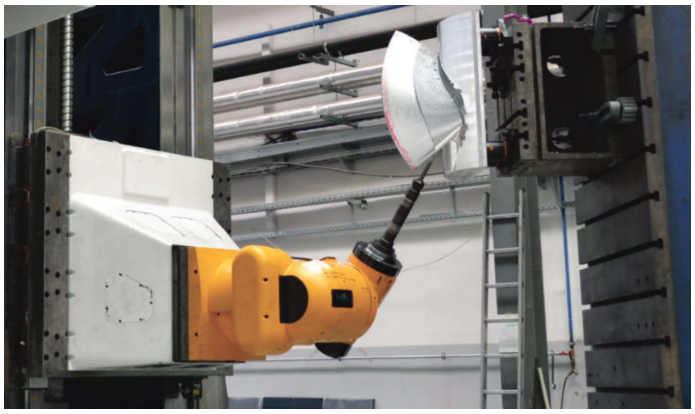

Figure 1.1: TOS Varnsdorf HPFL 50 pivot spindle head [1]

Chapter 2

Milling Technology

Milling is a cutting process, where the milling cutter removes material from a workpiece. It is the second most common machining technology after turning. With milling technology, we can machine even very complex and intricate shapes. It is mainly used to produce non-rotary surfaces such as faces, shaped surfaces, grooves, threads, gears, etc. The shape of the machined surface is determined by the shape of the tool and the relative movement of the tool and workpiece. [2, 3]

This chapter introduces the milling technology. First, the kinematics of milling is introduced, then the milling tool geometry and technological parameters are described and finally, the milling operations and strategies are presented.

2.1 Kinematics of the Milling Operation

In milling, the tool provides the main rotating motion, while the milling machine performs the secondary motion. The tool is placed in a holder and clamped in the spindle, while the workpiece is fixed on the table.

There are two main machining operations:

1. Peripheral (or slab) milling
2. Face milling

Peripheral (or slab) milling is a machining operation where the axis of the milling tool rotation is parallel to the workpiece surface. Material is removed by the outer edge of the tool. This operation is suitable for machining contours. Schema of the peripheral milling operation is shown in Figure 2.1a.

Face milling is a machining operation where the axis of the milling tool rotation is perpendicular to the workpiece surface. The purpose of this operation

is usually to create a flat surface or plane. The face milling tool is usually a milling head with large diameter and multiple cutting inserts. Schema of the face milling operation is shown in Figure 2.1b.

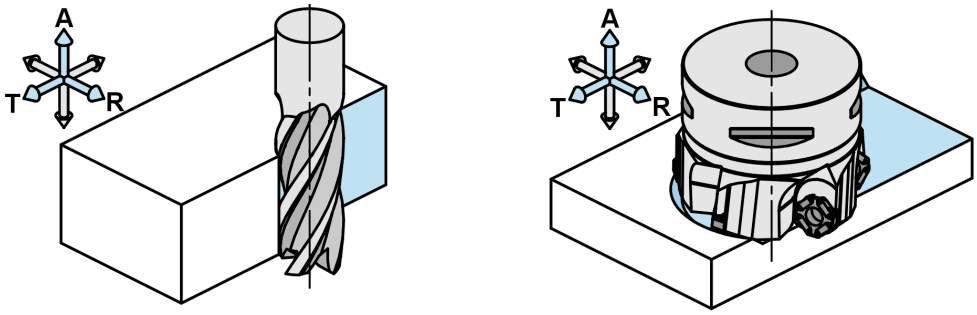

(a) Peripheral milling *(b) Face milling*

Figure 2.1: Kinematics of the milling operation

(the tool models have been downloaded from [4])

About the relation between the feed direction and the axis of the tool rotation, three directions (see Figures 2.1a and 2.1b) are defined:

1. Axial (A)
2. Radial (R)
3. Tangential (T)

Regarding the relation between the feed direction and the direction of the tool rotation, milling operations are classified as:

1. Up (or conventional) milling
2. Down (or climb) milling

In up (or conventional) milling, the direction of the cutting tool rotation is opposite to the feed direction of the cutting tool. This causes, that the chip thickness goes from zero to its maximum. Cutting edge is forced into the cut. Due to friction high temperatures can be reached. This can cause the welding of the chip to the cutting edge. Forces in this operation are higher than when milling down and the the cutting force tends to lift the workpiece from the table. Schema of the up milling is shown in Figure 2.2a.

In down (or climb) milling, the direction of the cutting tool rotation is the same as the feed direction of the cutting tool. Cutting force is at its maximum when the tool edge starts to cut and reaches zero at the end of the cut. This causes strong force impacts at the beginning of each cut. The impact

is usually eliminated by using cutting tools with helical cutting edges. The cutter tends to push the workpiece into the table in the direction of the table feed. That requires rigid milling machines with no backlash. The schema of the down milling is shown in Figure 2.2b. [3, 5, 6, 7]

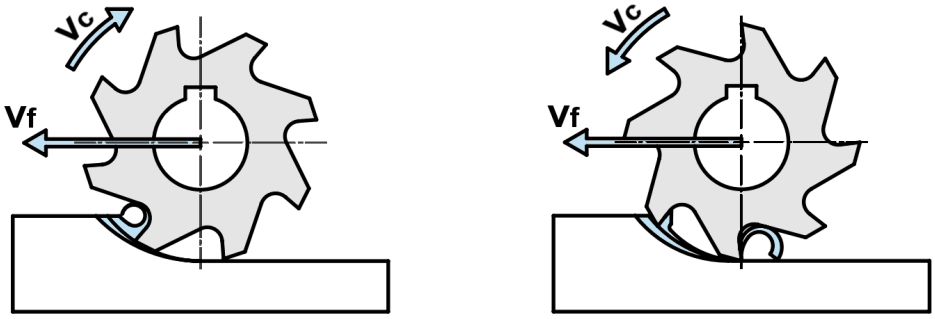

(a) Up milling *(b) Down milling*

Figure 2.2: Up and down milling

The actual cutting edge to workpiece movement is a combination of the tool axis translational movement and the tool rotation. The result of this combination is a cycloidal movement. Material removed in one cut is a volume bounded by the paths of two following teeth. The schema of the teeth engagement is shown in Figure 2.3.

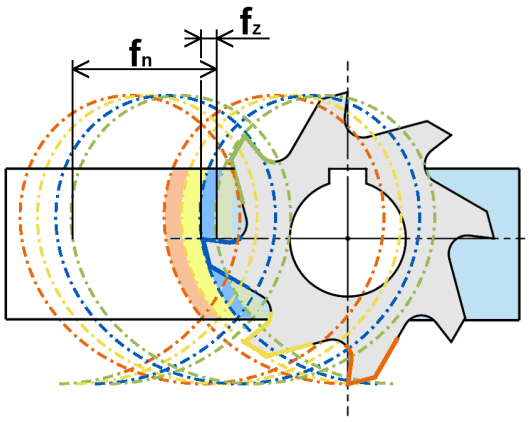

Figure 2.3: Material removed with one cutting edge

2.2 Tool Geometry and Technological Parameters

Choosing the proper tool and setting the appropriate cutting conditions is crucial for successful milling. If an improper tool or cutting condition is selected, it could lead to reduced tool life, tool damage, damage to the workpiece, roughness of the machined surface, etc. This section first describes the tool geometry and then the basic cutting parameters.

2.2.1 Geometry of the Milling Cutter

The milling tool is characterized by its geometry. The geometry has, among other things, a major influence on the mechanics of chip formation, the smoothness of tool loading, the dynamic behavior of the tool during machining, tool life, and the magnitude of cutting forces.

Manufacturers usually provide information about the tool diameter D, flute length L_c, overall length L, shank diameter D_S, number of teeth z, helix angle λ, and corner chamfer angle and width.

In addition to these geometric characteristics, other parameters such as radial rake angle γ_r and axial rake angle γ_a, radial relief angle α_r and axial relief angle α_a, and cutting edge angle κ_r are also relevant. [5, 8, 9]

The geometry of the end mill is depicted in Figure 2.4.

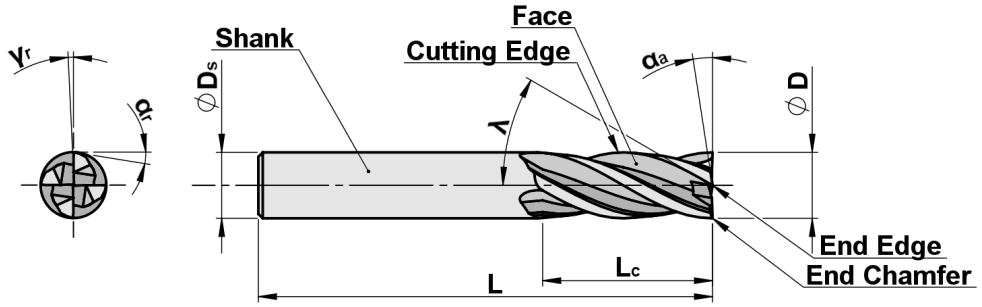

Figure 2.4: Geometry of the end mill

(the tool model has been downloaded from [4])

2.2.2 Cutting speed

The actual cutting speed is a vector sum of the feed rate and velocity of the primary rotary movement. Typically, only the surface speed of the rotating tool is considered, denoted as v_c. The calculation of the surface speed is described in Equation 2.1.

$$v_c = \frac{\pi \cdot D \cdot n}{1000} \tag{2.1}$$

where D is the tool diameter and n is the spindle speed. [5]

2.2.3 Feed Rate

For the desription of the spindle (tool) to workpiece relative movement a quantity called feed rate is usually used. Feed rate can be described as feed rate per minute v_f, feed rate per revolution f_n, or feed rate per tooth f_z. The feed rate per revolution and feed rate per tooth are apparent from Figure 2.3.

Feed rate per minute v_f describes the relative speed of the cutting tool axis to the worpiece. This parameter is described in Equation 2.2.

Feed rate per revolution f_n describes the relative tool movement per one tool revolution. This parameter is described in Equation 2.3.

Feed rate per tooth f_z describes relative tool movement that is done between cuts of two consecutive teeth. This quantity is a fundamental technological parameter.

$$v_f = f_z \cdot z \cdot n = f_n \cdot n \tag{2.2}$$

$$f_n = f_z \cdot z \tag{2.3}$$

where z is a number of cutting edges (teeth) and n is spindle speed. [5, 10]

2.2.4 Axial Depth of Cut

Axial depth of cut (or step-down) is usually denoted as a_p. It is defined as the distance between the machined surface and the surface being machined. The axial depth of the cut is shown in Figure 2.5. [11, 12]

2.2.5 Radial Depth of Cut

Radial depth of cut (or stepover) is usually denoted as a_e. It is defined as the distance a cutting tool is stepping over into the workpiece. Sometimes the stepover is defined as a percentage of the tool diameter. The radial depth of cut is shown in Figure 2.5. [11, 12]

2.3 Milling Operations and Strategies

Milling operations and strategies are two very close concepts. The definitions of these two terms vary in different sources. I would define these terms as follows:

- **Milling operation** is derived from what shape we need to machine. Such an operation can be i.e. face milling, groove and slot milling, shoulder milling, or copy milling. There are usually different types of cutting tools for each operation. We can also divide milling operations into roughing, semi-finishing, and finishing.
- **Milling strategy** determines the whole scenario of the individual milling operation. It defines the milling operation, milling cutter, cutting conditions, and tool trajectory.

In this chapter, selected milling operations and strategies are introduced. All of them are commonly used for roughing. Numerous other operations are widely used (i.e. contour milling, gear milling, ramping, thread milling, turn-milling, etc.) but they are not discussed in this thesis. [12, 13, 14, 15, 16]

2.3.1 Shoulder Milling

Two faces are generated simultaneously when employing the shoulder milling operation. That is achieved by combining peripheral milling with face milling. The true ninety-degree shoulder is often one of the most crucial requirements. Various types of milling cutters, such as square shoulder cutters, end milling cutters, long edge cutters, and side and face milling cutters, are suitable for this operation. The schema of the shoulder milling is in Figure 2.5.[17]

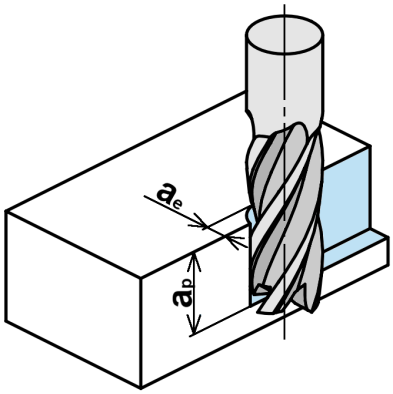

Figure 2.5: Shoulder milling - axial and radial depth of cut

(the tool model has been downloaded from [4])

2.3.2 Face Milling

The most common milling operation is the face milling. Many different types of milling tools are suitable for this operation. The most frequently used cutters for the face milling operation are face milling cutters with multiple

inserts. Usually, a tool with a 45° entering angle is used, but the round or square inserts are also common. The schema of the face milling is in Figure 2.1b. [18]

2.3.3 Groove and Slot Milling

Due to the variety of grooves and slots, numerous milling operations and strategies exist to machine the desired shape. For long, open, and deep slots, side and face milling cutters are usually used. Shorter, closed, and shallow slots are usually machined by using an end mill. For this type of slot, various strategies exist. Conventional slot milling, trochoidal milling, and plunge milling are just three of them. Choosing the proper strategy is key to achieve the required accuracy and production times. The schema of the conventional slot milling strategy is shown in Figure 2.6a. [19]

2.3.4 Adaptive Milling

Adaptive milling is a group of strategies usually used when roughing pockets, cavities, and holes. The main goal is to keep consistent cutting conditions during the milling operation. Usually, the tool load or the material removal rate are the key parameters. Adaptive milling strategies are:

1. **High Feed rate Cutting (HFC)** - high feed rate, small depth of cut, high width of cut
2. **High Dynamic Cutting (HDC)** - high feed rate, high depth of cut, small width of cut
3. **High Speed Cutting (HSC)** - high cutting speed, small depth of cut
4. **High Performance Cutting (HPC)** - combination of the high depth and width of cut

Some CAM systems provide milling strategy called *adaptive milling*. This strategy usually generates toolpaths with the condition of keeping the engagement angle or radial depth of cut a_e consistent. This strategy can be also called *slicing*. The adaptive strategy with the condition of keeping the radial depth of cut consistent was used in the experiment described in 9.3. The schema of the slicing strategy is shown in Figure 2.6b. [13, 14, 20, 21]

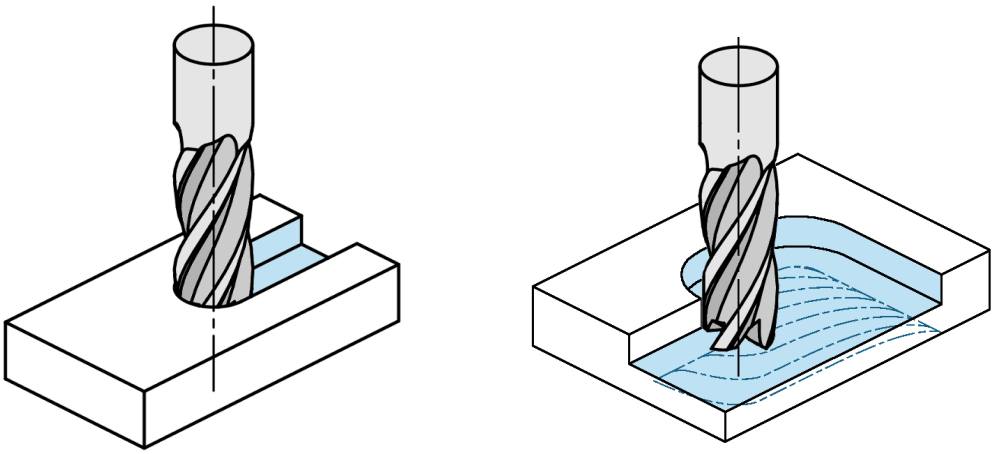

(a) Slot milling *(b) Adaptive milling (slicing)*

Figure 2.6: Milling strategies

(the tool model has been downloaded from [4])

Chapter 3

Fundamentals of the Cutting Process Dynamics

Machine tool, tool, and workpiece together form a dynamic system. Forced oscillations occur due to the force excitation from the cutting process, and self-excited oscillations can occur due to the instability of the dynamic system.

Vibrations have a crucial impact on the quality of the machined surface and the tool life. The machined surface shows a significant deterioration in quality and roughness, and the tool is subject to increased wear, chipping, or even breakage. Another symptom is an increased noise or vibrations of the machine or its parts. [3, 22, 23, 24]

The fundamentals of cutting process dynamics are introduced in this chapter. First the forced vibrations, then the self-excited vibrations, and the stability lobe diagram.

3.1 Forced Vibrations

The cutting process, especially the milling process, typically has a periodic evolution of cutting forces (see Figure 3.1). Another source of the excitation force can be unbalanced rotating components causing periodic forces, external periodic forces, or force impulses transmitted through the machine's foundation. As a result of these periodic forces or force impulses, forced vibrations can be excited. The frequency of the forced vibrations is, in a steady state for harmonic excitation, the same as the frequency of the excitation forces. [3, 8, 22, 23]

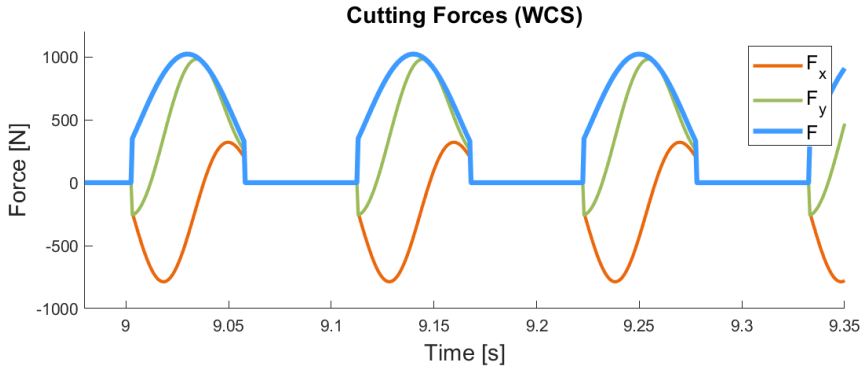

Figure 3.1: Demonstration of the periodic evolution of cutting forces during milling - simulation of the groove milling using one-flute cylindrical cutter

3.2 Self-Excited Vibrations

The self-excited vibrations are caused by the interaction between the cutting process and the machine tool. There are two basic principles of self-excited vibration in machining:

1. **Regenerative principle** - a scheme of this principle is shown in Figure 3.2. The cutting tool is engaged with a wavy surface that was machined in the previous cut. This wavy surface leads to periodic variations in the depth of the cut. These waves are regenerated with each successive cut. When the phase shift ψ between the waves on the machined surface and the tool vibrations is zero, the cross-sectional area of the chip remains constant, and so does the cutting force. In this case, self-excited vibrations will not occur. However, when the phase shift ψ exceeds its limit, self-excited vibrations can be excited. The extreme case occurs when ψ equals to 180°.

2. **Position feedback principle** - this principle assumes the development of two orthogonal dominant oscillation shapes with different natural frequencies. The periodic excitation force thus oscillates the cutting edge along an elliptical path. As the tool moves counterclockwise from point A to point B (see Figure 3.3), it supplies energy to the system. Subsequently, the system transfers energy back to the tool as it moves from point B to point A. Since the cross-section of the chip is larger during the motion from point B to point A than in the section from point A to point B, more energy is transferred to the tool. If not effectively damped, an overshoot will occur at point A, and trigger self-excited oscillation through this repeating process.

There are several other sources of self-excited vibrations, including changing coefficient of friction with the speed of movement, instability of the built-up

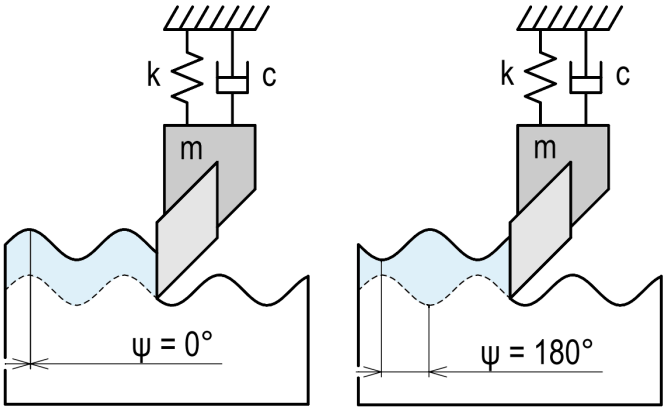

Figure 3.2: Regenerative principle - phase shift between the wavy surface machined in the actual and the previous cut $\psi = 0°$ (left), $\psi = 180°$ (right)

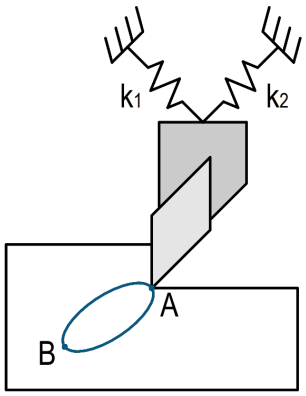

Figure 3.3: Position feedback principle

edge, and material slip at the boundary of the primary plastic deformation zone. [8, 23, 24, 25, 26]

A stability lobe diagram can be used to investigate machining stability. Lobes are curves that show the relation between the limit axial depth of cut a_p on the spindle speed n for stable machining. When these lobes are combined, a stability lobe diagram is generated (see Figure 3.4, one lobe is highlighted).

To ensure stable machining, it is essential to select the depth of cut values that are below the lobe curves corresponding to the spindle speed values. The region above the lobe curves represents unstable milling conditions, where self-excited oscillations occur.

Using the stability lobe diagram, the critical axial depth of cut $a_{p_{crit}}$ which ensures stable machining across the entire spindle speed range can be deter-

mined. Simultaneously, the appropriate speed to significantly increase the depth of the cut while maintaining stability can be identified. With this approach, we can use more of the spindle's power potential.

The creation of a stability lobe diagram involves measuring the amplitude-phase characteristics of a specific tool and a specific tool holder combination on the machine. For a more detailed explanation of the process, please refer to references [23] and [25]. [22, 23, 25, 26]

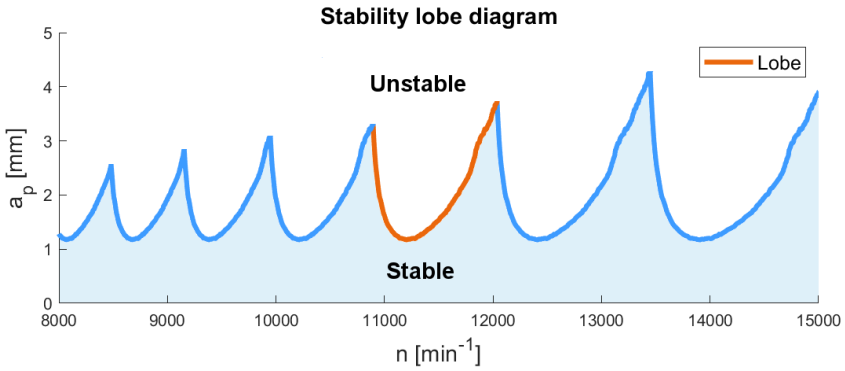

Figure 3.4: Stability lobe diagram with, single lobe is highlghited

Chapter 4

Digital Twins and Digital Models

This chapter introduces the concept of a digital twin. The first part introduces the general concept of digital twins and the definitions of digital twins, shadow, and model. The second part discusses the digital twins in the context of machining. It introduces the digital twin of machine and process. The last part discusses one of the key issues in the machining process virtualization, namely the geometric representation of the workpiece. The second issue in building a virtual model of the machining process is the description of cutting forces. This is treated separately in Chapter 5 due to its comprehensiveness.

4.1 The Concept of the Digital Twin

The definition of a digital twin according to ISO 23247-1:2021(E) is: "A digital twin in manufacturing is a fit for purpose digital representation of an observable manufacturing element with synchronization between the element and its digital representation." [27]

The concept of the digital twin dates back to 2002, when Michael Grieves from the University of Michigan first defined the term in relation to product lifecycle management. [28] Another definition was presented by NASA in 2010: "A digital twin is an integrated multi-physics, multi-scale, probabilistic simulation of a vehicle or system that uses the best available physical models, sensor updates, fleet history, etc., to mirror the life of its flying twin. The digital twin is ultra-realistic and may consider one or more important and interdependent vehicle systems, including propulsion/energy storage, avionics, life support, vehicle structure, thermal management/TPS, etc." [29] This definition refers to the digital twins that are used in the context of NASA space and air force vehicles.

Generally speaking, a digital twin is a realistic virtual representation of the physical system. It is necessary to distinguish the concepts of digital twin, digital shadow, and digital model. A digital model of a machine is a representation of a physical system, and there is no automatic data exchange between the physical system and the digital model. In the case of the digital shadow, there is already a one-way data flow from the physical system to the digital system. The highest form of the digital control and modeling of physical systems is then the digital twin, where data are exchanged in both directions, and the physical system is corrected or even controlled based on the data from the digital twin. The schema of the digital model, digital shadow, and the digital twin is depicted in Figure 4.1. [30]

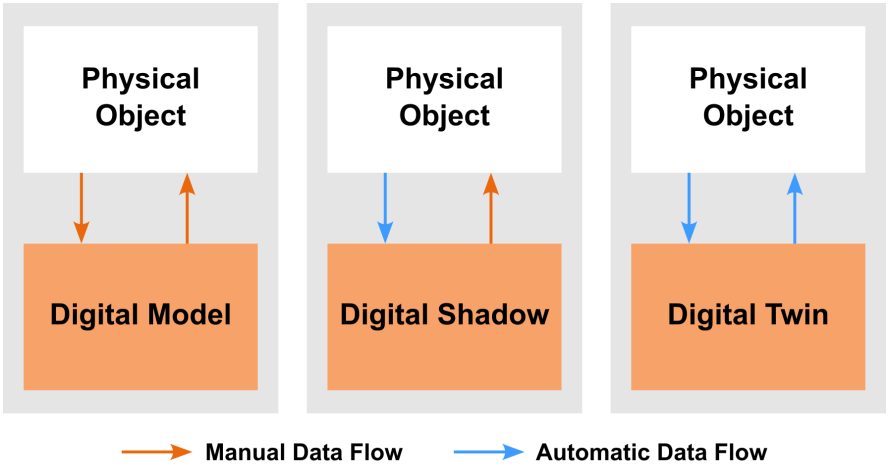

Figure 4.1: The schema of the digital model, digital shadow, and the digital twin

4.2 The Concept of the Digital Twin in Machining

In the context of manufacturing, the term *digital twin* usually means a *digital model* (as defined in the previous section). Two main categories can be distinguished: *digital twin of the machine tool*, and *digital twin of the machining process*.

Digital twin of a machine tool is a virtual representation of the actual machine tool. This model considers factors such as drive dynamics, the machine's mechanical structure, dynamic characteristics, and more. A validated digital model should accurately imitate the real-world behavior of the machine. [30]

Digital twin of the machining process offers a virtual representation of the machining process. Unlike the digital model of the machine tool, this model includes also information about tool and workpiece engagement. Therefore, in addition to simulating machine behavior, this model must also represent the geometry and properties of the tool and workpiece and a force model. This comprehensive knowledge enables the prediction of cutting forces, tool deflection, free and forced vibrations, and other technological phenomena. This virtual simulation is often referred to as *virtual machining*, resulting in a virtual workpiece model that predicts the final shape, tolerances, and surface quality under ideal machining conditions. Such a model can be used for support and optimization of the part manufacturing. [26, 31]

4.3 Geometric Representation of the Workpiece

Accurate geometry representation in a virtual environment is essential when evaluating tool-workpiece engagement in virtual machining. Various methods for describing geometry have been developed and are introduced in this section. Typically, virtual cutting is achieved by performing Boolean subtraction of the tool volume from the workpiece material volume. Some of the methods for body representation include:

- Z-map (dexel representation)
- Wire model
- Voxel representation
- Octree
- CSG
- B-Rep

These methods are introduced in the following sections.

4.3.1 Z-map

Z-map (or dexel representation) uses parallel vectors to describe a surface. This method typically employs a discretized x-y plane where each point on the plane has a corresponding Z-value. The accuracy and level of detail of the Z-map depend on the resolution of discretization. This method is straightforward and has a low computation time of $O(n^2)$. [32] However, a limitation of this method is that it can only be used for computing shapes without undercuts. While it is not suitable for five-axis milling, it can find application in 2.5D milling for some basic operations. An example of the Z-map is shown in Figure 4.2. [33]

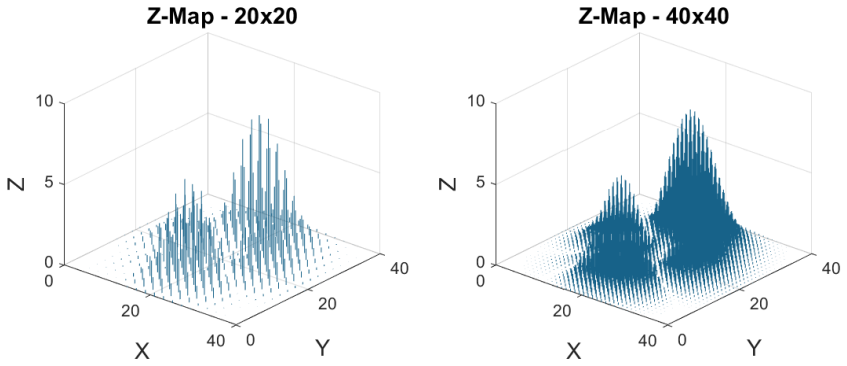

Figure 4.2: Z-map

4.3.2 Wire Model

These models represent the geometry of the body using points and lines. Wire models are more suitable for quick and simple visualization of the surface. The smoothness of the model is directly related to grid density, hence wire models are less smooth compared to solid models. An example of a wire model is shown in Figure 4.3. [33]

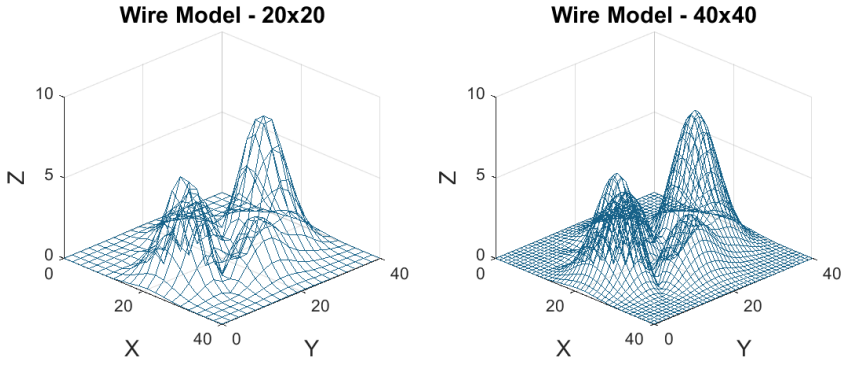

Figure 4.3: Wire model

4.3.3 Voxel Representation

Voxel representation is an approximation method based on discretizing a volume by small uniform cuboids called voxels. Voxels are binary units, either filled with material or empty. The smoothness, level of detail, and accuracy of the object represented by voxels depend on the resolution. Implementing this method is straightforward, but it comes with the drawback of significantly increased computational time and memory requirements (following an $O(n^3)$ relation) as the resolution increases. A simple example of a voxel representation is shown in Figure 4.4. [33, 34]

Another way of voxel representation is the distance field method. This method defines for each point how far it is from the object boundary. The sign of this value then determines whether the point is inside or outside the object. [35]

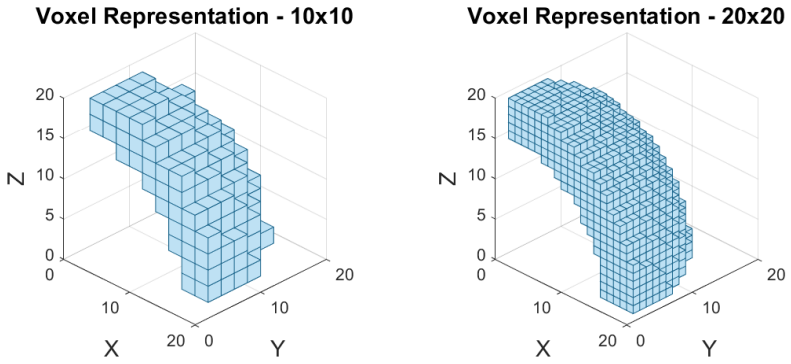

Figure 4.4: Voxel representation

4.3.4 Octree

Octree divides a volume into eight sub-volumes known as octants, as shown in the schema in Figure 4.5. Octants can be categorized as black (filled), gray (partially full), or white (empty). Black octants are entirely within the object, while white octants are entirely outside the object. If an octant is gray, it indicates that the object's boundary passes through it. In this case, this gray octant is subdivided into eight smaller octants. This process is repeated until the desired level of detail is achieved. This technique is straightforward to implement, has lower memory requirements, and carries the same level of detail compared to voxel representation. However, the downside of this method is that it offers lower object quality compared to solid model representation. [33, 36]

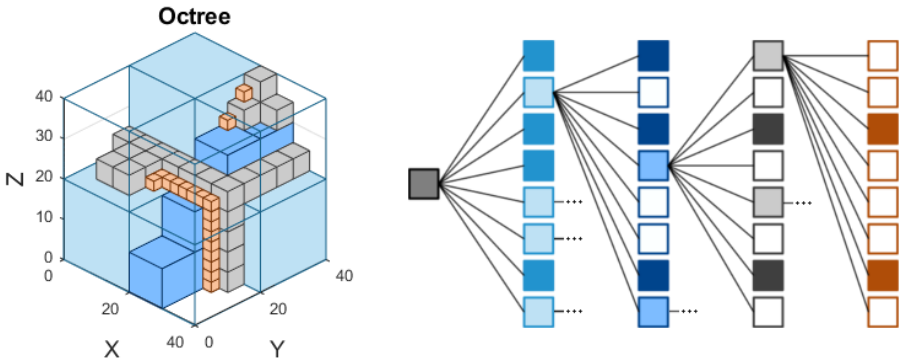

Figure 4.5: Octree

4.3.5 CSG

Constructive Solid Geometry is a solid modeling technique, that involves the combination of individual components (solid objects). The combination is achieved through Boolean operations, including union, difference, subtraction, or intersection. An example of a simple Boolean subtraction is illustrated in Figure 4.6. When simulating the cutting process, the intersection of the tool body and the workpiece is typically used to compute the material removal rate (MRR). [33]

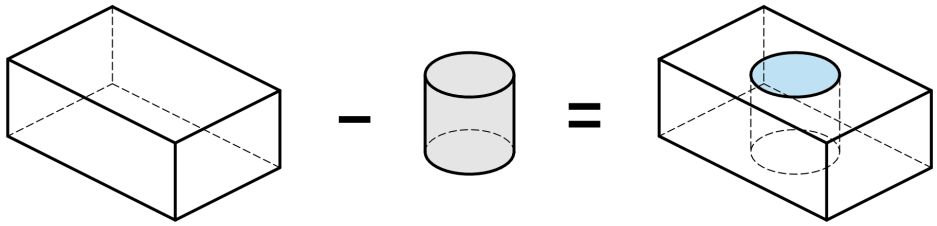

Figure 4.6: CSG - Boolean subtraction

4.3.6 B-Rep

Boundary representation (B-rep) is another technique for modeling solids. It characterizes solids using their boundary elements, which include surface patches, edges, and vertices. This method supports various mathematical descriptions such as Bézier curves, splines, NURBS, and more. An example of a boundary representation is provided in Figure 4.7. In this figure, the tool volume is swept along the toolpath from P_0 to P_1, and this volume is then subtracted from the workpiece (white).

B-rep offers a continuous and precise representation of free-form surfaces and tool-workpiece intersections. However, achieving this level of accuracy comes at the cost of complex intersection calculations and longer computation times. [33]

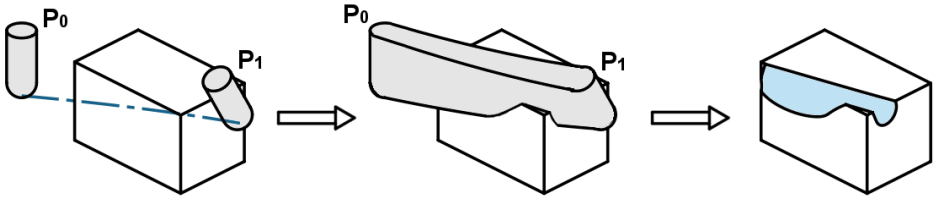

Figure 4.7: B-rep

Chapter 5

Modeling and Measurement of Cutting Forces

The goal of this work is to propose a strategy for adjusting the feed rates in NC code according to the tool load. Therefore, it is crucial to predict the force load that is created during machining. Therefore, this chapter is devoted to the description, modeling, and measurement of cutting forces.

The first part of this chapter discusses coordinate systems commonly used for describing cutting forces. The following sections cover modeling of cutting forces. The last section describes the methods for measuring cutting forces.

5.1 Coordinate Systems for the Description of Cutting Forces

The resultant cutting force can be described in numerous coordinate systems depending on the purpose of the force description. The coordinate systems are usually related on the machine motion axes (i.e. $x - y - z$ directions) or the kinematics of the milling operation, i.e. feed - tangential - radial direction ($f - t - r$) in case of turning [37]). When the calculation of the resultant cutting force is based on the mechanistic model (see Section 5.4), it is necessary to employ local coordinate systems on the cutting edge, i.e. tangential - normal - binormal ($t - n - b$). $t - n - b$ and $x - y - z$ coordinate systems are depicted in Figure 5.1.

The resultant cutting force F is a three-dimensional vector, which can be represented with three components, i.e. feed force F_f, tangential force F_t, and radial force F_r. Calculation of the resultant cutting force F is described by Equation 5.1.

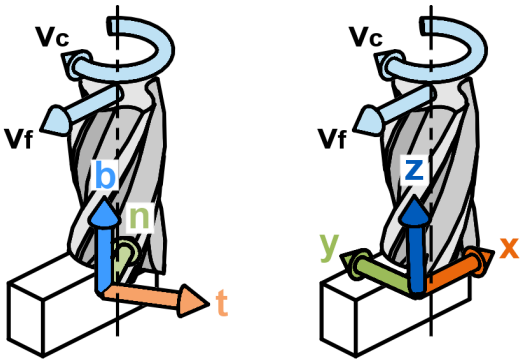

Figure 5.1: Cutting force bases: $t - n - b$, and $x - y - z$

(the tool model has been downloaded from [4])

The tangential force F_t is acting in the direction of the cutting velocity v_c and is the greatest of all the components. The feed force F_f is acting in the direction of the feed v_f and is usually about 50% of the tangential force F_t. The radial force F_r is the lowest component with its size of about 25% of the tangential force F_t. The passive force is directed perpendicular to the machined surface. When describing forces using these components, this is an $f - t - r$ basis. [3, 38]

The resultant cutting force F can be also decomposed into the direction of the workpiece coordinate system (WCS) or the global (machine) coordinate system (GCS). Individual components are F_x, F_y, and F_z, respectively to the WCS or F_X, F_Y, and F_Z respectively to the GCS.

$$F = \sqrt{F_f^2 + F_t^2 + F_r^2} \tag{5.1}$$

Numerous mathematical models for cutting forces exist. Some of them are provided in the following sections.

5.2 History of Modeling of Cutting Forces

Probably the first engineer who published works about cutting forces was Belgian general Casimir Erasme Cocquilhat in 1843 and 1850 [39, 40]. Another approach of cutting forces modeling was presented by Friedrich Karl Hermann Wiebe in 1858 in his book *Machine Building Materials and their Processing.* Wiebe's formula, rewritten in the contemporary annotation, is provided in Equation 5.2.

$$F_c = k_c \cdot h_D \cdot b_D \tag{5.2}$$

where F_c is the cutting force, k_c is a specific cutting resistance, h_D is the uncut chip thickness and b_D is the chip width. Wiebe considered constant k_c

to be the only sufficient workpiece material property, so the cutting force F_c is then a function of the uncut chip thickness h_D and the chip width b_D. The product of the uncut chip thickness and width (see equation 5.3) is the cut layer cross-section area A_D.

$$A_D = h_D \cdot b_D \tag{5.3}$$

So the cutting force F_c is a function of the cut layer cross-section area A_D.

Wiebe's formula laid the foundation for calculations of cutting forces and is still widely used today.

After Wiebe, Zvorykin, Merchant, Kienzle, Kline, and many others have developed other models and used other approaches to the phenomenon of cutting forces. Models can be divided into three main groups [26, 41]:

1. Analytical
2. Mechanistic
3. Empirical

Each group of the models is based on a different approach. Individual groups are presented in more detail in the following sections.

5.3 Analytical Models

Analytical models are derived from mechanics and material science. Due to the physical description of the model, these models use a minimum number of empirical coefficients obtained by machining measurements. Most of the models are based on the shearing mechanics in the chip formation process.

During the late 19th century, the first works presenting analytical models have been published. In 1870, Time's work described the formation of a chip as a result of shearing ahead of the tool. [42] Other engineers involved in the description of the chip formation were Tresca and Mallock. [42] In 1893, Zvorykin formulated the first physical explanation of this model and formed an equation for the shearing angle prediction. [42] The greatest expansion of analytical models followed after 1944 when Merchant published his model of the cutting forces for orthogonal cutting in his work *Basic Mechanics of the Metal Cutting Process*. [43] This model assumed homogenous and isotropic workpiece material with purely rigid plastic behavior. Unfortunately, this model can not be applied in most practical cases, due to the real cutting process is usually not a planar process.

Although the analytical models have been extended to cover oblique cutting as well, the following relations are derived for orthogonal cutting using the single shear plane model. These models exhibit a poor correlation with experimental data, but they serve well for explaining the main concepts of analytical modeling. Single shear plane models can also be extended to shear zone models, which assume that material deformation occurs within a narrow band centered on the shear plane.

Analytical single shear plane models assume, that the primary deformation takes place only in the shear plane, which is simplified as an infinitely thin layer. The angle between the motion vector and the shear plane is denoted ϕ_c and called the primary shear angle. The shear force F_S can be expressed as:

$$F_S = F \cdot \cos(\phi_c + \beta_a - \gamma) \tag{5.4}$$

where β_a is an angle of friction and γ is a rake angle. Friction angle β_a can be calculated from friction coefficient μ using relation:

$$\beta_a = \arctan(\mu) \tag{5.5}$$

Assuming uniform stress τ_s distribution in the shear plane, shear force F_S is described as:

$$F_S = \tau_S \cdot A_S = \frac{\tau_S \cdot A_D}{\sin(\phi_c)} \tag{5.6}$$

where A_S is the cross-section area of the shear plane. From equations 5.4 and 5.6 can be derived:

$$F = \frac{\tau_S \cdot A_D}{\sin(\phi_c)} \cdot \frac{1}{\cos(\phi_c + \beta_a - \gamma)} \tag{5.7}$$

$$F = b_D \cdot h_D \cdot \left[\frac{\tau_S}{\sin(\phi_c) \cdot \cos(\phi_c + \beta_a - \gamma)}\right] \tag{5.8}$$

From the geometry of the cut (see Figure 5.2), the tangential force F_t and the feed force F_f are deduced:

$$F_t = F \cdot \cos(\beta_a - \gamma) \tag{5.9}$$

$$F_f = F \cdot \sin(\beta_a - \gamma) \tag{5.10}$$

By combining equations 5.7 and 5.9, the result relation for the tangential force F_t can be derived:

$$F_t = \frac{\tau_S \cdot A_D}{\sin(\phi_c)} \cdot \frac{\cos(\beta_a - \gamma)}{\cos(\phi_c + \beta_a - \gamma)} \tag{5.11}$$

$$F_t = b_D \cdot h_D \cdot \left[\frac{\tau_S \cdot \cos(\beta_a - \gamma)}{\sin(\phi_c) \cdot \cos(\phi_c + \beta_a - \gamma)}\right] \tag{5.12}$$

Similarly by combining equations 5.7 and 5.10, feed force F_f can be expressed as follows:

$$F_f = \frac{\tau_S \cdot A_D}{\sin(\phi_c)} \cdot \frac{\sin(\beta_a - \gamma)}{\cos(\phi_c + \beta_a - \gamma)} \tag{5.13}$$

$$F_f = b_D \cdot h_D \cdot \left[\frac{\tau_S \cdot \sin(\beta_a - \gamma)}{\sin(\phi_c) \cdot \cos(\phi_c + \beta_a - \gamma)}\right] \tag{5.14}$$

In the equation 5.12, the part in square brackets is called *specific cutting pressure* or *tangential cutting force coefficient*. The specific cutting pressure K_{tc} is defined as follows:

$$K_{tc} = \tau_S \cdot \frac{\cos(\beta_a - \gamma)}{\sin(\phi_c) \cdot \cos(\phi_c + \beta_a - \gamma)} \tag{5.15}$$

The part in the square brackets in the equation 5.14 is called *feed force constant*. The feed force constant K_{fc} is defined as:

$$K_{fc} = \tau_S \cdot \frac{\sin(\beta_a - \gamma)}{\sin(\phi_c) \cdot \cos(\phi_c + \beta_a - \gamma)} \tag{5.16}$$

This model did not match the experimental data. Thus, Merchant published another model considering a linear dependency of the shear stress τ_S on the normal stress σ_S: [42]

$$\tau_S = \tau_0 - K \cdot \sigma_S \tag{5.17}$$

The value of the coefficient K varies for different workpiece and tool materials.

The problem with the shear plane models is that we can not calculate the shear angle ϕ_C analytically yet. Numerous approaches have been published, some of them are introduced in Table 5.1. Merchant used the same concept as Zvorykin and put the parameter A_1 equal to $\frac{\pi}{4}$ and A_2 equal to $\frac{1}{2}$. Lee and Shaffer used the same principle too, but assigned the value 1 to the parameter A_2. [26, 37, 41, 42, 44]

5.4 Mechanistic Models

Mechanistic models are based on the cutting mechanics combined with empirical data. Compared to analytical models, mechanistic models are usually simpler. They avoid phenomena such as shear angle, friction angle, etc. These parameters are simplified by constants obtained by processing the experimental data. Mechanistic models are suitable not only for orthogonal but also for oblique cutting. They provide all three components of the cutting force.

The resultant cutting force is usually described by its three components: tangential force F_t, normal force F_n, and binormal force F_b. (Binormal force is

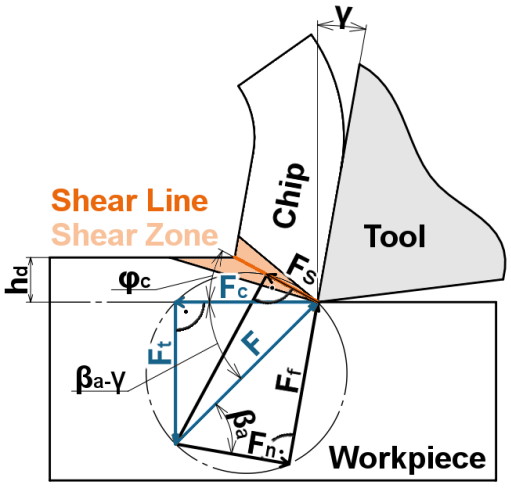

Figure 5.2: Geometry of the cut - Merchant's analytical model diagram

Table 5.1: Analytical force models - shear angle formulas [42]

Source	Equation	
Zvorykin, 1893	$\phi_c = A_1 + A_2 \cdot (\gamma - \beta_a)$	(5.18)
Merchant, 1944	$\phi_c = \frac{\pi}{4} + \frac{1}{2} \cdot (\gamma - \beta_a)$	(5.19)
Lee and Shaffer, 1951	$\phi_c = \frac{\pi}{4} + (\gamma - \beta_a)$	(5.20)
Sata, 1954	$\phi_c = \frac{\pi}{4} - \gamma \pm \frac{\gamma - 15^\circ}{2}$	(5.21)
Kronenberg, 1957	$\phi_c = arctg \left[\frac{e^{\mu(\frac{\pi}{2} - \gamma)} - \sin(\gamma)}{\cos(\gamma)} \right]$	(5.22)

acting in the direction perpendicular to the cutting plane.) These forces can be expressed using a linear mechanistic model as follows:

$$\begin{aligned} F_t(\phi) &= (K_{tc} \cdot h_D(\phi) + K_{te}) \cdot b_D \\ F_n(\phi) &= (K_{nc} \cdot h_D(\phi) + K_{ne}) \cdot b_D \\ F_b(\phi) &= (K_{bc} \cdot h_D(\phi) + K_{be}) \cdot b_D \end{aligned} \tag{5.23}$$

where K_{jc} are called *cutting* or *shear coefficients* and K_{je} are called *edge* or *friction coefficients* (the index j represents the general notation of the force component). These coefficients are obtained by linear regression of experimental data. All the coefficients differ for each tool geometry and workpiece material combination.

The friction coefficients K_{je} were introduced by Armerago in 1967. [26] He suggested, that the friction is not a function of the uncut chip thickness h_D. These coefficients are also strongly dependent on the tool micro geometry, so they change i.e. with tool wear.

The uncut chip thickness is a function of the instantaneous tool rotation ϕ. The dependency is evident from Figure 5.3 and can be described as provided in Equation 5.24.

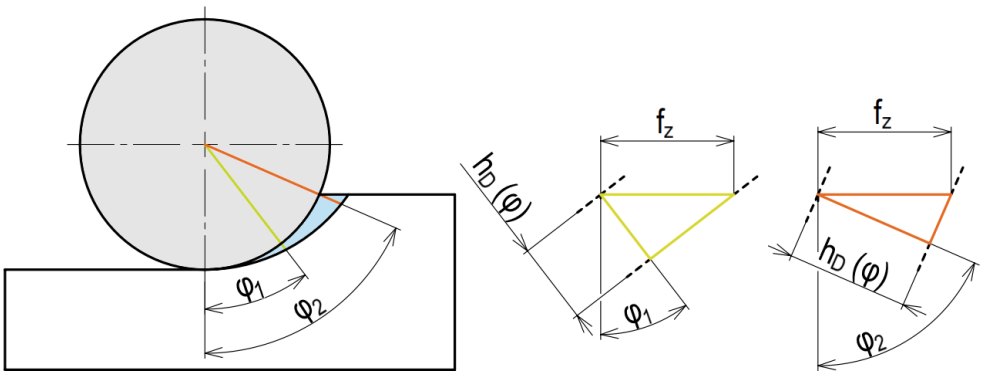

Figure 5.3: Dependence of the uncut chip thickness h_D on the current tool rotation angle ϕ

$$h_D = f_z \cdot \sin(\phi) \tag{5.24}$$

It becomes apparent that linear models of cutting forces do not show sufficient agreement with experiments. Therefore, models with up to cubic dependence on the uncut chip thickness h_D have been developed. The cubic mechanistic model is given in Equation 5.25.

$$\begin{aligned} F_t(\phi) &= (K_{t0} + K_{t1} \cdot h_D(\phi) + K_{t2} \cdot h_D(\phi)^2 + K_{t3} \cdot h_D(\phi)^3) \cdot b_D \\ F_n(\phi) &= (K_{n0} + K_{n1} \cdot h_D(\phi) + K_{n2} \cdot h_D(\phi)^2 + K_{n3} \cdot h_D(\phi)^3) \cdot b_D \\ F_b(\phi) &= (K_{b0} + K_{b1} \cdot h_D(\phi) + K_{b2} \cdot h_D(\phi)^2 + K_{b3} \cdot h_D(\phi)^3) \cdot b_D \end{aligned} \tag{5.25}$$

Another type of mechanistic model is the multiparametric model. These models are being developed also at the Department of Production Machines and Equipment (Czech Technical University in Prague, Faculty of Mechanical Engineering). [26] The challenge of the multiparametric models is to describe the

dependence of forces on tool geometry. Using a multiparametric model, the individual cutting and edge coefficients can be expressed according to Equation 5.26. The key parameters in this example are the cutting speed v_c, rake angle γ, helix angle λ, and the cutting edge radius R.

$$K_{ij} = C_{ij1} \cdot \gamma + C_{ij2} \cdot v_c + \ldots + C_{ijl} \cdot \gamma \cdot v_c \cdot R + \ldots + C_{ijk} \cdot \lambda \cdot v_c^3 + \ldots \quad (5.26)$$

In an attempt to simplify the description of the dependence of the forces on the tool geometry and the cutting speed, Falta developed a mechanistic multiparametric cubic pressure-friction model, presented in [45]. With this new approach, it is possible to achieve better fitting cutting and friction coefficients for the traditional mechanistic model describing the forces in the $t - n - b$ system. According to Falta, the cutting force can be decomposed into two components: the pressure force, denoted as F_P, acting perpendicular to the tool rake face, and the friction force, denoted as F_{fr}, acting on the surface of the tool rake face. The direction of the friction force is described using the chip flow angle η: the angle between the friction force and perpendicular to both the tool edge and the direction of the pressure force. The scheme of this model is depicted in Figure 5.4 and the calculation of the force components is described in Equation 5.27. Polynomial coefficients K_{ij} are obtained from equations considering the geometry of the tool and the material to be machined.

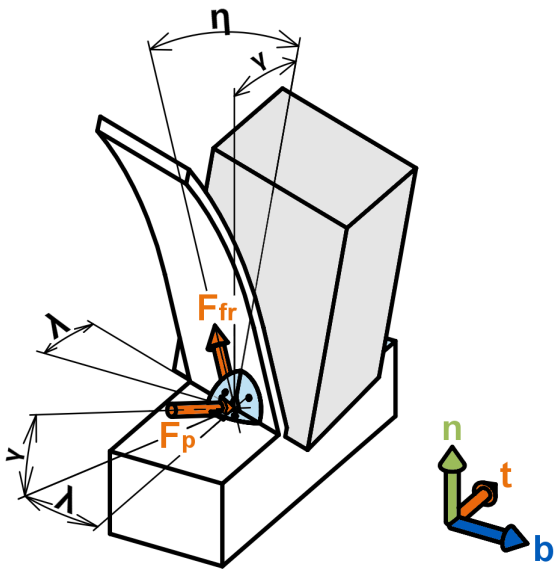

Figure 5.4: Scheme of the pressure-friction force model

$$\begin{aligned} F_P &= b_D \cdot (K_{P0} + K_{P1} \cdot h_D + K_{P2} \cdot h_D^2 + K_{P3} \cdot h_D^3) \\ F_{fr} &= b_D \cdot (K_{fr0} + K_{fr1} \cdot h_D + K_{fr2} \cdot h_D^2 + K_{fr3} \cdot h_D^3) \\ \eta &= f(R, \gamma, \lambda, v_c) \end{aligned} \quad (5.27)$$

The transformation from the pressure-friction model into the $t-n-b$ basis is provided in Equation 5.28.

$$\begin{aligned} F_t &= \cos(\lambda)\cdot\cos(\gamma)\cdot F_P + (\cos(\eta)\cdot\cos(\lambda)\cdot\sin(\gamma)+\sin(\eta)\cdot\sin(\lambda))\cdot F_{fr} \\ F_n &= -\sin(\gamma)\cdot F_P + \cos(\eta)\cdot\cos(\gamma)\cdot F_{fr} \\ F_b &= -\sin(\lambda)\cdot\cos(\gamma)\cdot F_P + (-\cos(\eta)\cdot\sin(\lambda)\cdot\sin(\gamma)+\sin(\eta)\cdot\cos(\lambda))\cdot F_{fr} \end{aligned} \tag{5.28}$$

When predicting cutting forces in a milling operation, multiple cutting edges, helix angles, and changing tool engagement conditions have to be considered. The cutting edges are divided into small slices axially (see Figure 5.5) and the force components are then integrated over each cutting edge. In that case, the linear mechanistic model can be expressed as follows:

$$\begin{aligned} dF_t(\phi) &= (K_{tc}\cdot h_D(\phi)+K_{te})\cdot db_D \\ dF_n(\phi) &= (K_{nc}\cdot h_D(\phi)+K_{ne})\cdot db_D \\ dF_b(\phi) &= (K_{bc}\cdot h_D(\phi)+K_{be})\cdot db_D \end{aligned} \tag{5.29}$$

where ϕ is instantaneous tool rotation, h_D is instantaneous cut layer thickness which varies according to the angle ϕ and db_D is the width of the cut layer for a small slice of the tool. [12, 26, 33, 37, 41, 44, 45, 46, 47]

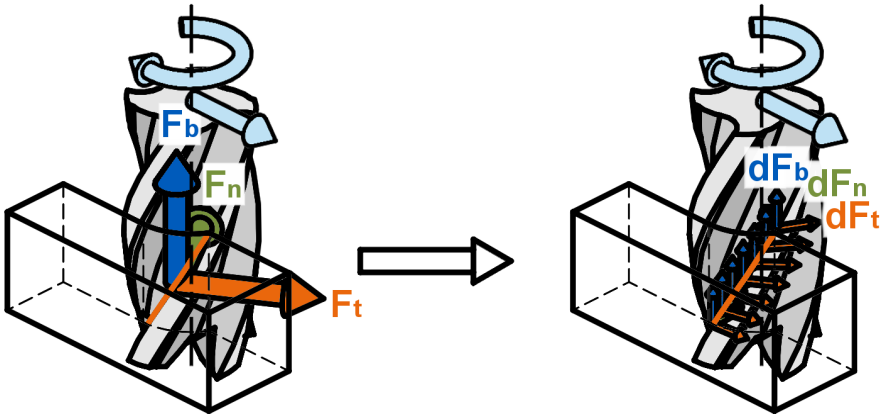

Figure 5.5: Force integration along the cutting edge

(the tool model has been downloaded from [4])

5.5 Empirical Models

Empirical models are built upon experimentally obtained data. They describe the force components using parameters that have the most significant impact on the cutting forces. These key parameters are usually the axial depth of cut a_p, feed rate per tooth f_z, and the cutting speed v_c (see Equation 5.30).

Additionally, other parameters, such as tool geometry parameters, can be considered. It is important to note that each model is specific to a particular technology of the machining process resulting in relatively low variability of these models.

When conducting experiments to obtain data for empirical models, the single-variable method is typically used. In this method, only one parameter is varied at a time while keeping other parameters constant. This process requires numerous measurements, making it a time-consuming task. [26, 48]

$$\begin{aligned} F_c &= K_{F_c} \cdot a_p^{X_{F_c}} \cdot f_z^{Y_{F_c}} \cdot v_c^{Z_{F_c}} \\ F_f &= K_{F_f} \cdot a_p^{X_{F_f}} \cdot f_z^{Y_{F_f}} \cdot v_c^{Z_{F_f}} \\ F_t &= K_{F_t} \cdot a_p^{X_{F_t}} \cdot f_z^{Y_{F_t}} \cdot v_c^{Z_{F_t}} \end{aligned} \tag{5.30}$$

5.6 Kienzle Force Model

Kienzle published his work in 1952. [49] His simple force model can be classified as a mechanistic or empirical cutting force model. Simple Kienzle force model takes into account only cut layer cross-section area A_D and the specific cutting resistance k_c. The main difference between Wiebe (see Section 5.2) and Kienzle's model is the fact, that according to Kienzle, the specific cutting resistance k_c is specific for each tool - workpiece material combination. The simple Kienzle force model can be described using the following equation:

$$F_c = k_c \cdot A_D \tag{5.31}$$

where the cutting coefficient k_c depends on the uncut chip thickness h_D. This dependency can be expressed as follows:

$$k_c = k_{c11} \cdot h_m^{-q_c} \tag{5.32}$$

where k_{c11} is a nominal cutting resistance, h_m is an average chip thickness and q_c is an exponent that signifies the impact of chip thickness on the cutting coefficient. The relation between specific cutting resistance k_c and average chip thickness h_m is shown in the logarithmic scale in Figure 5.6. Relation between inclination angle ξ and exponent q_c is described in Equation 5.33. The simple Kienzle model can be expressed as in Equation 5.34. [26, 41, 49, 50, 51]

$$q = \tan(\xi) \tag{5.33}$$

$$F_c = k_{c11} \cdot h_m^{1-q_m} \cdot b_D \tag{5.34}$$

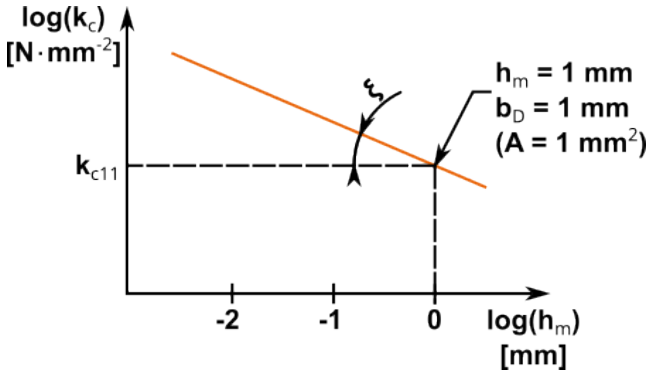

Figure 5.6: Relation between specific cutting resistance k_c and average chip thickness h_m in logarithmic scale

5.7 Measurement of Cutting Forces

To determine the cutting coefficients for force models, a set of measurements is conducted and subsequently analyzed. These measurements serve model development and model verification. This chapter does not address the methodology of measurement for modeling (such as cut conditions and number of measurements) but rather concentrates on the methods and instruments employed for measuring cutting forces. The methods of measuring forces can be distinguished into two groups:

- **Direct measurement** - this method involves the use of dynamometers
- **Indirect measurement** - it calculates forces from spindle or motion axis drive current or power

Direct measurements are more precise and repeatable, but on the other hand, they require expensive measurement instruments, and the data evaluation is time-consuming. They are typically employed in tool testing, machinability assessments, and process control and optimization. In contrast, indirect measurement methods are more straightforward to set up and evaluate, but they tend to offer lower accuracy. These are often used in roughing and high-performance machining.

Dynamometers, which are instruments for measuring forces, come in various types, including mechanical, hydraulic, pneumatic, and electric. For machining applications, piezoelectric dynamometers are commonly used.

Piezoelectric dynamometers are suitable especially for measurement of compressive and tensile forces in highly dynamic applications. Key requirements for a dynamometer include high stiffness, sensitivity, good dynamic properties (high natural frequencies), a wide measurement range, and low hysteresis.

When measuring with a piezoelectric dynamometer, a charge amplifier is also needed.

There are two main categories of piezoelectric dynamometers: stationary (see Figure 5.7a) and rotary (see Figure 5.7b). In the case of milling, the workpiece is attached to the stationary dynamometer. If the rotary dynamometer is needed for force measurement, it is held in the spindle and the tool is held in the dynamometer. Stationary dynamometers provide one to three axial force measurements in an orthogonal stationary system. Some can also measure corresponding moments on all three axes. In contrast, rotary dynamometers can measure one to three orthogonal force components and moments in the Z-axis, with the coordinate system rotating with the dynamometer, and the data acquisition is wireless. When turning, the cutter is attached to the stationary dynamometer. [12, 52, 53]

(a) Stationary dynamometer Kistler 9255B [54]

(b) Rotary dynamometer Kistler 9123C [55]

Figure 5.7: Piezoelectric dynamometers

The indirect measurement method involves measuring currents or power input to the spindle or drives of individual motion axes. From the measured data, cutting forces (when measured on the spindle) or forces in the direction of the motion axes (when measured in the axes of motion) can be calculated, considering the gear and motor constants. [53, 56]

Chapter 6

Approaches to Feed Rate Optimization

In the field of feed rate optimization, many different techniques, approaches, and algorithms have been developed over time. However, it is usually not optimization, but rather control of the feed rate about a given criterion. There are several ways to distinguish existing approaches. In general, the result should be a modified feed rate. This can be done online based on adaptive control or offline based on computer preprocess adjustment or optimization. The types of feed rate adjustments are introduced and discussed in this chapter. In the last section, the commercial software that deals with virtual machining and provides feed rate modifications is introduced.

6.1 Adaptive Control

Adaptive control, sometimes also called online optimization, is a hardware-based method that uses various sensors and real-time machine control to achieve optimal and safe cutting conditions during milling. These sensors can measure various quantities such as cutting forces, spindle speed, motor current, vibrations, chattering, or temperature. Adaptive control then evaluates these measurements and decides whether to adjust certain controlled cutting parameters, typically spindle speed or feed rate. This adjustment occurs in real-time during the cutting process. This method is suitable for large and heavily loaded cutting tools, such as face mills and large-diameter end mills.

However, adaptive control has several disadvantages. The most significant issues are associated with the sensors, including their high cost, low robustness, and difficulty in positioning them near the cutting zone. Other major drawbacks include the need for custom sensors and adaptive control systems

for each machine and the fact that optimization is performed separately for each part, even when the parts are identical. [46]

In 1988, Koren presented a paper on adaptive control systems for machining at the American Control Conference. In this paper, he summarized the research work that had been done on the topic since the mid-1960s. He considers Centner's paper *Final Report on Development of Adaptive Control Techniques for a Numerically Controlled Milling Machine* to be the best-known work in the field of adaptive control. Centner measured machine vibration, tool temperature, and cutting torque. Based on the values obtained, he adjusted the feed rate and spindle speed. Koren also notes that most adaptive controls require measuring tool wear, for which there is no direct method. Thus, wear has mostly been evaluated indirectly from measurements of cutting forces or tool temperature. The lack of reliable tool wear measurement greatly reduces the practical applicability of adaptive control. Another problem that arose from Koren's measurements in 1980 was the stability problem of the regulation circuit. [57]

6.2 Offline optimization

Offline optimization relies on virtual machining, employing a criterion function as the basis for optimization. Commonly, this criterion function is characterized by a constant material removal rate (MRR), cutting force limit, or drive movement smoothness. The subsequent sections will present works that address feed rate optimization using these criteria. [46]

6.2.1 Material Removal Rate Criterion

Optimization algorithms that use the material removal rate (MRR) as a key parameter typically aim to optimize the feed rate to maintain a constant MRR. However, some of these solutions assume that a constant MRR results in a constant tool load. Nevertheless, as discussed in Section 5, the magnitude of cutting forces is influenced by factors beyond just the MRR.

In 1988, Wang published probably the first research on offline feed rate optimization in milling. Wang published his paper *Solid Modeling for Optimizing Metal Removal of Three-dimensional NC End Milling.* He developed a solid modeling system to simulate and optimize three-dimensional (up to 5-axis) NC milling. The modeler can estimate the chip load and cutting force. Using the simulation, an adjusted feed rate is added to the NC code. [58]

In 1998, Altan et al. developed the optimization software *OPTIMILL* which was published in the article *High Performance Machining for Die/Mold Manufacturing – R&D in Progress.* The input for this software is NC code in

APT format. In the first step, the software analyses the tool engagement and cutting conditions. The next step is to compute the appropriate spindle speed and feed rate. New commands (words *SPINDL* and *FEDRAT*) are added to the original APT file if needed. The final step is to update the workpiece geometry according to the material removed by the current toolpath. Using *OPTIMILL*, a reduction of the machining time by 20–50% was reached. [59]

In 2022, Kůrka in his diploma thesis *NC Code Optimization Based on the Cutting Tool Load Considering the Machine Tool Dynamic Properties* introduced his two algorithms for feed rate optimization. The first was developed on the mechanistic force model, but the results were not satisfactory. Therefore he developed the second algorithm that uses the MRR as an optimization criterion. The main focus was on vibration reduction. After optimizing the feed rate, vibrations and chattering were reduced. [12]

6.2.2 Force Criterion

The criterion of maximum permissible cutting force is particularly useful when the objective is to prevent tool overload or minimize tool deflection. As discussed in Section 6.2.1, the material removal rate (MRR) course may not precisely correspond to the cutting force course. Consequently, more sophisticated algorithms have been developed to adapt the feed rate based on the force load calculated from the force model.

In 1992, Yazar et al. published a paper titled *Feed Rate Optimization Based on Cutting Force Calculations in 3-Axis Milling of Dies and Molds with Sculptured Surfaces*. In their work, they introduced the optimization software *FEDOPT*, which utilizes the ERC/NSM software with Z-map workpiece representation and force modeling. *FEDOPT* supports two types of mills: flat-end and ball-end mills, and it employs the Kienzle force model for its force calculations. *FEDOPT* assumes a linear relationship between cutting forces and feed rate and uses CL files as part of its operation. The primary criterion for optimization in *FEDOPT* is the minimization of machining time. [60]

In 2006, Salami et al. introduced an optimization algorithm for milling sculptured surfaces with one-flute ball-end mills in their work titled *Feed Rate Optimization for 3-Axis Ball-End Milling of Sculptured Surfaces*. The cutting force is calculated using the Kienzle force model based on the cutting edge generated by intersecting an inclined plane with the cutter nose. The model compares the maximal resultant force and shank stress with allowable values at each movement. Test results indicated a 10% time-saving. [61]

In 2014, Xu and Tang developed an algorithm to optimize toolpath and feed rate for ball-end mills. This algorithm is presented in the paper *Five-Axis*

Toolpath and Feed Rate Optimization Based on the Cutting Force-Area Quotient Potential Field. The mechanistic model for cutting forces calculation is used. To minimize the total machining time, the algorithm takes into account the force applied to the tool during deflection. First, the effect of tool orientation, local part surface geometry, feed direction, and feed rate on the deflection cutting force was investigated. Considering the limiting deflection force for each CC point, the effective MRR in each feed direction and feed rate was calculated. The potential field at the surface of the component was then determined. The toolpath is generated in the direction of maximum effective MRR and tries to follow the feed direction when the CC curves are determined. With this algorithm, the total machining time can be reduced by up to 25%. [62]

In 2018, Zhang et al. presented a method for feed rate optimization in their work named *A Force-Measuring-Based Approach for Feed Rate Optimization Considering the Stochasticity of Machining Allowance.* The main contribution of their work can be summarized in two main points. Firstly, "An instantaneous axial cutting depth calculation method by combining the analytical cutting force model with measured force data is proposed." [63] And secondly "A feed rate optimization method according to the actual instantaneous axial cutting depth to improve machining efficiency is proposed." [63] The method was experimentally validated and the results showed more than 19% timesaving. [63]

In 2019, Kokotovic et al. focused on planar milling operations with flat-end mills and the optimization of these operations using MATLAB. They employed a Z-map representation for model geometry. Mechanistic force models and simulation of one spindle revolution were used for milling force prediction. This algorithm is detailed in the paper *Feed Rate Optimization for 2.5D Milling Operations.* [32]

6.2.3 Machine Drive and Higher Order Dynamic Constraints Criterion

Typically, when optimizing the feed rate, usually only the speed is considered. However, methods that incorporate machine drive and higher-order dynamic constraints as criteria also account for drive limits and include factors such as limits, continuity, and smoothness of acceleration, jerk, jounce, and other higher dynamic constraints. This section introduces selected studies in this domain.

In 2013, Erkorkmaz et al. presented a paper titled *Feed Rate Optimization for Free Form Milling Considering Constraints from the Feed Drive System and Process Mechanics.* They introduced a novel strategy for planning minimum

cycle time tool trajectories. This optimization strategy takes into account constraints imposed by the feed drive control system, specifically acceleration and jerk, as well as process mechanics, including maximum milling forces. A Parasolid kernel was used for the tool-workpiece engagement. A mechanistic force model was applied to predict the cutting forces. [64]

In 2015, Bharathi and Dong concluded their work *A Smooth Trajectory Generation Algorithm for Addressing Higher-Order Dynamic Constraints in Nanopositioning Systems* as follows: "This paper presents a computationally efficient heuristic algorithm for feed rate optimization that can generate a near-optimal trajectory for a toolpath incorporating constraints with higher order dynamic states (e.g. jerk, jounce, and derivative of jounce). Instead of optimizing the trajectory along the toolpath, in our algorithm, the trajectory is constructed from a set of knot points on the position-velocity phase plane by piecewise spline interpolation with higher-order continuity. The algorithm starts with a non-optimal but feasible velocity trajectory, and the trajectory is improved in its traverse time by multiple scanning iterations to move the velocity profile upward. In each iteration, the velocity at the knot points is improved one by one while maintaining the feasibility of the resulting trajectory. A near-optimal trajectory is achieved when the improvement in travel time is negligible from the last two scan iterations. The developed heuristic algorithm supports the incorporation of constraints with higher order states without sacrificing the computational efficiency." [65]

In 2020, Lu et al. introduced a novel method for time-optimal tool motion planning, which has been implemented into the ROS (Robot Operating System) platform. This optimization is subject to constraints on jerk, acceleration, and feed rate. The optimization process starts with the highest-order parameter, the jerk, and then numerically integrates the other variables, observing their upper and lower bounds. The paper also includes a case study in which the toolpath for a 6-DoF robotic arm was optimized using this strategy. You can find a detailed description of this optimization approach in the paper titled *Time-Optimal Tool Motion Planning with Tool-Tip Kinematic Constraints for Robotic Machining of Sculptured Surfaces.* [66]

6.2.4 Using Artificial Intelligence

In the last few years, artificial intelligence (AI) has been used in many fields, so in the field of machining. Although the use of these relatively new methods is not yet widespread, several works using AI have already been produced. Most of them deal with the prediction of a technological parameter, but they are usually not used for any further optimization.

In 2007, Aykut et al. developed a model of cutting forces using the artificial neutral network. The work presenting this method is titled *Modeling of Cutting Forces as Function of Cutting Parameters for Face Milling of Satellite 6 Using an Artificial Neural Network*. Cutting forces were described as functions of cutting parameters such as cutting speed, feed rate, and depth of cut. This model was not used for any further optimization. The model showed accurate results, so it could be used to optimize the feed rate. [50]

In 2017, Mundada and Narala focused on developing a method using artificial neural networks and a simulated annealing algorithm to optimize cutting parameters to achieve the minimum surface roughness. They concluded their work titled *Optimization of Milling Operations Using Artificial Neural Networks (ANN) and Simulated Annealing Algorithm (SAA)* as follows: "The results indicate that to obtain good surface finish, high cutting speed, lower feed rate and medium values for the other two variables (rake angle and nose radius), gives optimized results according to problem condition." [67]

6.3 Commercial Software for Feed Rate Optimization

In addition to academic and research work, commercial software solutions also offer feed rate optimization capabilities. Some advanced computer-aided manufacturing (CAM) software, such as *CutPro, Npro,* and others from *MAL Inc.*, as well as modules like *OptiPath* and *Force* for *VERICAD, NCG CAM, SmartFEED™, Production Modeule - Third Wave System, Eureka Chronos, NC Simul, NC Brain, Saveapp*, and *MillVis* employ feed rate optimization algorithms. Many companies do not publicly disclose or describe the specific details of their optimization algorithms, making the optimization process a black box for end users. [68, 69, 70, 71, 72, 73]

6.3.1 MAL Inc. Optimization Software

Canadian company *MAL Inc.* (*Manufacturing Automation Laboratories*) develops a range of software solutions for machining simulations and optimizations. Among their notable products are *CutPro®, MACHpro™, DELPro,* and *Npro*. These software packages typically encompass not only the geometric aspects of the machining process but also consider the physics of machining and the dynamic behavior of both the machine and the tool. The company introduces their product as follows: "*MACHPRO™* is the most advanced process simulation and NC program optimization software. It enables engineers to visualize and simulate real-world performance of machining operations early in the process planning stage. Unlike competitor software, we do not simply look at geometry calculations to optimize programs; we look

at the physics involved in machining process, which include machine drives, the CNC, and geometries involved. Since *MACHpro* covers aspects from the entire machine tool, *MACHpro™* is the most accurate machining optimization software. *MACHpro* is the only NC program optimization software which can simulate machining vibrations and true cycle time within 80% accuracy." [68]

6.3.2 VERICUT

VERICUT is a product of the American company *CG Tech*. There are some modules for milling optimization. Two of them are for the feed rate optimization – *Force* and *OptiPath*.

According to *CG Tech*, *Force* module employs the material properties and the cutting edge geometry to simulate cutter contact conditions and to predict cutting forces and chip load. "The software then automatically adjusts the feed rate to stay within desired force, chip load and power limits. Force predicts cutting conditions using a proprietary set of material coefficients that account for the shear-strength of the workpiece material and the effects of friction and temperature." [69]

The *OptiPath* module adjusts feed rate according to the user's desired material removal rate, chip chiskness, and surface speed. [69]

6.3.3 NCG CAM

German company NC Graphics developed software *NCG CAM* that includes also feed rate optimization. The authors present the functionalities of the software as follows:

"*NCG CAM* has feed-rate optimization for area-clearance, core roughing, rest roughing and water-line machining.

The software is aware of the cutting conditions, if the current toolpath is machining an external corner, then the feed-rate specified can be maintained. In areas such as internal corners where the cutter will be in full contact, *NCG CAM* looks ahead and adjusts the feed-rate down to maintain accuracy and prolong tool-life.

When *NCG CAM* is performing a ramping entry move for area clearance roughing, the ramping feed rate is used. Once the cutter is to depth, the cutting feed-rate can also be reduced as this first cut will be the full width of the cutter. This is then returned to the normal feed-rate once the cutter is not making a full width cut." [70]

6.3.4 SmartFeed™

Canadian company *ICAM Technologies Corporation* developed software *SmartFEED™*. The company introduces their software as follows: "*SmartFEED™* optimizes cutting feed-rates by using material removal simulation to automatically recalculate the best machining feed-rate based on the machine tool capabilities, tool reference cuts and the real-time engagement of the cutting tool in the in-process stock material." [71]

6.3.5 Production Module

Production Module, developed by an American company *Third Wave System*, is an CAE software for modeling machining at the toolpath level. According to authors "*Production Module* integrates advanced, experimentally validated, FEA driven material models, with CAD/CAM into an easy to use system for analyzing and improving machining progress ... users can balance loads, pressures and even temperatures across the entire toolpath." [74]

6.3.6 Eurekea Chronos

The company *Roboric Srl.* developed the software *Eureka Chronos* for the feed rate optimization. As the authors present: "*Chronos* optimizes G-code program feedrates using AI based algorithms to maintain constant tool engagement and material removal, while maintaining the original CAM programs toolpath geometry. *Eureka Chronos* is compatible with all popular CAM software." [75]

6.3.7 NCSIMUL

NCSIMUL is a software suite developed by the Swedish company *Hexagon*. *NCSIMUL* provides comprehensive control over the machining process, including tasks such as NC code modifications, simulations, and real-time machine monitoring. The *NCSIMUL Optitool* module specializes in the analysis and optimization of cutting conditions, including spindle speeds and feed rates. Feed rate adjustments are particularly applied in regions where the tool is not actively machining, improving efficiency. The solution provides up to five-axis machining. [76]

6.3.8 NCBrain

NCBrain is another Czech software specializing in NC code optimization. Based on NC code, workpiece geometry, and tooling information, *NCBrain* conducts machining simulations and automatically optimizes the NC code. These optimizations are probably based on Material Removal Rate (MRR) analysis. *NCBrain* performs several optimizations, including adjusting the

feed rate, optimizing toolpaths in areas where minimal material is being machined, adjusting tool approach, detecting and preventing collisions, adding toolpaths in regions with non-constant material removal rates, and offering recommendations for optimal tool overhang. [77]

6.3.9 MillVis

MillVis is not a commercial milling optimization solution; rather, it is a software in ongoing research development, focused on creating a virtual model of the cutting process. This software is being developed at the Department of Production Machines and Equipment at the Czech Technical University in Prague, Faculty of Mechanical Engineering. There are plans to incorporate optimization features in future versions of *MillVis*. *MillVis* employs a voxel distance field workpiece representation, and mechanistic force models are utilized for force calculations. Toolpath files can be either NC code, CL data, or interpolated data. The workpiece is imported in .stl format. This software has been used extensively in the work on this thesis. [35, 78]

Chapter 7

Assumptions for Feed Rate Control

Two assumptions had to be examined before a feed rate control strategy are proposed. The first is that the effect of the feed rate on the force load is sufficient that a desired change in load can be achieved by adjusting the feed rate. The second assumption is that the feed rate adjustment can be based on the force load evolution obtained by virtual machining based on programmed feed rates. These two investigations are described in this chapter.

7.1 Cutting Force Dependency on Feed Rate

The initial question in developing this algorithm is how much the feed rate reduction will affect cutting forces. As shown in Section 5, in all force models, feed rate occurs in some relation, typically either as a feed rate per tooth f_z or as the uncut chip thickness h_D, which is directly dependent on the feed rate per tooth.

Throughout this work, a mechanistic cutting force model was used (see Section 5.4). With this model, tangential force F_t, normal force F_n, and binormal force F_b can be calculated using Equation 5.23, which is restated here in differential form.

$$\begin{aligned} dF_t(\phi) &= (K_{tc} \cdot h_D(\phi) + K_{te}) \cdot db_D \\ dF_n(\phi) &= (K_{nc} \cdot h_D(\phi) + K_{ne}) \cdot db_D \\ dF_b(\phi) &= (K_{bc} \cdot h_D(\phi) + K_{be}) \cdot db_D \end{aligned} \tag{7.1}$$

With the knowledge of the tool geometry and the current tool rotation ϕ, the directional forces F_x, F_y, and F_z can be calculated.

The cutting force component F_{ic} (also called the shearing component) and edge force component (also called the ploughing component) of the directional force F_{ie} (the index i represents the general notation of the force direction) are introduced as follows:

$$dF_{ic} = K_{ic} \cdot h_D(\phi) \cdot db_D \tag{7.2}$$

$$dF_{ie} = K_{ie} \cdot db_D \tag{7.3}$$

It becomes evident, that only the cutting force component F_{jc} depends on the feed rate. The edge force component F_{je} is feed rate independent. The ratio of the cutting and edge force components then determines how the magnitude of the total force changes with a change in feed rate.

$$\begin{aligned} F_{ic} &= f(v_f) \\ F_{ie} &\neq f(v_f) \end{aligned} \tag{7.4}$$

The directional force F_i can be written as the sum of these two components:

$$dF_i(\phi) = dF_{ic} + dF_{ie} \tag{7.5}$$

To investigate the contribution of the feed-dependent component, the simulation has been conducted using actual cutting and edge coefficients. It was carried out in *MillVis* software with settings for four-flute cylindrical 12mm end mill *ISCAR EC120A25-4C12* and the workpiece material was carbon steel C45. Values corresponding to this combination of the tool and workpiece material were entered into the force model. The simulation was run for two different toolpaths.

The first toolpath for the cutting force analysis is shown in Figure 7.1a. The shape of the path was designed so that the tool moves first in the X-direction, then along an arc, and then in the Y-direction. Thus, it is possible to show the effect of the feed rate on the directional components of the cutting force for different directions of motion.

The second toolpath is depicted in Figure 7.1b. The shape of this toolpath was designed so there is no radius in the tool motion and the motion direction changes at one point. Also the axial depth of cut a_e is not 12 mm, but only 4 mm. This case was chosen to demonstrate the change in force when the engagement angle increases in the corner. Cutting and edge coefficients and other simulation parameters are listed in Table 7.1.

Forces obtained from the first simulation (toolpath 1) are presented in Figures 7.2, 7.3, 7.4, and 7.5. In Figures 7.2 and 7.5, the resultant directional force is decomposed into all six cutting components, and it can be described using the following equation:

$$F_i = F_{itc} + F_{inc} + F_{ibc} + F_{ite} + F_{ine} + F_{ibe} \tag{7.6}$$

where the individual force components refer to the contributions of the respective cutting and edge coefficients. In Figures 7.3 and 7.5, the force is decomposed as described in Equation 7.5. What percentage of the total directional force is the feed rate dependent component is shown in Figure 7.6.

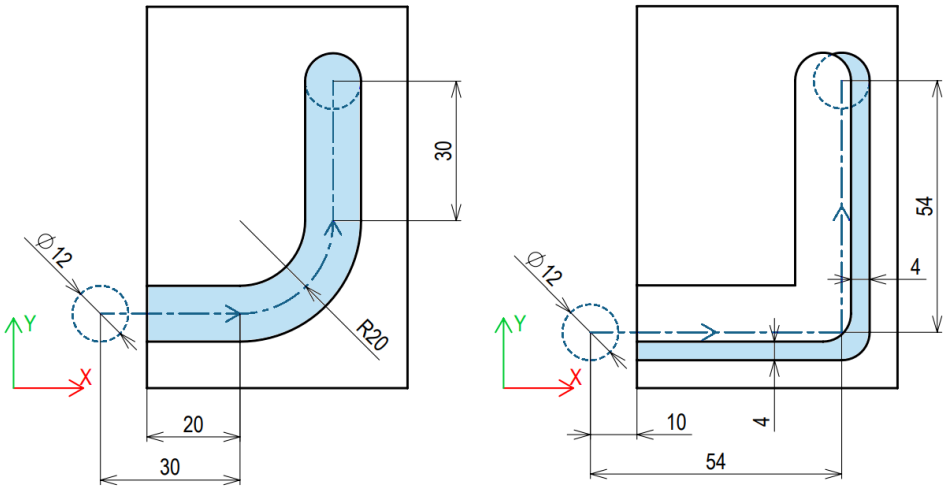

(a) Toolpath 1 *(b) Toolpath 2*

Figure 7.1: Force analysis - toolpaths

Table 7.1: Force component dependent on feed rate - simulation settings

Parameter	Value	Units
K_{tc}	1640	$\mathrm{N \cdot mm^{-2}}$
K_{nc}	390	$\mathrm{N \cdot mm^{-2}}$
K_{bc}	550	$\mathrm{N \cdot mm^{-2}}$
K_{te}	51	$\mathrm{N \cdot mm^{-1}}$
K_{ne}	65	$\mathrm{N \cdot mm^{-1}}$
K_{be}	0	$\mathrm{N \cdot mm^{-1}}$
n	4775	$\mathrm{min^{-1}}$
v_f	2101	$\mathrm{mm \cdot min^{-1}}$
f_z	0.11	mm
a_p	4	mm
D	12	mm
z	4	
λ	30°	

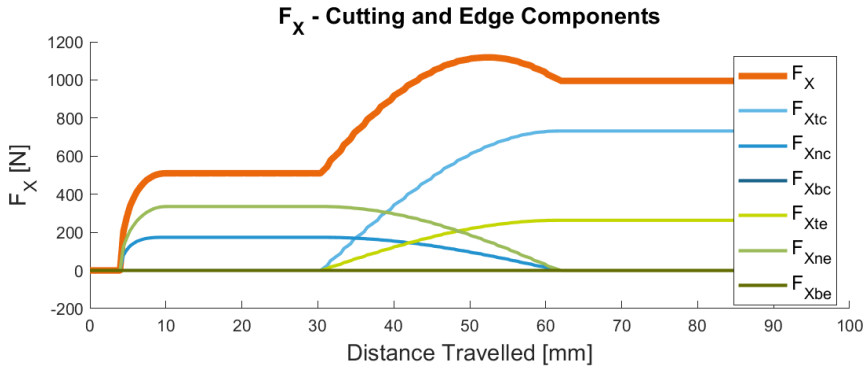

Figure 7.2: F_X - contribution to overall directional force from individual cutting and edge coefficients (toolpath 1)

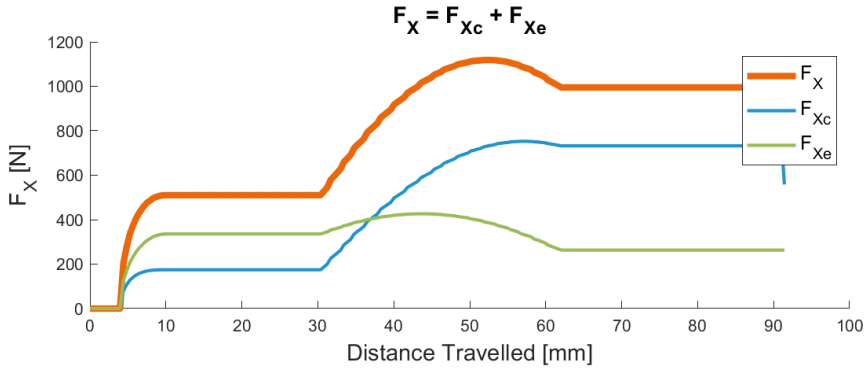

Figure 7.3: $F_X = F_{Xc} + F_{Xe}$ (toolpath 1)
F_{Xc} - feed-dependent component of the F_X
F_{Xe} - feed-independent component of the F_X

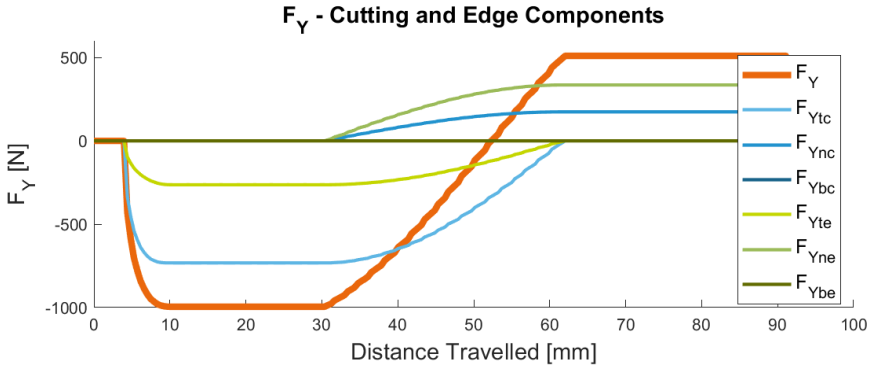

Figure 7.4: F_Y - contribution to overall directional force from individual cutting and edge coefficients (toolpath 1)

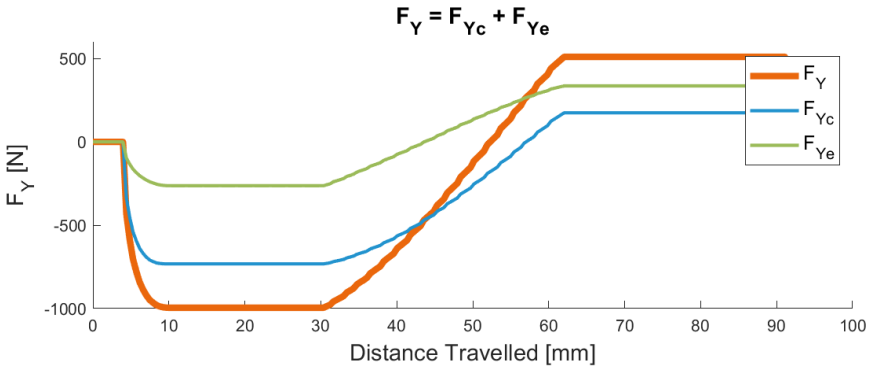

Figure 7.5: $F_Y = F_{Yc} + F_{Ye}$ (toolpath 1)
F_{Yc} - feed-dependent component of the F_Y
F_{Ye} - feed-independent component of the F_Y

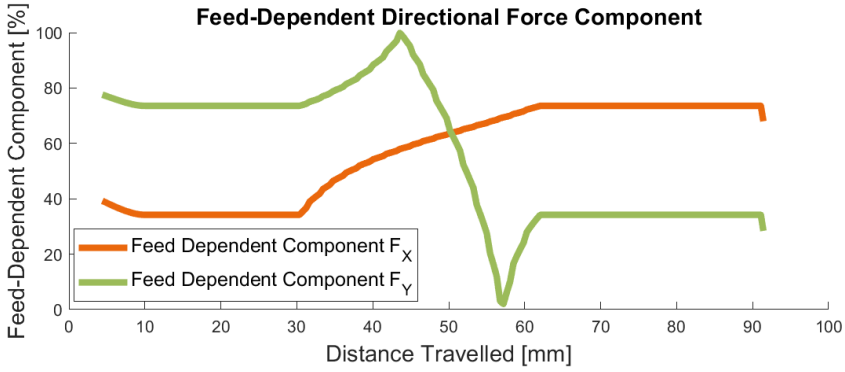

Figure 7.6: Feed-dependent component of the overall directional force (toolpath 1)

Results of the second simulation (toolpath 2) are presented in Figures 7.7, 7.8, 7.9, and 7.10. Figure 7.11 illustrates a significant increase in the cutting force at the corner and, as can be seen from Figure 7.8, the feed rate dependent component of the force in the X-direction is only approximately 8%. That implies that assuming the validity of the force model, these force peaks that arise at locations with increased engagement angles can not be reduced by simply reducing the feed rate. In Chapter 10, this problem is discussed in more detail. It is shown that at very low feed rates the force models used are not valid, and a reduction in cutting force will occur. That comes at the cost of possibly unstable machining.

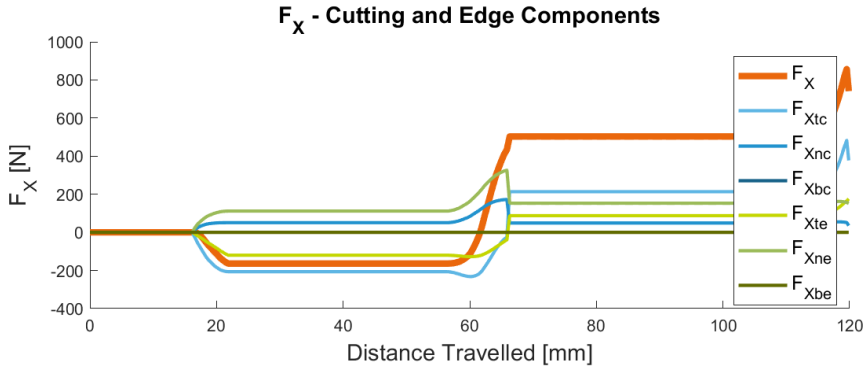

Figure 7.7: F_X - contribution to overall directional force from individual cutting and edge coefficients (toolpath 2)

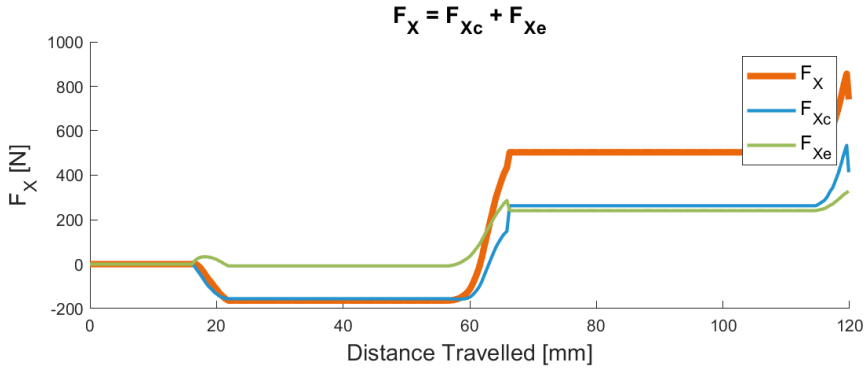

Figure 7.8: $F_X = F_{Xc} + F_{Xe}$ (toolpath 2)
F_{Xc} - feed-dependent component of the F_X
F_{Xe} - feed-independent component of the F_X

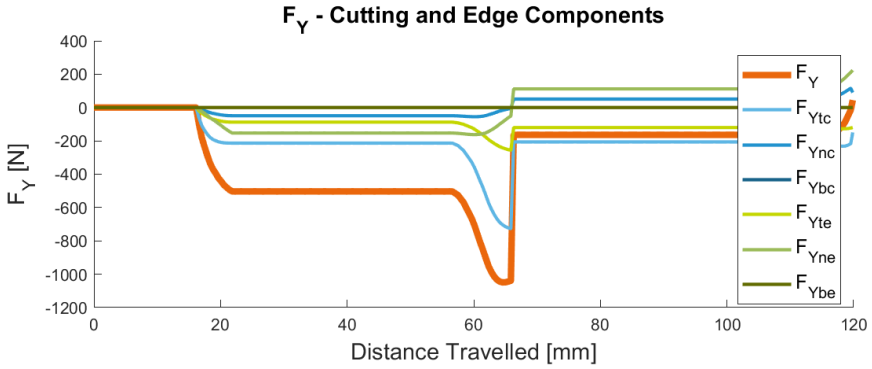

Figure 7.9: F_Y - contribution to overall directional force from individual cutting and edge coefficients (toolpath 2)

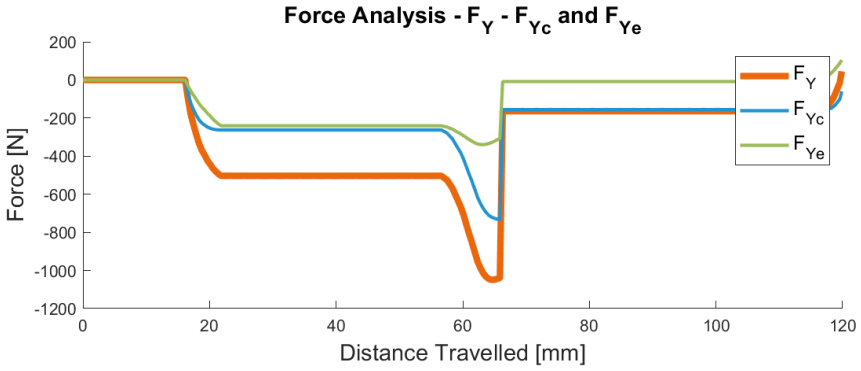

Figure 7.10: $F_Y = F_{Yc} + F_{Ye}$ (toolpath 2)
F_{Yc} - feed-dependent component of the F_Y
F_{Ye} - feed-independent component of the F_Y

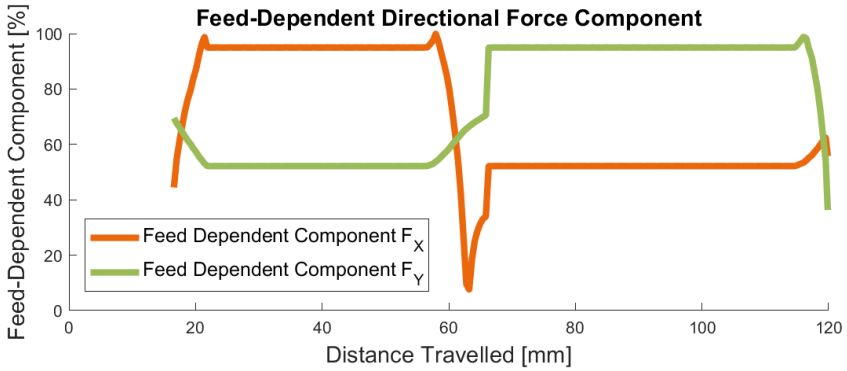

Figure 7.11: Feed-dependent component of the overall directional force (toolpath 2)

The feed rate dependent force component significantly contributes to the magnitude of the resultant directional force. However, the extent of this influence depends on various factors, including tool geometry, engagement conditions, tool and workpiece materials, and the direction of movement. To optimize the feed rate effectively, it is necessary to consider the magnitude of its contribution to the cutting forces at each point. It is not possible to determine its contribution from the directional force evolution alone. Since *MillVis* does not export these values, simulations need to be run twice, once with zero cutting coefficients and once with zero edge coefficients.

For better illustration, Figures 7.12 and 7.13 display the changes in directional forces when the feed rate is reduced by 50%. This reduction results in force reductions of approximately 32% for the X-axis and 37% for the Y-axis for the first toolpath, and approximately 29% for the X-axis and 35% for the Y-axis for the second toolpath. However, in the second example, the force

in the X-direction reduces only approximately 4% in the corner (marked in Figure 7.13).

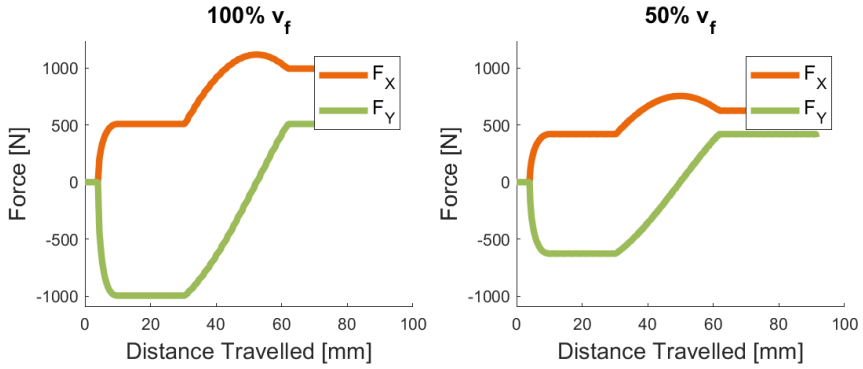

Figure 7.12: Change in directional load when the feed rate is reduced by 50% (toolpath 1)
$v_f = 2101\,\text{mm} \cdot \text{min}^{-1}$ *(100%)*
$v_f = 1050\,\text{mm} \cdot \text{min}^{-1}$ *(50%)*

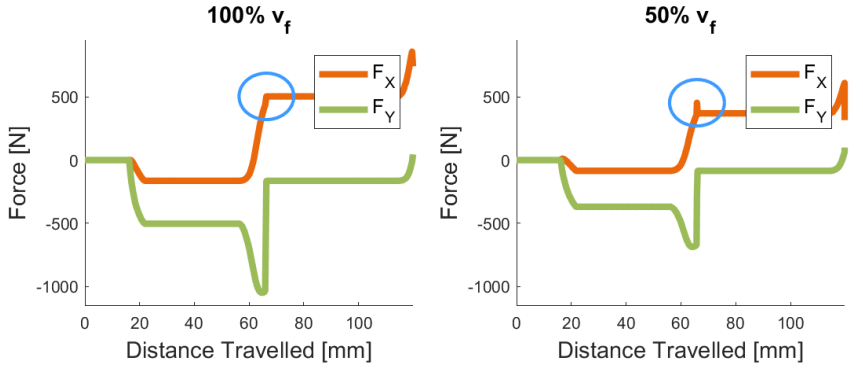

Figure 7.13: Change in directional load when the feed rate is reduced by 50% (toolpath 2)
$v_f = 2101\,\text{mm} \cdot \text{min}^{-1}$ *(100%)*
$v_f = 1050\,\text{mm} \cdot \text{min}^{-1}$ *(50%)*

7.2 Analysis of the Impact of Programmed, Set-Point, and Actual Feed Rates on Cutting Forces

Different machine tools have different drive dynamics. In general, the larger the machine, the less dynamic it has, which means it has a lower maximum permissible jerk and acceleration. As a consequence, the machine will take

longer to reach the programmed feed rate. If the feed rate change is required over a short distance, the machine may not reach the programmed feed rate at all. For this reason, it was essential to determine whether the optimization algorithm can be based on the programmed feed rate, whether it will always require a prior execution of the NC program in a virtual station, or even if it should be based on actual positions and feeds that would necessitate dry run of the code on the real machine.

In the context of this analysis, three types of feed rates can be distinguished:

- **Programmed feed rate** - is written in the NC program
- **Set-point feed rate** - is obtained from the NC interpolator, or from the virtual machine (simulation)
- **Actual feed rate** - is the actual tool-to-workpiece speed and can only be obtained from the NC program execution on a real machine

In the same way, we can also distinguish positional data.

Two analyses have been carried out for the same toolpath depicted in Figure 7.14 (for the highlighted section, detailed results are provided below). Virtual machining was conducted for all position data, and the resulting forces were compared as part of the analysis. Cutting condition and simulation parameters are listed in Table 7.2. The material of the workpiece was carbon steel C45, used tool was the flat-end mill *ISCAR EC120A25-4C12*.

Table 7.2: Analysis of the impact of programmed, set-point, and actual feed rates on cutting forces - cutting conditions and simulation settings

Parameter	Value	Units
K_{tc}	1640	$\mathrm{N \cdot mm^{-2}}$
K_{nc}	390	$\mathrm{N \cdot mm^{-2}}$
K_{bc}	550	$\mathrm{N \cdot mm^{-2}}$
K_{te}	51	$\mathrm{N \cdot mm^{-1}}$
K_{ne}	65	$\mathrm{N \cdot mm^{-1}}$
K_{be}	0	$\mathrm{N \cdot mm^{-1}}$
n	4775	$\mathrm{min^{-1}}$
v_f	1910	$\mathrm{mm \cdot min^{-1}}$
f_z	0.10	mm
a_p	3	mm
D	12	mm
z	4	
λ	30°	

The first analysis compares programmed, set-point, and actual feed rates. The second analysis compares programmed and set-point for two different machines. The analyses are compared in the following sections.

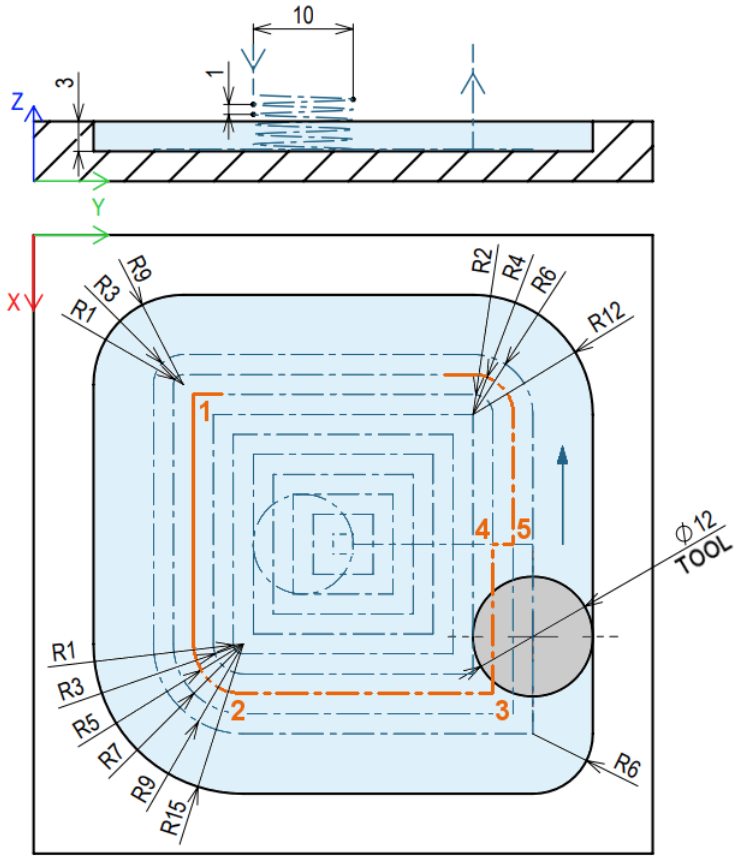

Figure 7.14: Pocket toolpath with different inner radii

7.2.1 Programmed, Set-Point, and Actual Feed Rate Comparison

The first analysis contained only constant feed rates (except rapid movements at the beginning and end of the toolpath). It compares programmed, set-point, and actual feed rates. The set-point feed rates and actual feed rates from a prior experiment conducted at the Department of Production Machines and Equipment, Czech Technical University in Prague, Faculty of Mechanical Engineering, were used for this analysis. This experiment was performed on the horizontal milling machine *TAJMAC-ZPS H630*, which is further detailed in Section 9.1.1.

From this analysis, it is evident, that as the interpolator regulates the position and the feed rate, set-point feed rate and actual feed rate are almost identical (see Figure 7.16). Similarly, the force load courses are almost identical (see Figures 7.17 and 7.18). That allows us to eliminate the possibility of having to obtain actual data from the machine and perform a dry-run before each optimization.

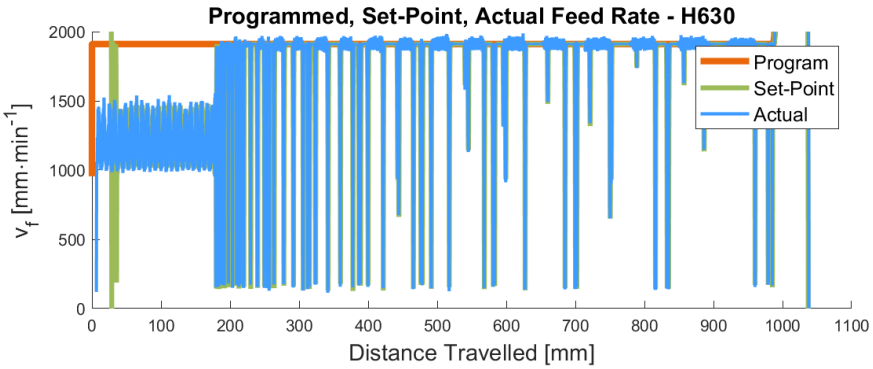

Figure 7.15: Programmed, set-point, and actual v_f comparison feed rate v_f

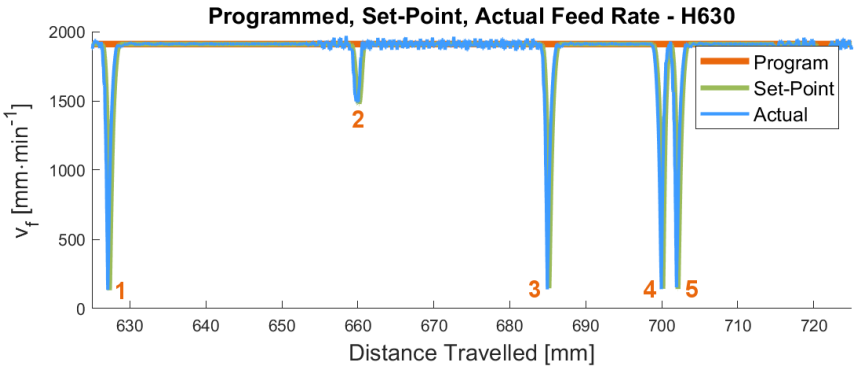

Figure 7.16: Programmed, set-point, and actual feed rate comparison feed rate v_f - detail

(the corresponding section of the toolpath is highlighted in Figure 7.14) the numbers in the figure refer to the corners shown in Figure 7.14

Figure 7.15 also shows that although the programmed feed rate is constant, the machine is not able to meet this requirement at all points along the toolpath. The reduction in feed rate is most noticeable when helical plunging at the beginning of the program. The largest, but only local, decreases in feed rate then occur at the pocket corners, where the machine must always stop in one axis and accelerate in the other. Figure 7.18 shows that there is a reduction in the force peaks at the corners as a result of this deceleration.

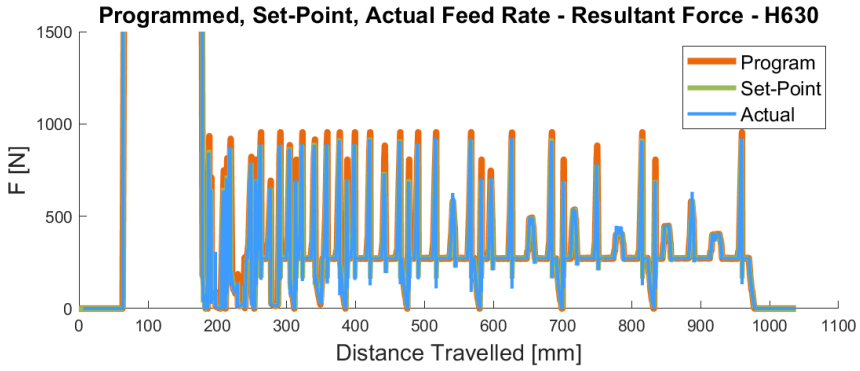

Figure 7.17: Programmed, set-point, and actual feed rate comparison resultant force F

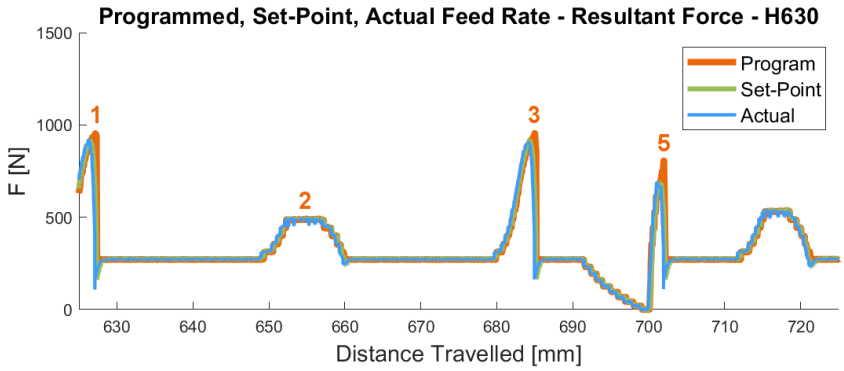

Figure 7.18: Programmed, set-point, and actual feed rate comparison resultant force F - detail

(the corresponding section of the toolpath is highlighted in Figure 7.14) the numbers in the figure refer to the corners shown in Figure 7.14

7.2.2 Set-Point Feed Rate Comparison for Different Machines

The second analysis was performed on the same toolpath as the first one with the same programmed feed rates. It compares set-point feed rates for two different machine dynamics. In this case, set-point feed rates were obtained from the virtual machine *SINUMERIK ONE Create MyVirtual Machine*. The first setting of accelerations and jerks corresponded to that of the H630 machine, and the second one to that of the *TOS Varnsdorf WHT 110* machine. *WHT 110* machine is a big horizontal machining center (range X, Y, Z is up to 3 x 2 x 2.5 m [1].) Values of jerks and accelerations are provided in Table 7.3.

Table 7.3: H630 and WHT 110 - acceleration and jerk

Parameter	*H630*	*WHT 110*	Units
a_X	2.5	2	$\mathrm{m} \cdot \mathrm{s}^{-2}$
a_Y	2.5	2	$\mathrm{m} \cdot \mathrm{s}^{-2}$
a_Z	2.5	2	$\mathrm{m} \cdot \mathrm{s}^{-2}$
e_X	20	3	$\mathrm{m} \cdot \mathrm{s}^{-3}$
e_Y	37	3	$\mathrm{m} \cdot \mathrm{s}^{-3}$
e_Z	20	3	$\mathrm{m} \cdot \mathrm{s}^{-3}$

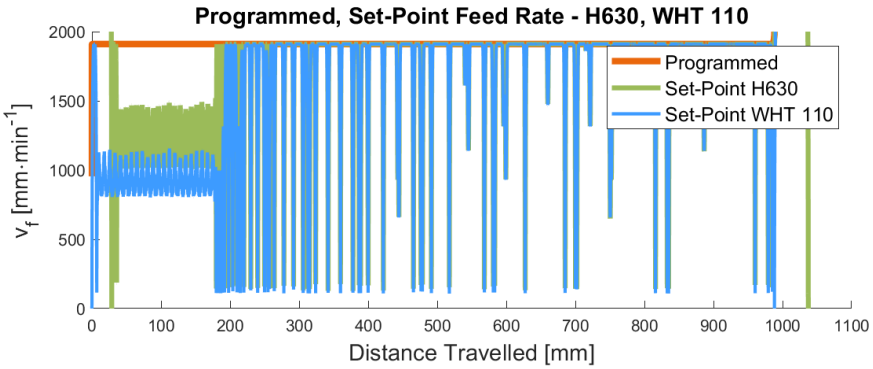

Figure 7.19: Programmed and set-point feed rate comparison H630, WHT 110 - feed rate v_f

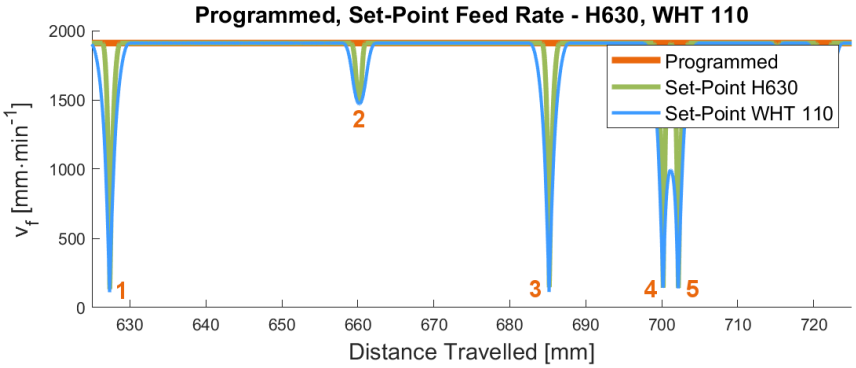

Figure 7.20: Programmed and set-point feed rate comparison H630, WHT 110 - feed rate v_f - detail

(the corresponding section of the toolpath is highlighted in Figure 7.14) the numbers in the figure refer to the corners shown in Figure 7.14

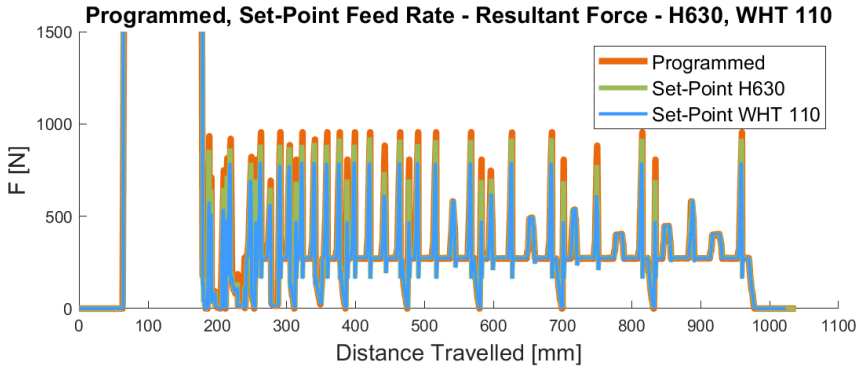

Figure 7.21: Programmed and set-point feed rate comparison H630, WHT 110 - resultant force F

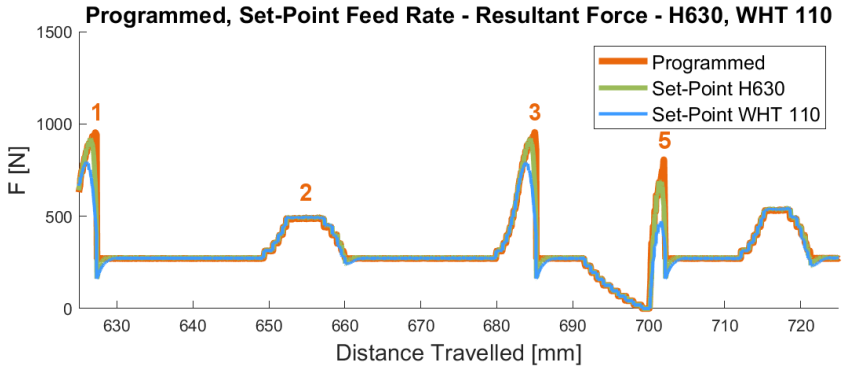

Figure 7.22: Programmed and set-point feed rate comparison H630, WHT 110 - resultant forces F - detail

(the corresponding section of the toolpath is highlighted in Figure 7.14) the numbers in the figure refer to the corners shown in Figure 7.14

The results of this analysis are shown in Figures 7.19 and 7.20. From the results, it is clear, that the H630 machine has higher drive dynamics compared to the larger *WHT 110* machine. Therefore the reduction of the feed rate during helical plunging was lower for *H630* than for *WHT 110*. Also, the H630 can reach the programmed feed rate after each corner faster. Figures 7.21 and 7.22 show that as the machine dynamics decrease, the force peaks at locations with higher engagement angles also decrease.

This analysis of the impact of programmed, set-point, and actual feed rates on cutting forces shows that although the machine is not always able to follow the programmed feed rates, the force load is not significantly affected. The initial motivation for optimizing the feed rate according to the directional force load is to avoid overloading the rotary axes of large machining centres

during roughing. Given this assumption, it can be expected that large parts will be machined, larger tools will be used, and lower feed rates will be set. Therefore, the machine will probably have sufficient travel distance to reach the desired feed rate. If the machine does not reach the required feed rate, the cutting forces will also be lower than programmed, and therefore, the machine will not be overloaded. Therefore, when optimizing the feed rate, the programmed feed rate can be used as a basis for optimizing the feed rate without significantly complicating the pre-process preparation of the machining. If the analysis showed that it is necessary to start from the set-point feed rate, it would mean for each optimization to execute the program first in the virtual machine and then to optimize it, which would be a significant complication and delay for practical use.

Chapter 8

Feed Rate Optimization Process

One of the goals of this thesis was to design a strategy for optimizing the feed rate in NC programs according to the defined limits of the directional force load of the tool. This strategy was designed and tested. Key parts and insights of the optimization algorithm are described in this chapter.

Although the term *optimization* is used, throughout this thesis, the more accurate term would be *adjustment* of the feed rate in the NC code according to the directional load and algorithmization of this strategy. Optimization usually means the search for a local or global minimum or maximum, for example, optimization with the aim of cost minimization. However, the term *optimization* is widely used for similar challenges both in the scientific research community and in commercial software.

After the assumptions stated in the previous chapter were proved, a strategy for adjusting the feed rate according to the directional load was proposed. Furthermore, an algorithmization of this strategy was designed.

This section describes the optimization process. The first step is to run the simulations in *MillVis* and save the selected results. This is described in Section 8.1. Next, the user has to set numerous parameters at the beginning of the script, such as force limits, tool parameters, etc. The parameter settings are described in Section 8.2. Section 8.3 describes how the multi-axis indexed machining optimization was approached. If everything is set up, the optimization starts by loading the NC code, which is described in Section 8.4. Section 8.5 then describes the subsequent loading and processing of the *MillVis* simulation results. The optimization process itself is described in Section 8.6. How the code is modified before exporting is summarised in Section 8.7.

8.1 Simulation Run

The first step of the optimization process is to obtain cutting forces from the simulation run in *MillVis* software (MillVis is introduced in Section 6.3.9). It is necessary to utilize the linear mechanical force model. The simulation needs to be executed twice: firstly, with zero edge coefficients K_{ie}, and secondly, with zero cutting coefficients K_{ic}. This dual simulation approach is essential because the optimization algorithm relies on information regarding the impact of the feed rate on the resultant directional cutting force. For a more detailed explanation of this concept, refer to Section 7.1.

At the end of each simulation, it is crucial to export the results. This involves obtaining the tooltip position in the workpiece coordinate system (File → Export → Tool Tip in WCS) and exporting the mean directional cutting forces in the tooltip coordinate system (File → Export → Mean Cutting Forces).

8.2 Optimization Settings

The simulation requires and offers numerous settings. The first thing to set up is the paths to the source files. These include the NC code file and simulation result files. From simulations in the *MillVis* software, the optimization script takes the resulting tooltip positions, corresponding mean cutting forces, and feed rates at specific points.

The input simulation results can be filtered, and one of two methods (floating average or floating median) can be used, along with the number of elements over which should be averaged. Another filtering parameter is *FilterPointsLength*, which specifies the minimum number of points in an optimized section. That filters out parts, typically at the beginning and end of optimized sections, where the force value may fluctuate around the specified force limit due to simulation inaccuracies, and then connects these sections into one. The distance between individual points is determined by the *MillVis* simulation resolution.

Another necessary parameters are the limits of all machine axes to be considered in the simulation. The algorithm allows optimization based on linear (X, Y, and Z) or rotary (A, B, and C) axes. If the user wants to optimize according to rotary axes, the distance from the tool tip to the corresponding rotary axis has to be entered. This option is further described in Section 8.3. The user can also set which axes should be taken into account. Force limits are entered as upper and lower limits. The upper force limit must not be exceeded after optimization. For the lower force limit, if all forces in a given section are below the lower limit, the algorithm will increase the feed rate in

that section. A safety coefficient can also be set, which linearly adjusts all specified force limits.

Another value entered by the user is the *rapid feed rate* value, which is applied where interpolation is commanded (G01, G02, or G03) but the tool does not cut.

The optimization algorithm also requires information about the tool used, specifically the number of cutting edges, diameter, and the manufacturer's recommended minimum and maximum feed rate per tooth. The user can then choose whether to adhere to the manufacturer's recommendation, or allow to adjust the feed rates to the lower values, that is the recommended minimum feed rate per tooth.

Finally, the script offers two last settings related to the optimization outputs. The first one toggles the rendering of certain process graphs, and the second one allows for the export of the optimized NC code.

8.3 4th and 5th Indexed Axes

If the objective of the optimization is to prevent overloading of the rotary axis, it is possible to define the moment limits of the rotary axes and the distance of the tooltip from the respective rotary axis. With this information, calculating the maximum relevant turning moment acting on the axis becomes straightforward. The instantaneous turning moment from the cutting process can then be determined as the product of the cutting force in the respective direction (in TCS) and the arm length L_a on which the force is applied. Therefore,

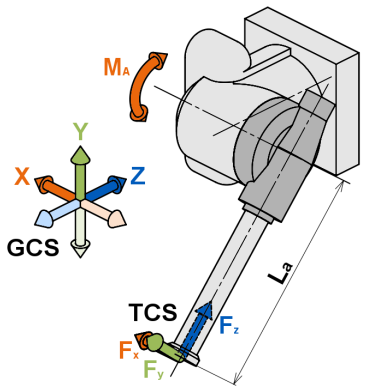

Figure 8.1: Schema of the milling using A-axis pivot spindle head

when optimization is conducted with constraints based on the rotary axes, the script recalculates the maximum allowable force for a given rotation, aligns it

with the limit of the linear axis, and proceeds with the optimization as usual. Figure 8.1 illustrates an example of milling using a pivot milling head with the A-axis. The procedure for recalculating the rotational axis limit (for the case depicted in Figure 8.1) is then indicated in Equation 8.1.

$$\begin{aligned} M_A &= F_y \cdot L_a \\ M_{Amax} &= F_{ymax} \cdot L_a \\ F_{ymax} &= \frac{M_{Amax}}{L_a} \end{aligned} \tag{8.1}$$

8.4 NC Code Processing

For this work, an interpreter of the NC code has been developed. Currently, it supports only ISO code, and other standard NC instruction formats are not integrated yet.

Upon loading the NC code, the interpreter initially distinguishes individual sentences and separates the NC words based on their address. If parameters are defined, their values are left-non-associative evaluated and then inserted into the appropriate positions.

In ISO code, only values that change are explicitly specified; those that remain constant are not included in the line. However, for optimization purposes, missing values need to be filled in. Each motion instruction sentence is therefore completed to ensure completeness. The values G, X, Y, Z, A, B, C, S, and F are added for the G00, G01, G02, and G03 instructions, while I, J, and K are included only for circular interpolation G02 and G03.

8.5 Simulation Results Processing

In Section 7.1, it is noted that the algorithm relies on the outcomes of two simulations, which are nearly identical but differ in the cutting and friction coefficients within the force model. Firstly, the friction coefficients are nullified, and secondly, the cutting coefficients are nullified. In both cases, the directional cutting forces are evaluated in a tool coordinate system (TCS) whose orientation is usually the same as the workpiece coordinate system (WCS) and the machine coordinate system (GCS) in case of the three-axis machining.

Another necessary output from the simulation is the position of the tool in the WCS. Since the WCS offset from the GCS is usually not introduced in the simulation, the tool position values in the GCS can be used.
During this phase, the identification of overloaded and underloaded sections is conducted. Each simulation point is categorized based on the directional loads relative to the directional limits as follows:

1. **Overloaded point** - when at least one directional force exceeds the corresponding upper force limit
2. **Underloaded point** - when all directional forces are below their respective lower force limits
3. **No optimization** - when all directional forces are below their upper force limit and at least one force is above its lower limit

Consecutive points with the same classification form a segment, with an *optimization point* at the beginning and end. The *optimization points* are newly defined points that will be subsequently added to the NC program. Between the *optimization points*, the endpoints of all NC motion instructions (G00, G01, G02, and G03) are incorporated to create smaller *optimization segments*. The optimal feed rate is then calculated for each *optimization segment*, as described in the subsequent Section 8.6.

8.6 Optimization

As mentioned in the previous Section 8.5, the optimization is performed on the *optimization segments* that are bounded by *optimization points* and the endpoints of all NC motion instructions. If the segment belongs to the *overloaded* category, it is first evaluated whether it is even possible to achieve a force below its upper limit by reducing the feed rate (this issue is discussed in Section 7.1). If not, the optimal feed rate value is set to the minimum feed rate value determined from Equation 8.3. If a sufficient reduction in directional load can be achieved by reducing the feed rate, the optimal feed rate is calculated from Equation 8.2. If the *keep minimum feed rate per tooth* function (*keep* f_{zmin}) is enabled, the optimal feed rate is compared to the minimum feed rate determined by Equation 8.3. If the optimal feed rate is lower than the minimum feed rate, the optimal feed rate is set to the minimum feed rate, otherwise it does not change.

For the *underloaded* and *no optimization* sections, the calculation of the optimal feed rate is more straightforward. If there is no optimization, the feed rate remains the same as in the original NC code. The optimal feed rate in the *underloaded* sections is calculated using Equation 8.2 in case of cutting. If the optimal feed rate exceeds the maximum feed rate, the optimal feed rate is set to the maximum feed rate determined from the maximum feed rate per tooth. That is described in Equation 8.4. When the tool is not in the cut and moves in the air, a *rapid feed rate* is set.

The entire decision scheme is shown in Appendix A. In this scheme and related equations, F_{cmax} is the maximum cutting force component of the most

overloaded directional force in the investigated section, F_{emax} is the maximum edge force component of the most overloaded directional force in the investigated section, F_{max} is the upper force limit of the respective directional force, v_f is the original feed rate, v_{fopti} is the optimal feed rate, v_{fmin} is the minimum feed rate determined from the minimum feed rate per tooth f_{zmin}, v_{fmax} is the maximum feed rate determined from the maximum feed rate per tooth f_{zmax}, f_{rapid} is the rapid feed rate, n is the spindle speed, and z is the number of the cutting edges.

$$v_{fopti} = \left\lfloor v_f \cdot \frac{F_{max} - \mid F_{emax} \mid}{\mid F_{cmax} \mid} \right\rfloor \tag{8.2}$$

$$v_{fmin} = f_{zmin} \cdot n \cdot z \tag{8.3}$$

$$v_{fmax} = f_{zmax} \cdot n \cdot z \tag{8.4}$$

If one NC instruction is divided into more separate sections with different feed rates, a new NC line needs to be added. The new instruction is inserted before the original one. Interpolation G-command is kept, and the new X, Y, and Z coordinates are added from the original simulation results (tooltip position in WCS), and the optimal feed rate v_{fopti} is set. In the case of circular interpolation (G02, G03), when the circle center coordinates are given relative to the tool position, a new circle center needs to be calculated and edited in the new NC line.

For better illustration, the example of optimizing NC code with a circular interpolation segment is introduced below. In Figure 8.2a, the toolpath is described, and numbers in circles describe the optimization segments. Figure 8.2b shows the calculation of new circle center coordinates, which are determined using Equation 8.5. The simulation parameters are the same as those used for the force analysis on the arc path (see Section 7.1) listed in Table 7.1. This optimization was conducted with the axis limits set according to Table 8.1, resulting in the feed rate being limited only by the x-axis limit. Other directional components are below their upper limits. The original x-force, including its cutting and edge components, is shown in Figure 8.3. The evolutions of the feed rate before and after optimization are shown in Figure 8.4, and the comparison of the x-force evolution before and after the feed rate optimization is shown in Figure 8.5. The original and optimized NC codes are provided in Table 8.2.

$$[I_2,\ J_2] = [I_1 + (X_1 - X_0),\ J_1 - (Y_1 - Y_0)] \tag{8.5}$$

Where $[I_2,\ J_2]$ are the circle center coordinates for the new NC command, $[I_1,\ J_1]$ are the circle center coordinates from the original NC command, $[X_0,\ Y_0]$ are the coordinates of the endpoint of the NC block before the optimized circular interpolation, and $[X_1,\ Y_1]$ are the coordinates of the endpoint

of the original NC block with circular interpolation. Referring to Figure 8.2b, it should be mentioned that $[X_2, Y_2]$ were the coordinates of the endpoint of the original circular interpolation, now they are the endpoints of the new NC block.

In the first section, the X-force F_x did not exceed its upper limit F_{xmax} and was below its lower limit F_{xmin}. Unfortunately, the force in the y-direction was not below its lower limit. Therefore, it was not possible to increase the feed rate v_f. In the second section, the tool enters the arc, and the force in the X-direction starts to increase. For this section, the same applies as for the previous one. In the third section, the force limit in the x-direction is exceeded, and therefore, it is necessary to slow down. The optimal feed rate was determined by calculating Equation 8.2. That is lower than the minimum feed rate per tooth f_{zmin} (determined by Equation 8.3), but since the minimum feed rate function is disabled, the value originally calculated is applied. For the last section, the same applies.

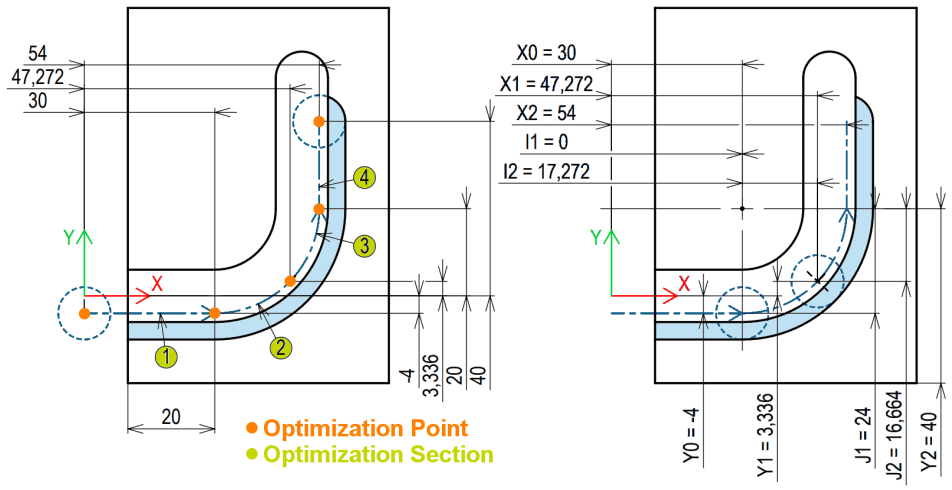

(a) Optimization - toolpath *(b) Circle center calculation*

Figure 8.2: Optimization - example

Table 8.1: Optimization example - optimization settings

Parameter	Value	Units
F_{xmin}	250	N
F_{ymin}	250	N
F_{zmin}	250	N
F_{xmax}	300	N
F_{ymax}	1000	N
F_{zmax}	1000	N
f_{zmin}	0.04	mm
f_{zmax}	0.11	mm
v_{fmax}	2101	$\text{mm} \cdot \text{min}^{-1}$
f_{rapid}	6000	$\text{mm} \cdot \text{min}^{-1}$
keep minimum f_z	disabled	

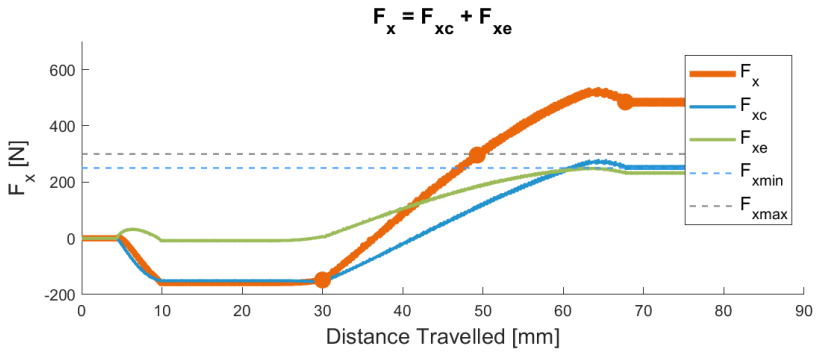

Figure 8.3: Optimization example - $F_x = F_{xc} + F_{xe}$
the orange points show the optimization points
dashed lines show the F_x force lower and upper limits

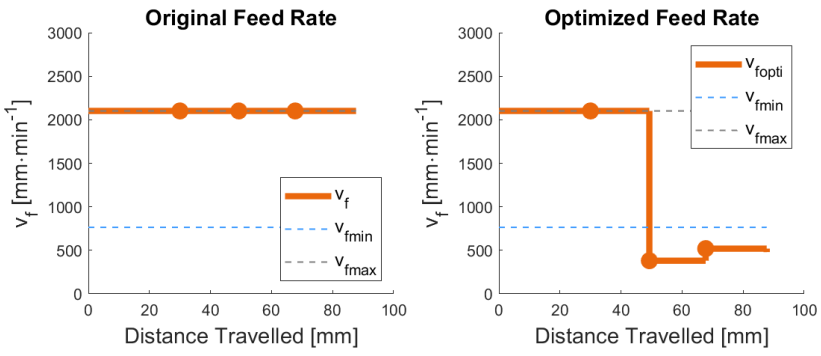

Figure 8.4: Optimization - comparison of the original and optimized v_f
the orange points show the optimization points
(the corresponding section of the toolpath is highlighted in Figure 9.8)
Dashed lines show recommended feed rate range for the cutting tool.

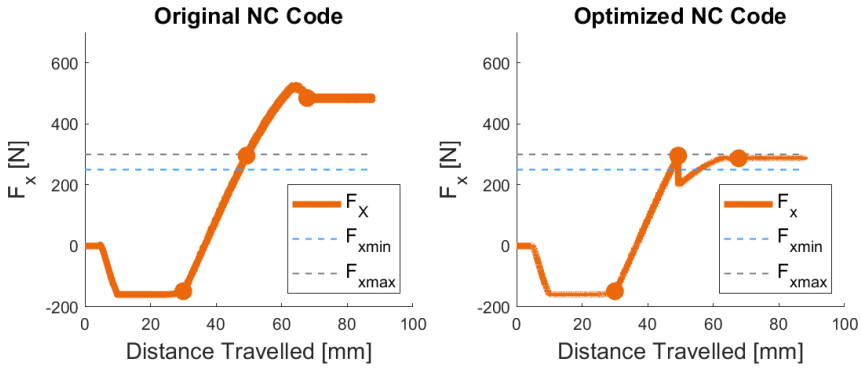

Figure 8.5: Comparison of the F_x before and after optimization the orange points show the optimization points dashed lines show the F_x force lower and upper limits

Table 8.2: Optimized NC code

Original NC Code	Optimized NC Code
M3 S4775	M3 S4775
G0 X0 Y-4 Z-4	G0 X0 Y-4 Z-4
G1 X30 F2101	G1 X30 F2101
G3 X54 Y20 I0 J24	G3 X47.272 Y3.336 I0 J24
	X54 Y20 I-17.272 J16.664 F381
G1 Y40	G1 Y40 F520

8.7 NC Code Export

Once the NC code is optimized, some final editing has to be done. Firstly, throughout the calculations, numerical and rounding errors may arise, leading to non-zero results in situations where zero is expected. These commands are identified and zeroed out. Secondly, when the same addresses have the same values in the consecutive NC blocks, there is no need to write the address with its value in the second NC block. Therefore the NC code is freed from unnecessarily repetitive commands. After these two final edits, the optimized NC code is exported into a text file with the same name as the original file name but extended with *"_opti.mpf"*.

8.8 Case Study

In this section, a case study is presented to demonstrate the functionality of the algorithm. The case study was performed for the pocket machining case

used in Section 7.2 and shown in Figure 7.14. All results of this case study were obtained by the simulation on programmed data only and were not verified by experiment. The machining parameters, force model coefficients, and other settings are listed in Table 8.3. The milling tool used for this simulation was a four-flute cylindrical 12mm end mill *ISCAR EC120A25-4C12*. The material of the workpiece was carbon steel C45.

Two optimizations were performed, one with the *keep* f_{zmin} function enabled, and the other one without this condition.

In Figure 8.6, the evolution of the feed rates are shown. Programmed feed rate v_f is constant, while the optimized feed rate with the condition of the minimum feed rate per tooth is inconstant, but it is kept between its limits v_{fmin} and v_{fmax}. Optimized feed rate without the condition of the minimum feed rate per tooth is also inconstant but is repeatedly below the lower feed rate limit. The detail shown in Figure 8.7 shows this more clearly.

Figures 8.8 and 8.10 show the evolutions of forces (F_x and F_y along the toolpath, which is shown in more detail in Figures 8.9, and 8.11. It can be clearly stated from these figures that keeping the minimum feed rate per tooth in places where the feed would otherwise be reduced to a lower value causes the maximum allowable force to be exceeded. Reducing the feed rate below the minimum feed rate results in a reduction in force below its limit. But as discussed in Chapter 10, it can cause unstable machining.

According to the simulations performed in this case study, it can be stated that the proposed algorithm can achieve a reduction of the directional forces below the specified limit, but not always with the minimum feed rate per tooth limit. Following this conclusion, an experiment was designed and carried out, which is presented in the following Chapter 9.

8.9 Summary

In this chapter, the optimization algorithm was introduced and described in detail. Based on the results from virtual machining and set limits, optimization is performed. The product of optimization is a new optimized NC code, which represents the same toolpath with edited feed rates.

The case study presented in Section 8.8 shows, that the optimization algorithm might be well designed, and the simulations show a reduction in directional forces below the required limit. An experiment was designed to validate the algorithm, which is described in the following chapter.

Table 8.3: Optimization case study - simulation and optimization settings

Parameter	Value	Units
K_{tc}	1640	$\mathrm{N \cdot mm^{-2}}$
K_{nc}	390	$\mathrm{N \cdot mm^{-2}}$
K_{bc}	550	$\mathrm{N \cdot mm^{-2}}$
K_{te}	51	$\mathrm{N \cdot mm^{-1}}$
K_{ne}	65	$\mathrm{N \cdot mm^{-1}}$
K_{be}	0	$\mathrm{N \cdot mm^{-1}}$
F_{xmin}	200	N
F_{ymin}	250	N
F_{zmin}	500	N
F_{xmax}	250	N
F_{ymax}	300	N
F_{zmax}	2000	N
n	4775	$\mathrm{min^{-1}}$
v_{fmin}	764	$\mathrm{mm \cdot min^{-1}}$
v_f	1910	$\mathrm{mm \cdot min^{-1}}$
v_{fmax}	2101	$\mathrm{mm \cdot min^{-1}}$
f_{zmin}	0.04	mm
f_z	0.10	mm
f_{zmax}	0.11	mm
f_{rapid}	6000	$\mathrm{mm \cdot min^{-1}}$
a_p	3	mm
D	12	mm
n_z	4	
λ	30°	

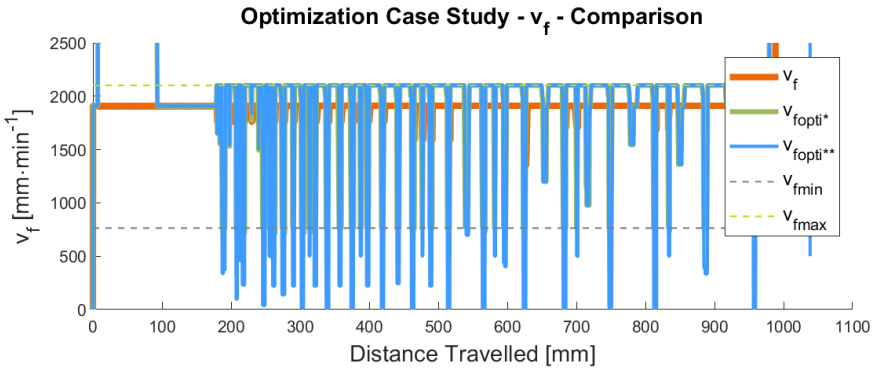

Figure 8.6: Case study - v_f comparison

(the corresponding section of the toolpath is highlighted in Figure 9.8) Dashed lines show recommended feed rate range for the cutting tool.

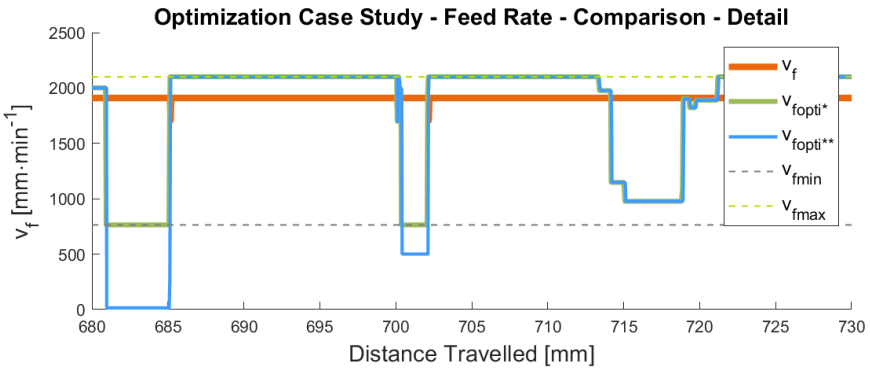

Figure 8.7: Case study - v_f comparison - detail

(the corresponding section of the toolpath is highlighted in Figure 9.8)
Dashed lines show recommended feed rate range for the cutting tool.

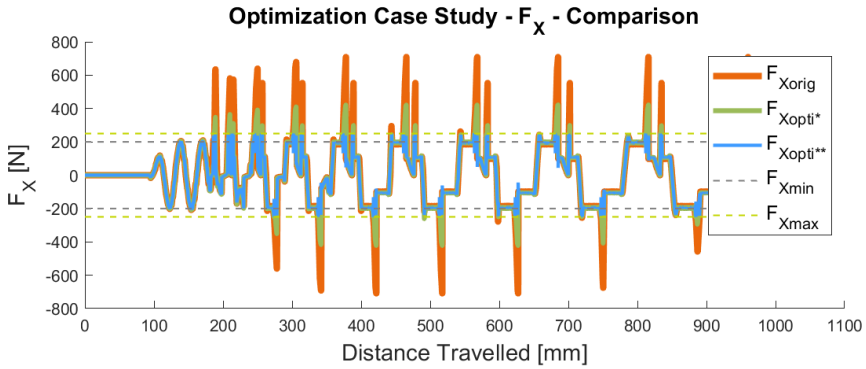

Figure 8.8: Case study - F_x comparison
dashed lines show the F_x force lower and upper limits

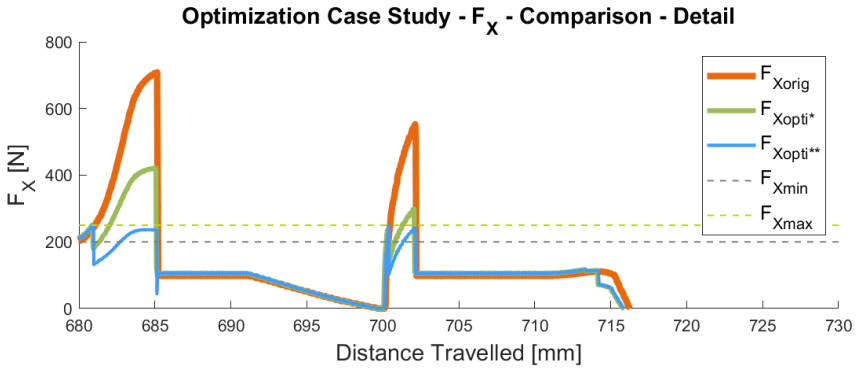

Figure 8.9: Case study - F_x comparison
dashed lines show the F_x force lower and upper limits

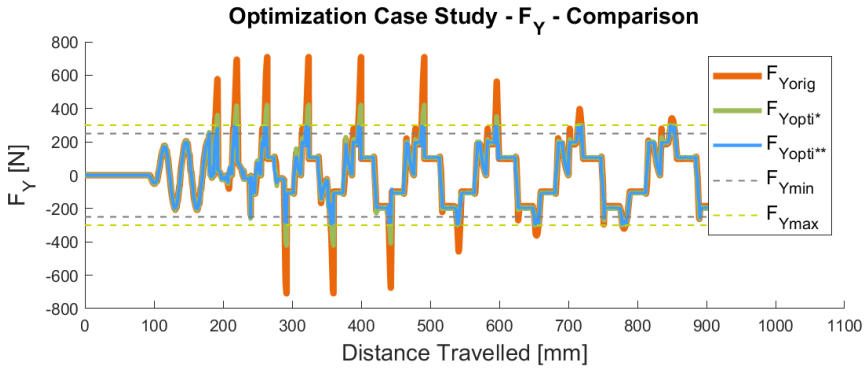

Figure 8.10: Case study - F_y comparison
dashed lines show the F_y force lower and upper limits

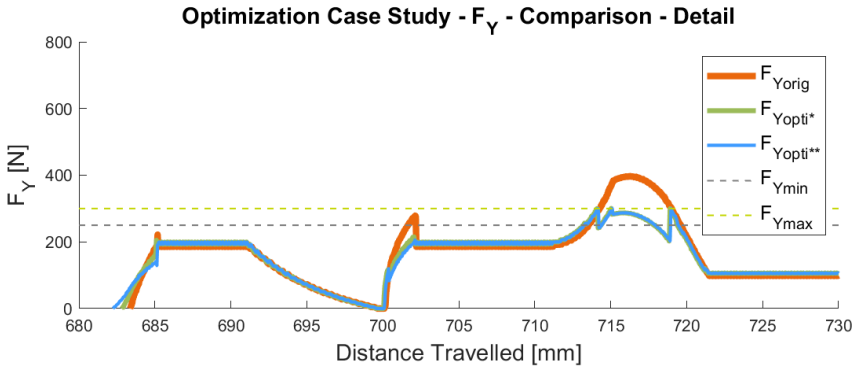

Figure 8.11: Case study - F_y comparison

Original - original NC code
Optimized - optimized NC code (keepf_{zmin} function enabled)*
*Optimized** - optimized NC code (keepf_{zmin} function disabled)*
dashed lines show the F_y force lower and upper limits

Chapter 9

Validation of the feed rate control strategy

Since the simulations demonstrated the functionality of the proposed algorithm, an experiment was designed to validate the feed rate control strategy. The conducted experiment is described in this chapter. Firstly, the design of the experiment and the experiment equipment is presented. Subsequently two settings of the algorithm for two different machining strategies, and the results are presented.

9.1 Design and Setup of the Experiment

This chapter describes the design and set-up of the experiment. First, the milling machine and milling tools are introduced. Then, the workpiece is described, followed by a description of the selected milling strategies and toolpaths, and lastly, a selection of the measured quantities and the measurement instruments.

Although the main motivation for the development of the presented algorithm is to prevent overloading of the pivot spindle heads, the experiment had to be adapted to the time and equipment availability. The machined workpiece was relatively small (180 x 180 x 10 mm) and was machined with a 12mm flat-end mill. Thus, the experiment verifies the algorithm's functionality that a reduction in directional load can be achieved by reducing the feed rate, but does not test whether it would solve the initial motivation problem of overloading pivot spindle heads.

9.1.1 Milling Machine

The horizontal machining centre (with a rotary B axis) *TAJMAC-ZPS H630* was selected for the experiment.

The movement in the X and Y-axis is realized by the movement of the spindle structure, and the movement in the Z axis and B axis is realized on the side of the workpiece. The machine characteristics are described in more detail in Table 9.1. A picture of the machine is shown in Figure 9.1. The structure of the machine is depicted in Figure 9.2.

Figure 9.1: TAJMAC-ZPS H630 horizontal machining centre [79]

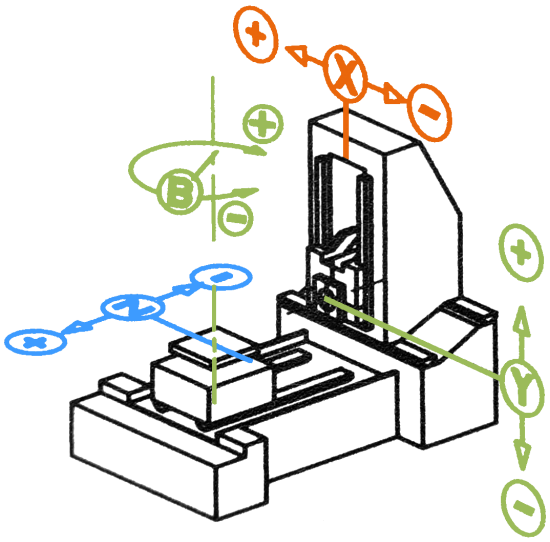

Figure 9.2: TAJMAC-ZPS H630 horizontal machining centre structure (after the diagram on the machine)

Table 9.1: TAJMAC-ZPS H630 characteristics [79]

Parameter	Value	Units
Working travel (X)	750	mm
Working travel (Y)	700	mm
Working travel (Z)	770	mm
B-axis	360°	
Positioning accuracy (X, Y, Z)	0.008	mm
Positioning accuracy (B)	0.006	rad sec
Repeatability (X, Y, Z)	0.005	mm
Repeatability (B)	3	rad sec
Pallet size	630 x 630	mm
Maximum pallet load	800	kg
Working feed (X, Y, Z)	50	$m \cdot min^{-1}$
Acceleration (X, Y, Z)	5	$m \cdot s^{-2}$
Spindle torque (S1 / S6-40%)	159 / 197	$N \cdot m$
Spindle power (S1 / S6-40%)	25 / 31	kW
Maximum electrospindle speed	18 000	min^{-1}
Tool interface	HSK-A63	
Control system	*Siemens SINUMERIK 840d*	

9.1.2 Milling Tool

Two milling cutters were used during the experiment. Both tools were 12mm flat-end mills made by *ISCAR*. The first tool was the *EC120A25-4C12 IC900* end mill. It was damaged during the experiment (contour milling), so the *EC120B25-4C12 IC900* end mill was used for the second milling strategy (adaptive milling). The tool characteristics are described in more detail in Table 9.2. Pictures of the milling tools are shown in Figures 9.3a and 9.3b.

(a) ISCAR EC120A25-4C12 IC900 flat-end mill [80]

(b) ISCAR EC120B25-4C12 IC900 flat-end mill [80]

Figure 9.3: Milling tools used in experiment

Figure 9.4: ISCAR EC120B25-4C12 IC900 flat-end mill in SCHUNK TENDO Slim 4ax HSK-A63 Ø12x120 hydraulic tool holder

Table 9.2: Milling tools - characteristics [26]

Parameter	*ISCAR EC120A25-4C12 IC900*	*ISCAR EC120B25-4C12 IC900*	Units
Material	solid carbide	solid carbide	
D	12	12	mm
z	4	4	
γ_r	12°	14.4°	
γ_a	9.8°	15°	
λ	30°	45°	
R	30	30	μm

The tool was held in the HSK-A63 hydraulic tool holder *SCHUNK TENDO Slim 4ax HSK-A63 Ø12x120*. Picture of the milling cutter *EC120B25-4C12 IC900* in the *SCHUNK* tool holder is shown in Figure 9.4.

9.1.3 Workpiece

Since a directional load optimization algorithm is proposed, it was requested that the forces act in several different directions under different loading conditions. Therefore, the geometry of the workpiece was designed to contain segments in the X-direction, in the Y-direction, inclined differently to these two directions, and the arcs were designed to have different radii.

The size of the workpiece was 180 x 180 x 10 mm. It was subsequently divided into four squares (80 x 80 x 5 mm). The milling operation then run on these squares (one measurement for each square) up to a depth of 4 mm. The shape and the dimensions of the machined contour are shown in Figure 9.5.

The dimensions and shape of the workpiece are depicted in Appendix B. Picture of the workpiece clamped on the dynamometer is shown in Figure 9.6.

Workpiece material is carbon steel C45 with hardness 13 ± 1 HRC.

The workpiece model was created in *SolidWorks 2017* CAD software.

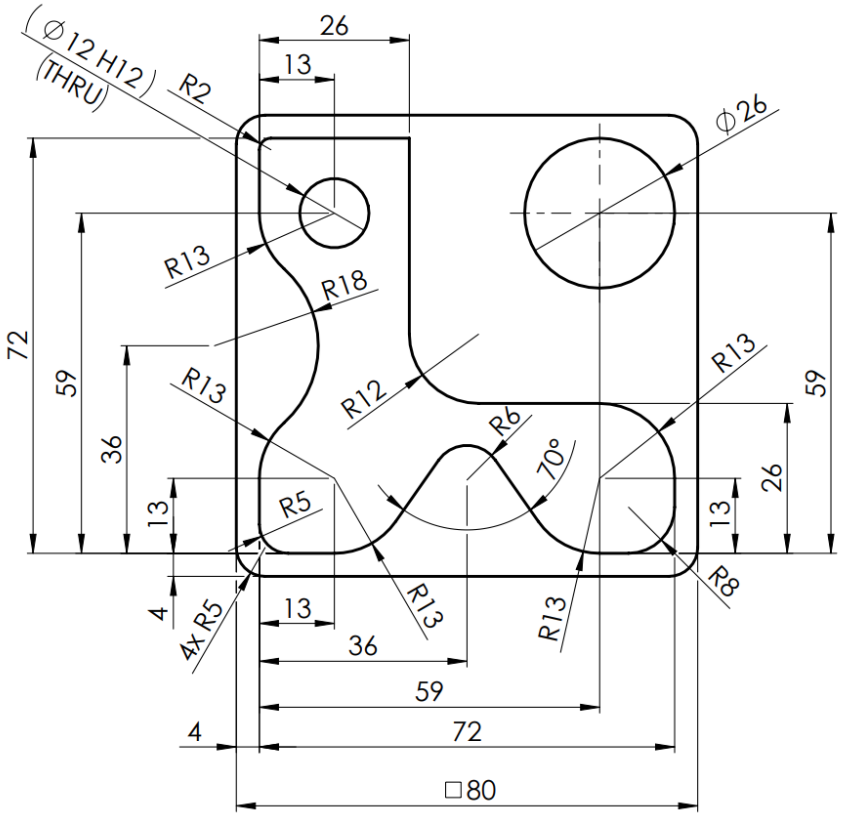

Figure 9.5: Experiment - machined contour dimensions

9.1.4 Milling Strategies

Two milling strategies were chosen for the experiment. The first strategy was contour milling, where material is removed sequentially by tool passes along paths equidistant from the contour of the workpiece. The second strategy was adaptive machining, where the paths were generated in an attempt to keep the radial depth of the cut constant.

Contour milling was chosen for its simplicity and clarity. During contour milling, in the selected case, the direction of movement is constant when

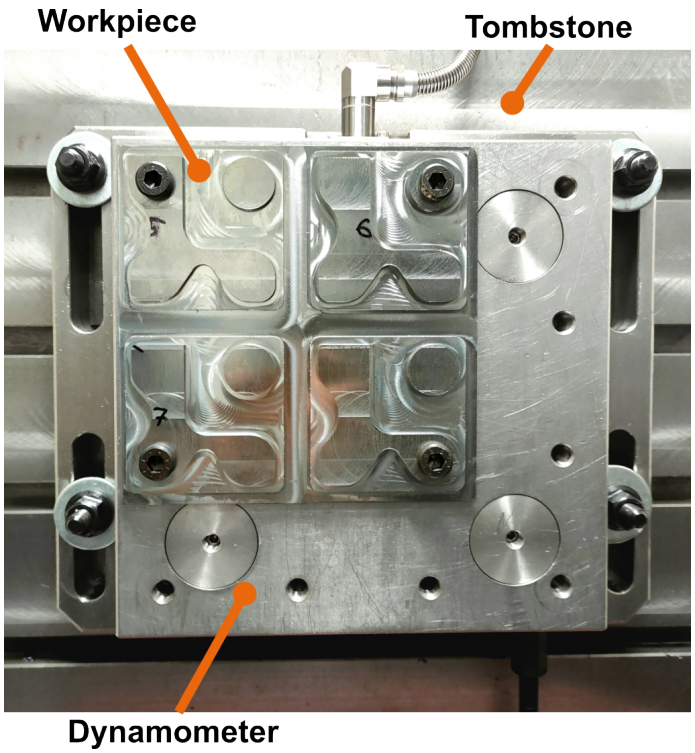

Figure 9.6: Experiment - workpiece on the dynamometer

milling a given linear part of the workpiece, as well as the angle of engagement and therefore the directional force load. Only during the transitions from linear to circular interpolation and during circular interpolation does the directional load change.

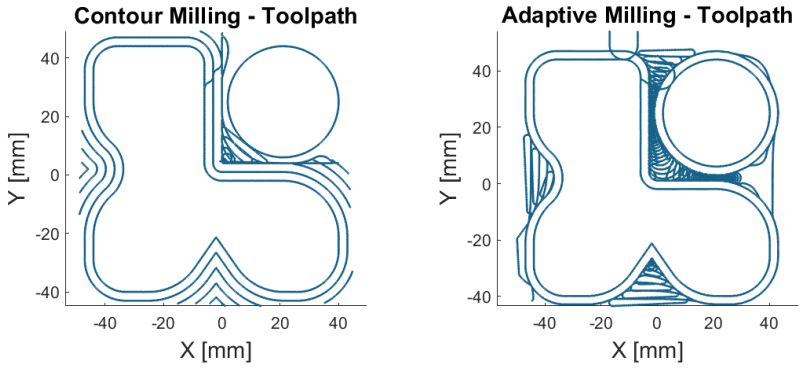

Figure 9.7: Experiment - contour milling and adaptive milling - toolpaths

In contrast, the chosen adaptive strategy is a dynamic strategy that attempts to keep the radial depth of cut constant, resulting in a practically constant change in the direction of motion and thus in the directional load.

The toolpaths were generated in the *HSMExpress 2018* CAM module for *SolidWorks 2017*.

9.1.5 Measured Quantities and Measurement Equipment

Since the criterion function for optimization is not to exceed the force limit, the forces F_x, F_y, and F_z were measured with a stationary piezoelectric dynamometer *KISTLER 9255B* (see Figure 5.7a). The electric signal from the dynamometer has to be amplified, therefore *KISLTER Type 5017 multichannel charge amplifier* was used. *KISTLER DAQ for DynoWare Type 5697* provided data acquisition. *DynoWare* is software by *KISTLER* for measured data acquisition and processing. All the measurement equipment is listed in Table 9.3.

Table 9.3: Measurement equipment

Instrument	Manufacturer	Type	Serial Number
Stationary piezoelectric dynamometer	*KISTLER*	9255B	1211090
Multichannel Charge Amplifier	*KISTLER*	5017B1500	1233960
DAQ for DynoWare	*KISTLER*	5697A	4698276

In addition, the set-point positions in the machine coordinate system (GCS) and the set-point speed of each axis were obtained using SinuTrace software.

9.2 Contour Milling

As mentioned above, the first milling strategy was contour milling, where toolpaths equidistant to the reference surface (contour) were generated. However, this wasn't the only strategy used in the NC program. Initially, the cylindrical part was machined as the tool followed a helical toolpath. Subsequently, the adaptive strategy was used to rough out the middle section of the machined part, to ensure a consistent allowance along the main contour. Finally, the contour milling strategy was applied to machine the contour itself.

In this section, the contour milling strategy, its simulation, optimization, and results are presented. The toolpath is shown in Figure 9.8 and its detail shows the part of the toolpath, for which detailed views of the time evolution of the feed rate and the cutting forces are presented below.

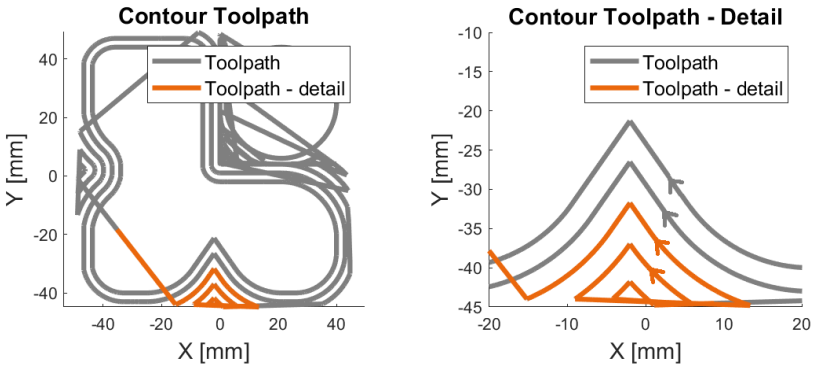

Figure 9.8: Experiment - contour milling toolpath

Table 9.4: Contour milling simulation and optimization settings

Parameter	Value	Units
Tool	*ISCAR EC120A25-4C12 IC900*	
K_{tc}	1640	$\mathrm{N \cdot mm^{-2}}$
K_{nc}	390	$\mathrm{N \cdot mm^{-2}}$
K_{bc}	550	$\mathrm{N \cdot mm^{-2}}$
K_{te}	51	$\mathrm{N \cdot mm^{-1}}$
K_{ne}	65	$\mathrm{N \cdot mm^{-1}}$
K_{be}	0	$\mathrm{N \cdot mm^{-1}}$
F_{xmin}	250	N
F_{ymin}	300	N
F_{xmax}	300	N
F_{ymax}	350	N
n	4775	$\mathrm{min^{-1}}$
v_{fmin}	764	$\mathrm{mm \cdot min^{-1}}$
v_f	1528	$\mathrm{mm \cdot min^{-1}}$
v_{fmax}	2101	$\mathrm{mm \cdot min^{-1}}$
f_{zmin}	0.04	mm
f_z	0.08	mm
f_{zmax}	0.11	mm
f_{rapid}	6000	$\mathrm{mm \cdot min^{-1}}$
a_e^*	3	mm
a_p	4	mm

* *in this case, a_e is the nominal axial depth of cut, which is the distance of the equidistant paths from each other*

9.2.1 Simulation and Optimization

The simulation was performed in *MillVis* software using a linear mechanistic model with cutting and edge coefficients listed in Table 9.4. The input data for the tool motion was the NC code generated in *HSMExpress 2018*. The density of points at which cutting forces were calculated was 10 points per tool revolution. The result simulated feed rate and directional forces F_x and F_y are shown in Figures 9.9 and 9.10. The calculated forces F_x and F_y are shown in more detail in Figure 9.11. The figures show that there are zero loads in some sections. These sections are tool traverses when the tool is out of the cut.

Two optimizations were performed for the contour milling strategy according to the simulation results. One optimization with the condition of keeping the minimum feed per tooth f_{zmin} recommended by the tool manufacturer, the other without this condition. The given directional limits are listed in Table 9.4.

9.2.2 Results

After all three contour milling NC codes were executed, the measurement results were processed. First of all, programmed and set-point feed rates were compared. This comparison shows, that the milling machine is able to reach the programmed feed rate almost every time. Only in areas where there is an abrupt change in direction of movement, set-point feed rate dropped down to almost zero. Evolution of the simulated and set-point feed rates is shown in Figures 9.12 and 9.13.

The simulated and measured forces were then compared. As shown in Figures 9.14 and 9.15, the force model used for the simulation did not sufficiently match the measurements. As it was later discovered, the cutting and edge coefficients used were set for a larger chip thickness than was set for milling. Since measured forces were lower than simulated, optimized feed rates were lower than they could be. For the adaptive milling, more appropriate force model was used (described in Section 9.3.1).

The measured set-point feed rates of the original and both optimized NC programs are shown in Figure 9.18. Comparison of the feed rates is shown in Figure 9.19 and in more detail in Figure 9.20.

The measured forces F_x and F_y are shown in Figures 9.21 and 9.24. Their comparison is then shown in Figures 9.22 and 9.25, and the selected part is shown in more detail in Figures 9.23 and 9.26.

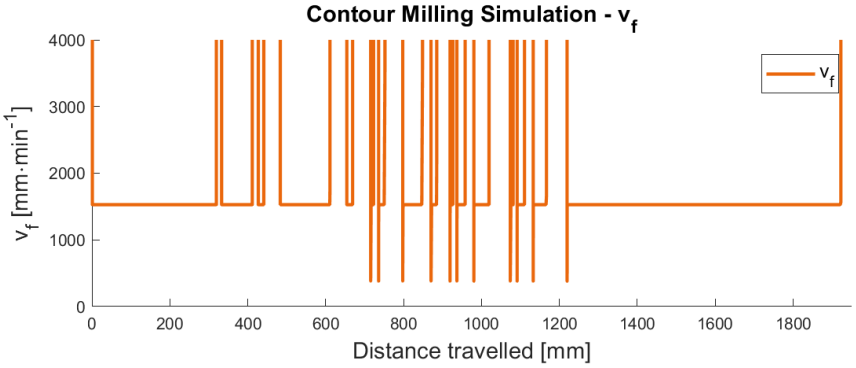

Figure 9.9: Contour milling simulation based on programmed data feed rate v_f

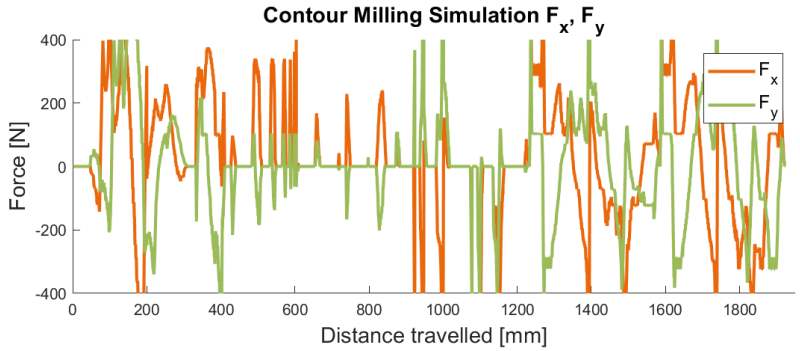

Figure 9.10: Contour milling simulation based on programmed data directional forces F_x, F_y

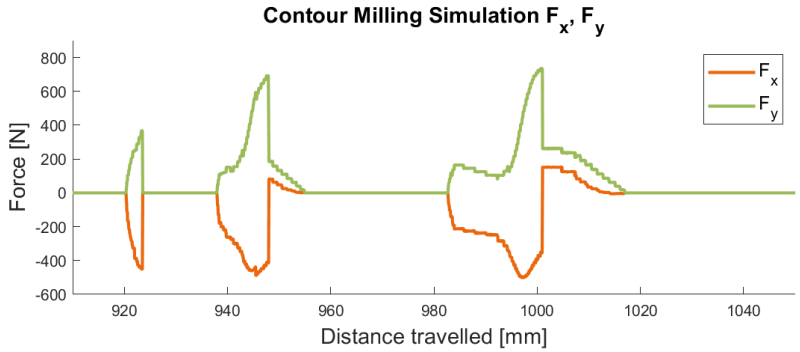

Figure 9.11: Contour milling simulation based on programmed data directional forces F_x, F_y - detail

(the corresponding part of the toolpath is highlighted in Figure 9.8)

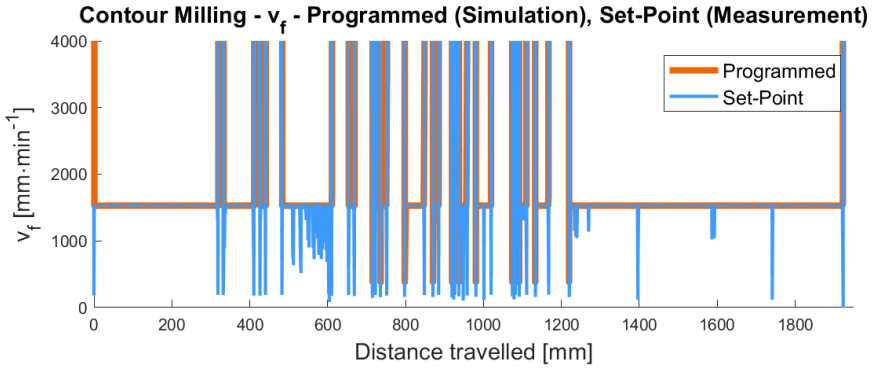

Figure 9.12: Contour milling - comparison of the programmed (simulation) and set-point (measurement) feed rate v_f

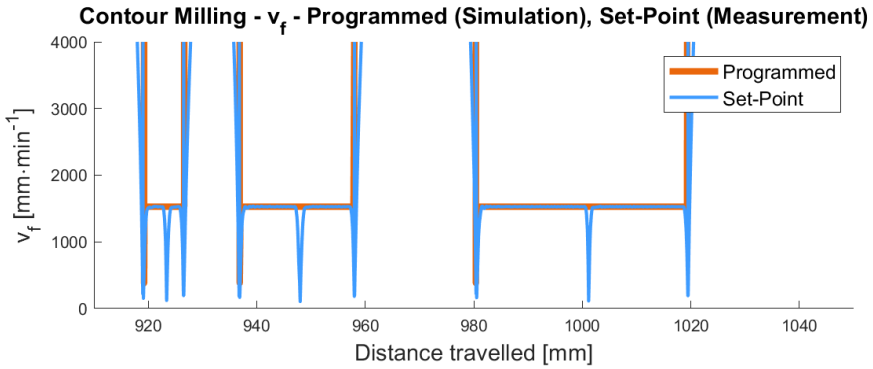

Figure 9.13: Contour milling - comparison of the programmed (simulation) and set-point (measurement) feed rate v_f - detail

(the corresponding part of the toolpath is highlighted in Figure 9.8)

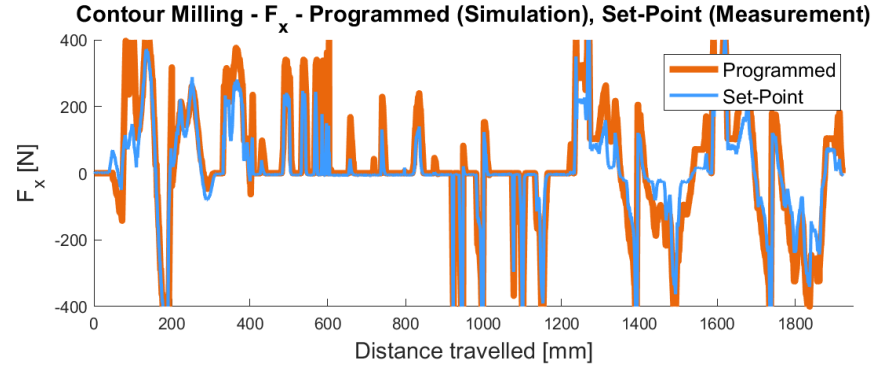

Figure 9.14: Contour milling - comparison of the programmed (simulation) and set-point (measurement) feed rate - force F_x

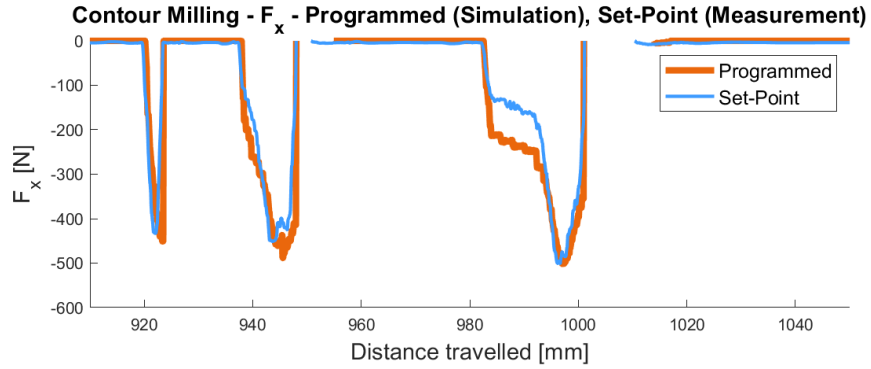

Figure 9.15: Contour milling - comparison of the programmed (simulation) and set-point (measurement) feed rate - force F_x - detail

(the corresponding part of the toolpath is highlighted in Figure 9.8)

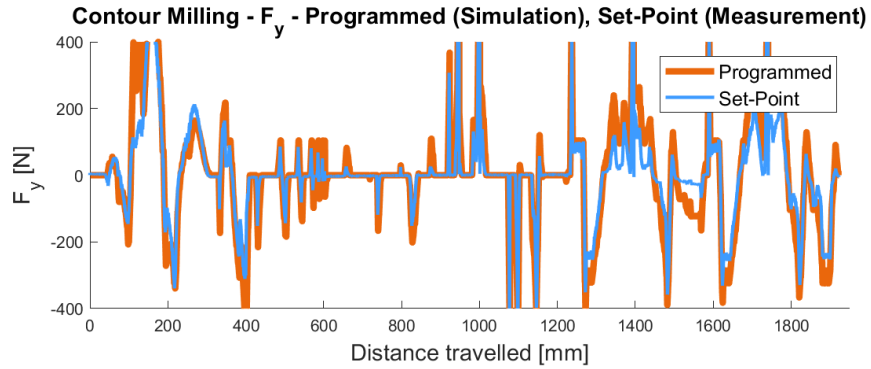

Figure 9.16: Contour milling - comparison of the programmed (simulation) and set-point (measurement) feed rate - force F_y

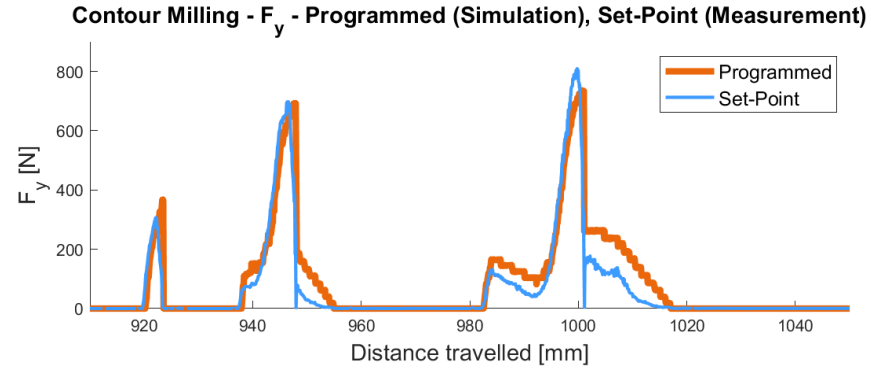

Figure 9.17: Contour milling - comparison of the programmed (simulation) and set-point (measurement) feed rate - force F_y - detail

(the corresponding part of the toolpath is highlighted in Figure 9.8)

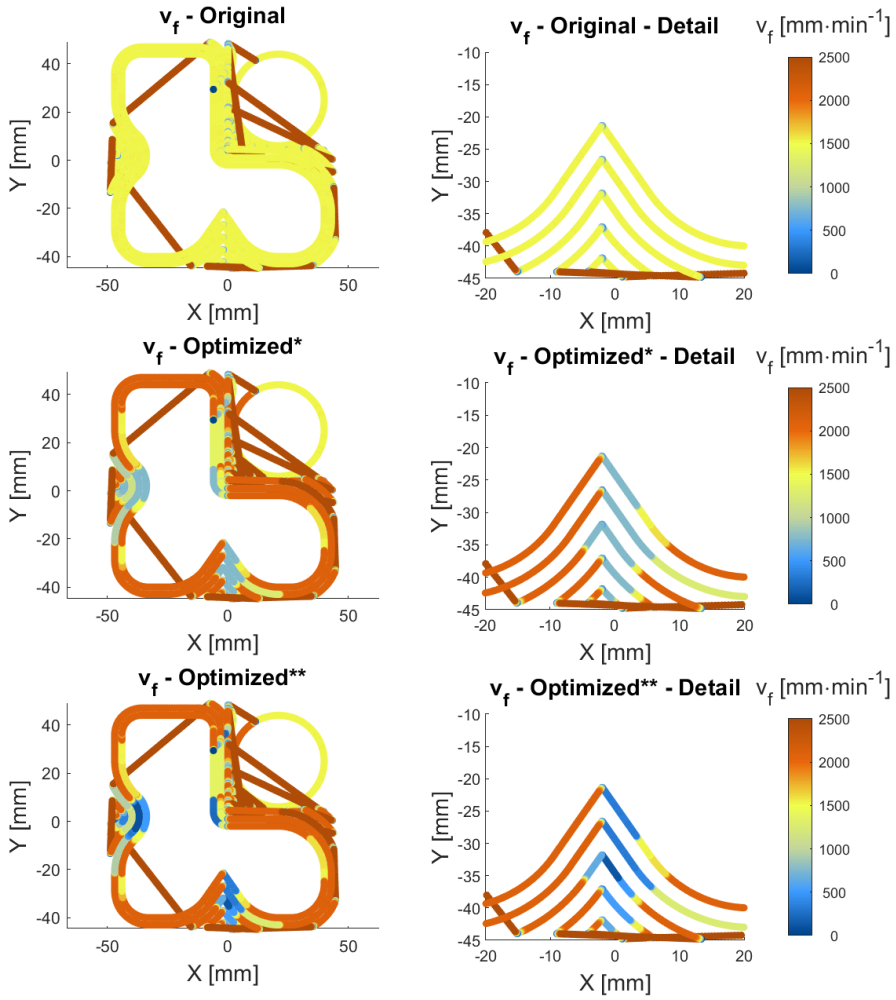

Figure 9.18: Contour milling - v_f

Original - original NC code
Optimized - optimized NC code (keep f_{zmin} function enabled)*
*Optimized** - optimized NC code (keep f_{zmin} function disabled)*

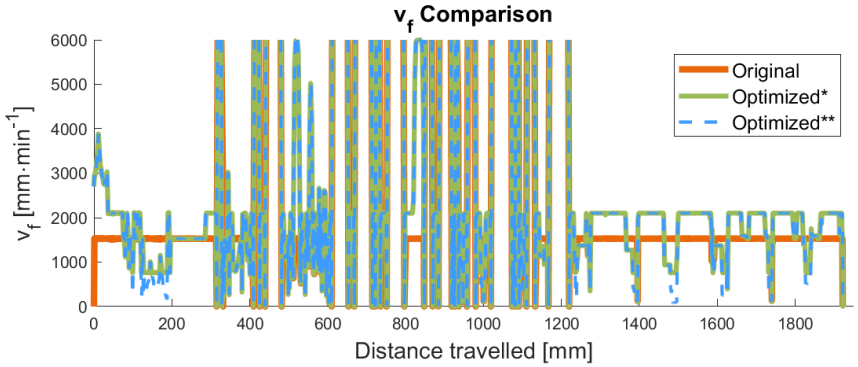

Figure 9.19: Contour milling - v_f comparison

Original - original NC code
Optimized - optimized NC code (keep f_{zmin} function enabled)*
*Optimized** - optimized NC code (keep f_{zmin} function disabled)*

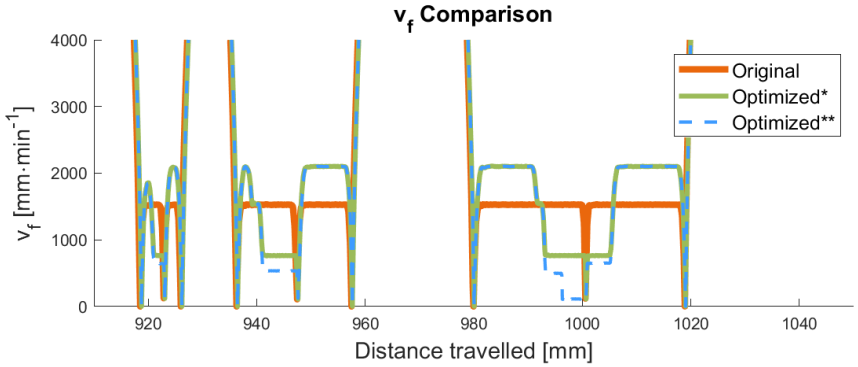

Figure 9.20: Contour milling - v_f comparison - detail

(the corresponding section of the toolpath is highlighted in Figure 9.8)
Original - original NC code
Optimized - optimized NC code (keep f_{zmin} function enabled)*
*Optimized** - optimized NC code (keep f_{zmin} function disabled)*

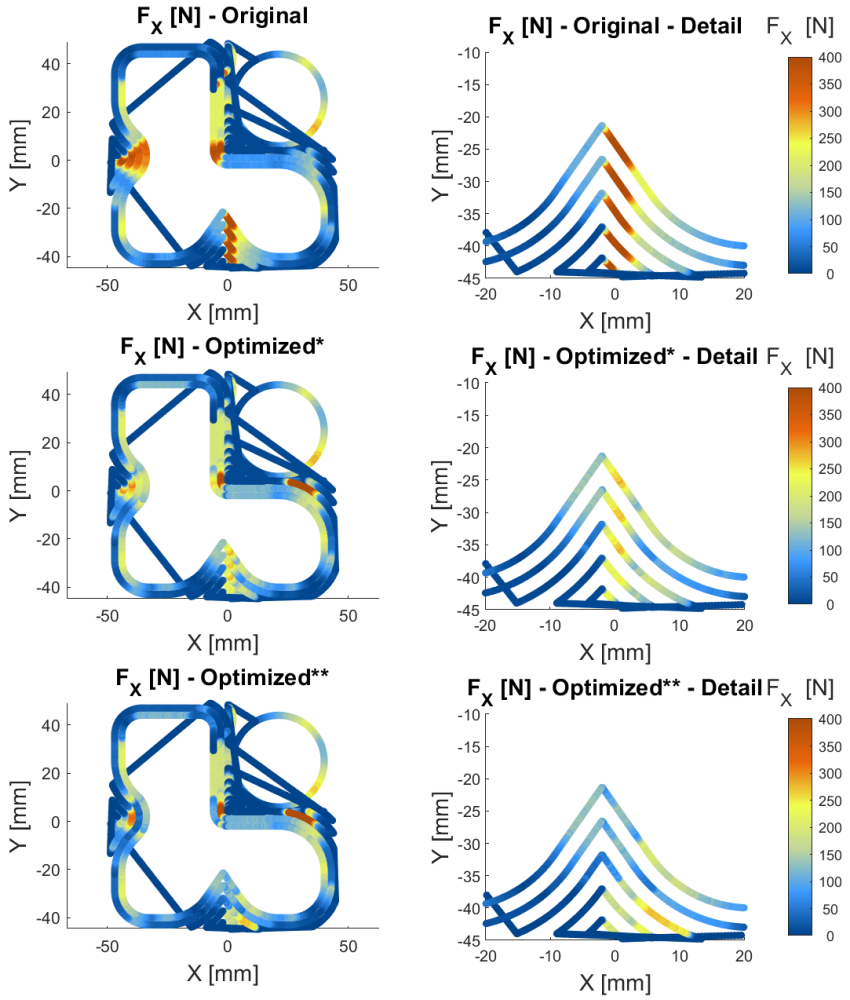

Figure 9.21: Contour milling - F_x

Original - original NC code
Optimized - optimized NC code (keep f_{zmin} function enabled)*
*Optimized** - optimized NC code (keep f_{zmin} function disabled)*

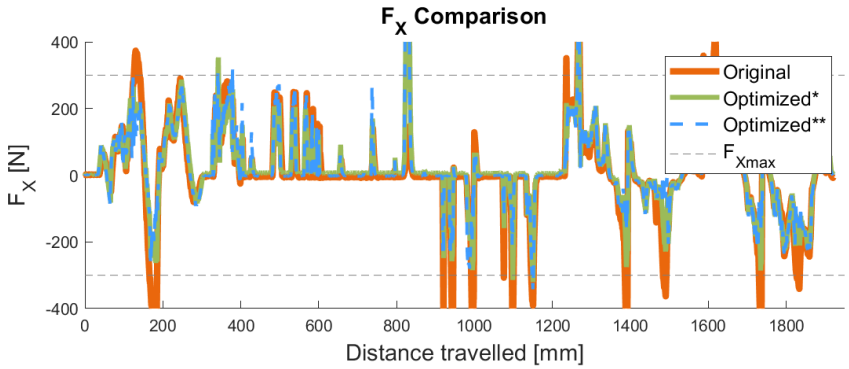

Figure 9.22: Contour milling - F_x comparison

Original - original NC code
Optimized - optimized NC code (keep f_{zmin} function enabled)*
*Optimized** - optimized NC code (keep f_{zmin} function disabled)*
dashed lines show the F_x force upper limits

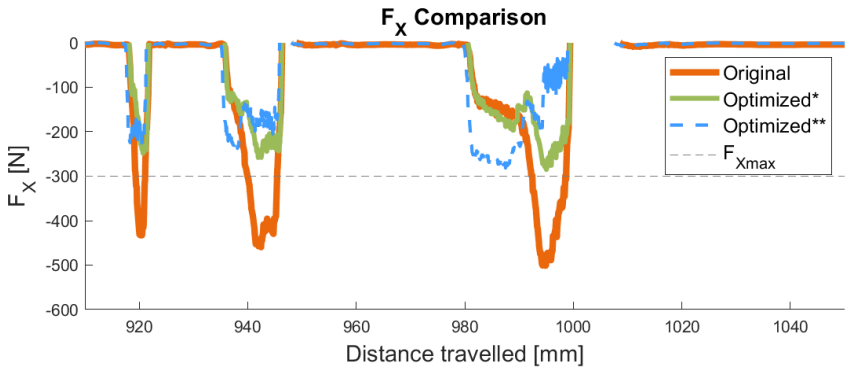

Figure 9.23: Contour milling - F_x comparison - detail

(the corresponding section of the toolpath is highlighted in Figure 9.8)
Original - original NC code
Optimized - optimized NC code (keep f_{zmin} function enabled)*
*Optimized** - optimized NC code (keep f_{zmin} function disabled)*
dashed lines show the F_x force upper limits

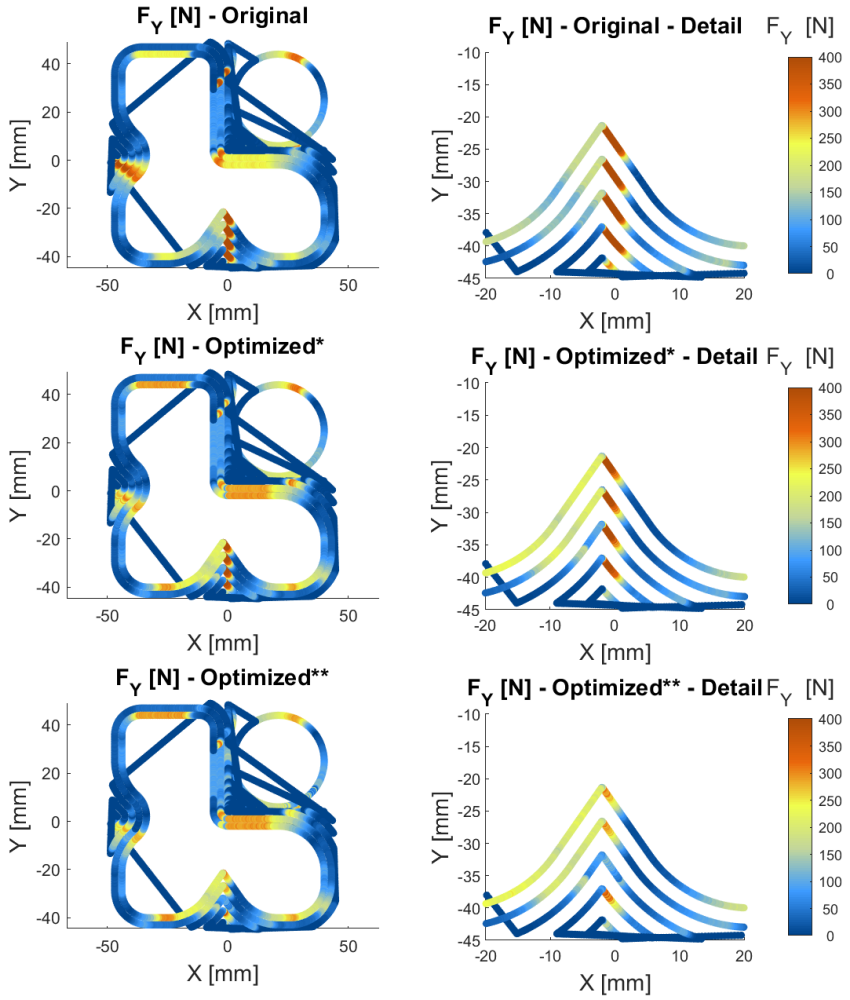

Figure 9.24: Contour milling - F_y

Original - original NC code
Optimized - optimized NC code (keep f_{zmin} function enabled)*
*Optimized** - optimized NC code (keep f_{zmin} function disabled)*

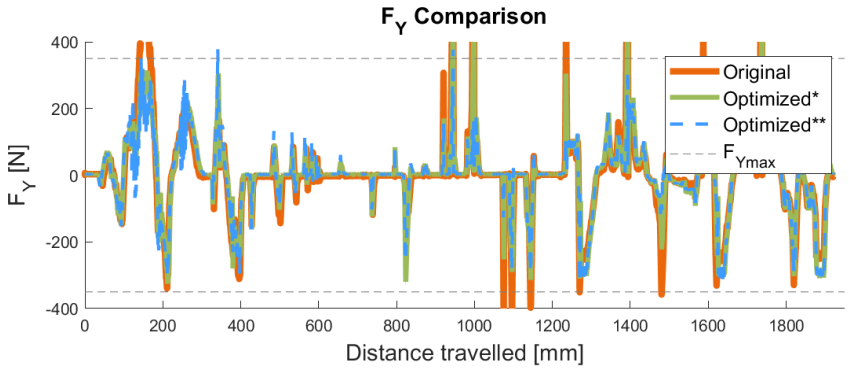

Figure 9.25: Contour milling - F_y comparison

Original - original NC code
Optimized - optimized NC code (keep f_{zmin} function enabled)*
*Optimized** - optimized NC code (keep f_{zmin} function disabled)*
dashed lines show the F_y force upper limits

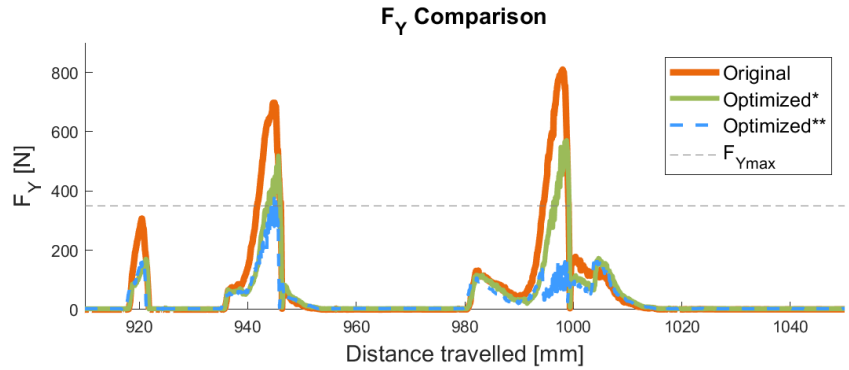

Figure 9.26: Contour milling - F_y comparison - detail

(the corresponding section of the toolpath is highlighted in Figure 9.8)
Original - original NC code
Optimized - optimized NC code (keep f_{zmin} function enabled)*
*Optimized** - optimized NC code (keep f_{zmin} function disabled)*
dashed lines show the F_y force upper limits

When contour milling optimized NC code (optimized without the condition of keeping the minimum feed per tooth recommended by the tool manufacturer) was run, the minimum feed rate of 88 mm · min^{-1} resulted in unstable machining leading to the tool damage (see Figure 9.27).

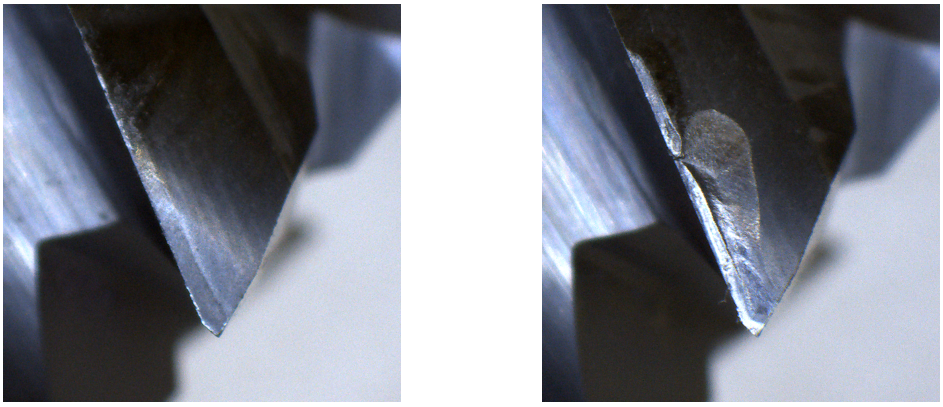

(a) Undamaged tool *(b) Damaged tool*

Figure 9.27: Tool damage caused by the unstable machining

The change in feed rates naturally results in a change in the overall machining time. Machining according to the original program took 90 seconds, according to the optimized program with keeping the minimum feed per tooth recommended by the tool manufacturer 78 seconds, and according to the program that did not have to meet this condition, the machining took 97 seconds.

9.2.3 Conclusions for Contour Milling

The first part of the experiment was contour milling. This strategy does not require any high machine dynamics, and it was shown that in almost all places the machine reached the programmed feed rate.

Furthermore, the experiment confirmed that it is possible to reduce the directional load below the desired limit in most points by adjusting the feed rate. However, there are problematic sections, where there is a significant increase in engagement angle. In these areas, either the force limit was exceeded, but the set minimum feed per tooth was met, or a reduction in directional load below the required limit was achieved but at the cost of very low feed rates (88 mm · min^{-1}). Such drastic reductions in feed rates result in increased machining time and, in the presented case, a shift into the area of unstable machining and the tool damage.

However, the whole experiment was burdened by an inappropriately chosen force model that predicted higher forces than were measured.

9.3 Adaptive Milling

The second strategy chosen for the validation of the proposed control strategy was adaptive milling. This strategy attempts to maintain a constant radial depth of cut a_e. This strategy requires significantly higher machine dynamics as the direction of tool movement is almost constantly changing. This NC program consisted of two parts, the first was adaptive milling, which removed most of the material, and the final pass was a contour milling operation.

In this section, the adaptive milling strategy, its simulation, optimization, and results are presented. The toolpath is shown in Figure 9.28, and its detail shows the part of the toolpath for which detailed views of the evolution of the feed rate and the cutting forces are presented below.

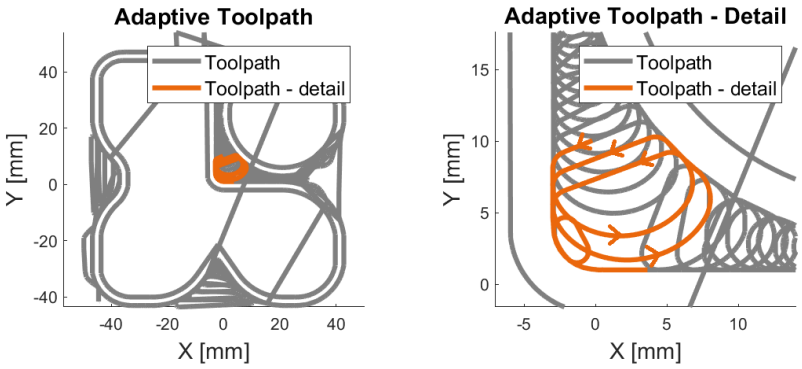

Figure 9.28: Experiment - adaptive milling toolpath

9.3.1 Simulation and Optimization

The simulation was again performed in *MillVis* software and the density of calculation points was set to 10 points per tool revolution. A linear mechanistic force model was used, however the cutting and edge coefficients (see Table 9.5) were derived from the multiparametric pressure-friction model (after [26]). The calculation of the coefficients is provided in Appendix C. This force model has a significantly better match with the measured data. The simulation results of the directional load F_x and F_y are shown in Figures 9.30 and 9.31. Simulated feed rate is shown in Figure 9.29.

Same as for the first milling strategy, two optimizations were performed according to the simulation results. One optimization with the condition of keeping the minimum feed per tooth f_{zmin} recommended by the tool manufacturer, the other without this condition. Results of this experiment are presented in the following section.

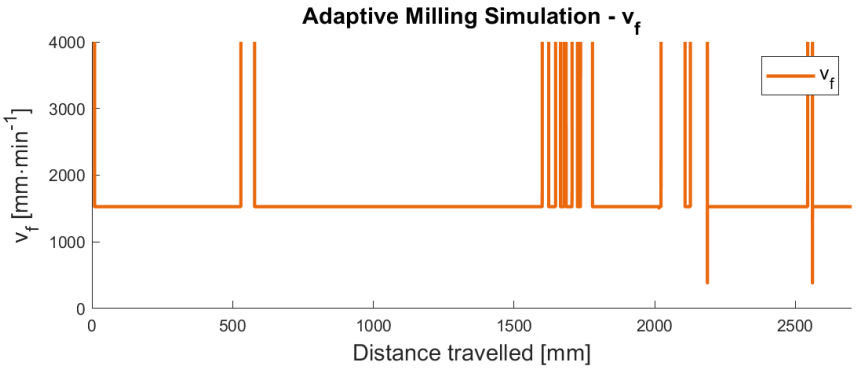

Figure 9.29: Adaptive milling simulation based on programmed data feed rate v_f

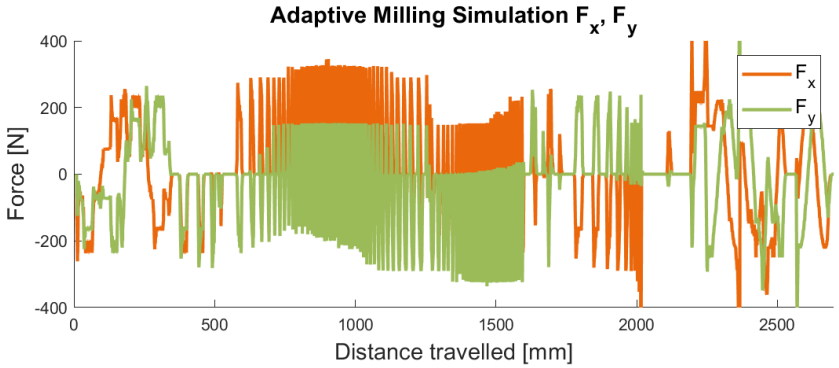

Figure 9.30: Adaptive milling simulation based on programmed data directional forces F_x, F_y

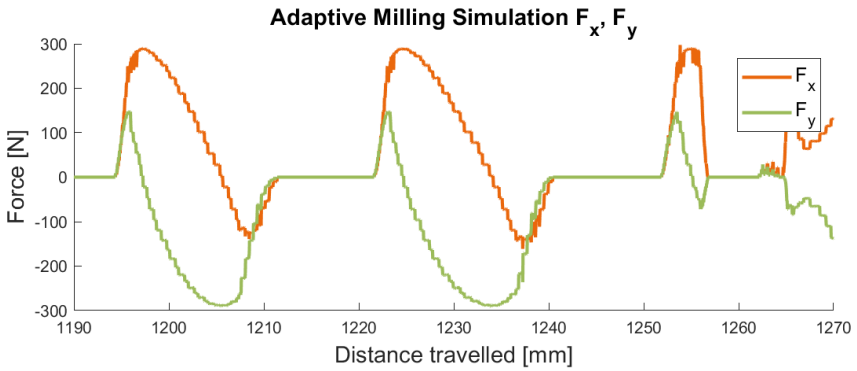

Figure 9.31: Adaptive milling simulation based on programmed data directional forces F_x, F_y - detail

(the corresponding section of the toolpath is highlighted in Figure 9.28)

Table 9.5: Adaptive milling simulation and optimization settings

Parameter	Value	Units
Tool	*ISCAR EC120A25-4C12 IC900*	
K_{tc}	1863	$\mathrm{N \cdot mm^{-2}}$
K_{nc}	445	$\mathrm{N \cdot mm^{-2}}$
K_{bc}	820	$\mathrm{N \cdot mm^{-2}}$
K_{te}	29	$\mathrm{N \cdot mm^{-1}}$
K_{ne}	22	$\mathrm{N \cdot mm^{-1}}$
K_{be}	2	$\mathrm{N \cdot mm^{-1}}$
F_{xmin}	120	N
F_{ymin}	170	N
F_{xmax}	170	N
F_{ymax}	220	N
n	4775	$\mathrm{min^{-1}}$
v_{fmin}	764	$\mathrm{mm \cdot min^{-1}}$
v_f	1528	$\mathrm{mm \cdot min^{-1}}$
v_{fmax}	2101	$\mathrm{mm \cdot min^{-1}}$
f_{zmin}	0.04	mm
f_z	0.08	mm
f_{zmax}	0.11	mm
f_{rapid}	6000	$\mathrm{mm \cdot min^{-1}}$
a_e^*	3	mm
a_p	4	mm

* in this case, a_e is the axial depth of cut, that the adaptive strategy attempts to keep constant and also the axial depth of cut of the last contour milling pass

9.3.2 Results

Processing the results of the adaptive milling strategy showed that the machine was not able to achieve programmed feed rates where the change in the direction of movement was too fast. That can be seen in Figure 9.32 and also had the effect of the cutting forces reduction in such areas. However, as discussed in Section 7.2, this does not affect the functionality of the optimization algorithm.

The comparison of the simulated (based on programmed feed rate) and measured forces is shown in Figures 9.34 and 9.35. As mentioned above, the difference between the simulated and measured forces is caused by the difference between programmed and set-point feed rates.

The measured set-point feed rates are shown in Figure 9.40. This graph shows in detail how the optimised feed rate varies with the engagement angle and the direction of tool movement relative to the X and Y-directions. Comparison of the feed rates is shown in Figure 9.38 and in more detail in Figure 9.39.

The measured forces F_x and F_y are shown in Figures 9.41 and 9.44. Their comparison is then shown in Figures 9.42 and 9.45, and the selected part is shown in more detail in Figures 9.43 and 9.46.

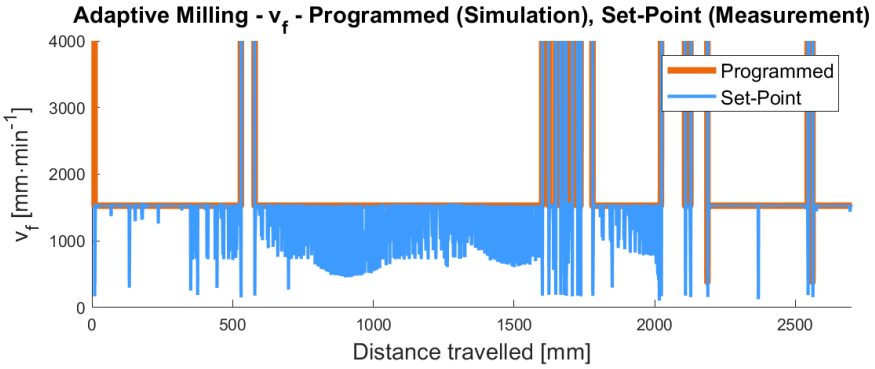

Figure 9.32: Adaptive milling - comparison of the programmed (simulation) and set-point (measurement) feed rate v_f

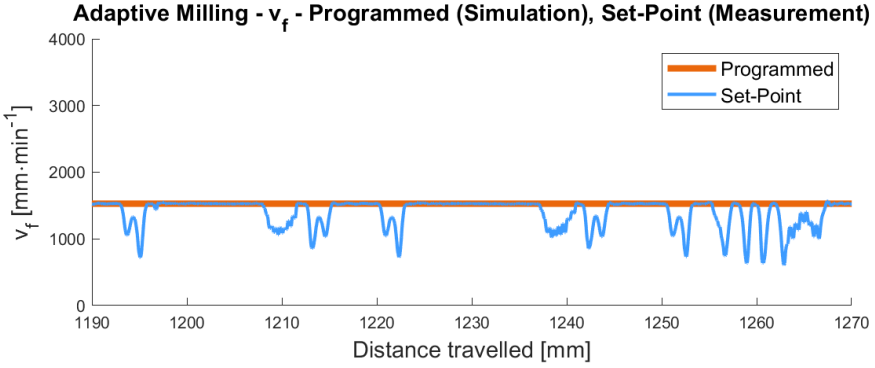

Figure 9.33: Adaptive milling - comparison of the programmed (simulation) and set-point (measurement) feed rate v_f - detail

(the corresponding section of the toolpath is highlighted in Figure 9.28)

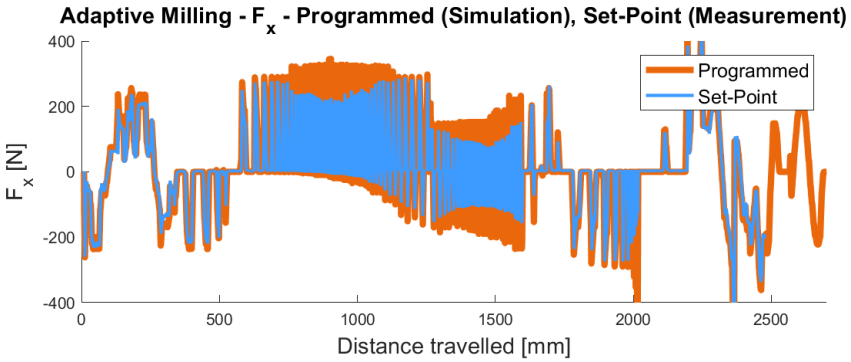

Figure 9.34: Adaptive milling - comparison of the programmed (simulation) and set-point (measurement) feed rate - force F_x

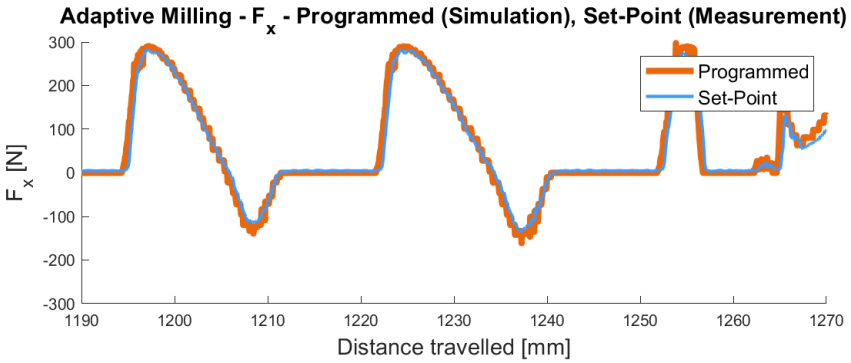

Figure 9.35: Adaptive milling - comparison of the programmed (simulation) and set-point (measurement) feed rate - force F_x - detail

(the corresponding section of the toolpath is highlighted in Figure 9.28)

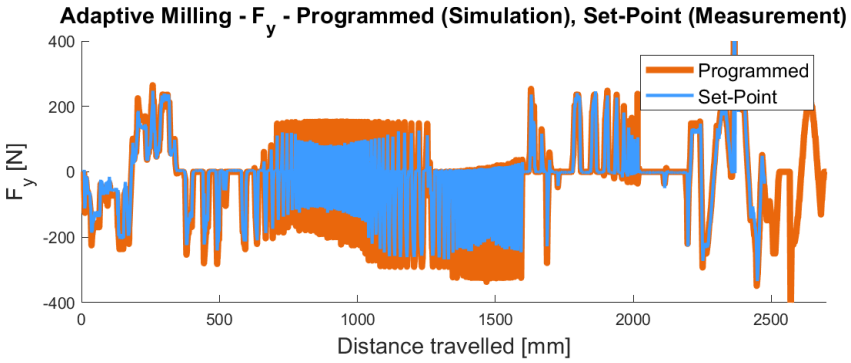

Figure 9.36: Adaptive milling - comparison of the programmed (simulation) and set-point (measurement) feed rate - force F_y

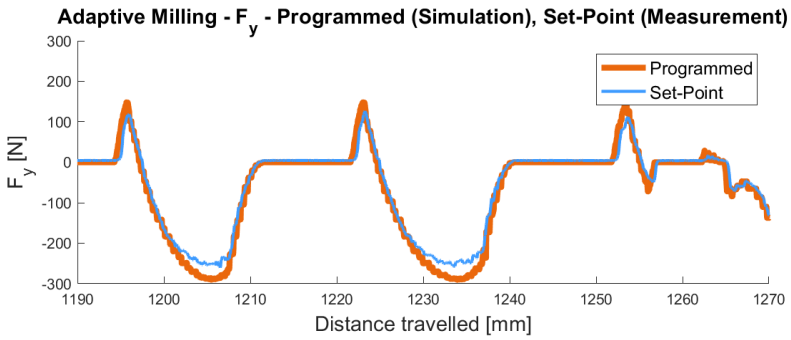

Figure 9.37: Adaptive milling - comparison of the programmed (simulation) and set-point (measurement) feed rate - force F_y - detail

(the corresponding section of the toolpath is highlighted in Figure 9.28)

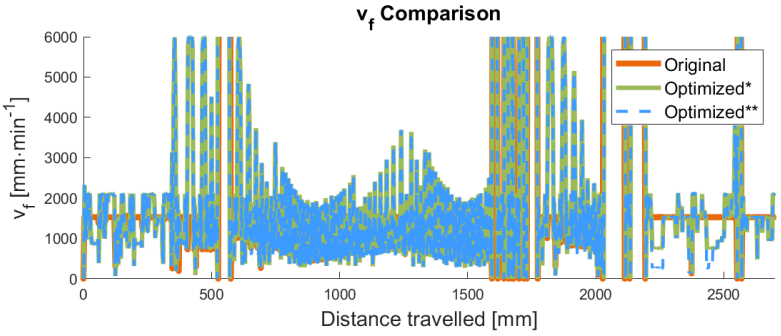

Figure 9.38: Adaptive milling - v_f comparison

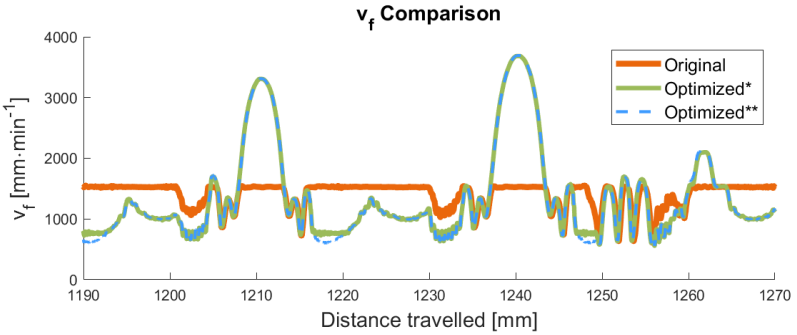

Figure 9.39: Adaptive milling - v_f comparison - detail

(the corresponding section of the toolpath is highlighted in Figure 9.28)
Original - original NC code
Optimized - optimized NC code (keep f_{zmin} function enabled)*
*Optimized** - optimized NC code (keep f_{zmin} function disabled)*

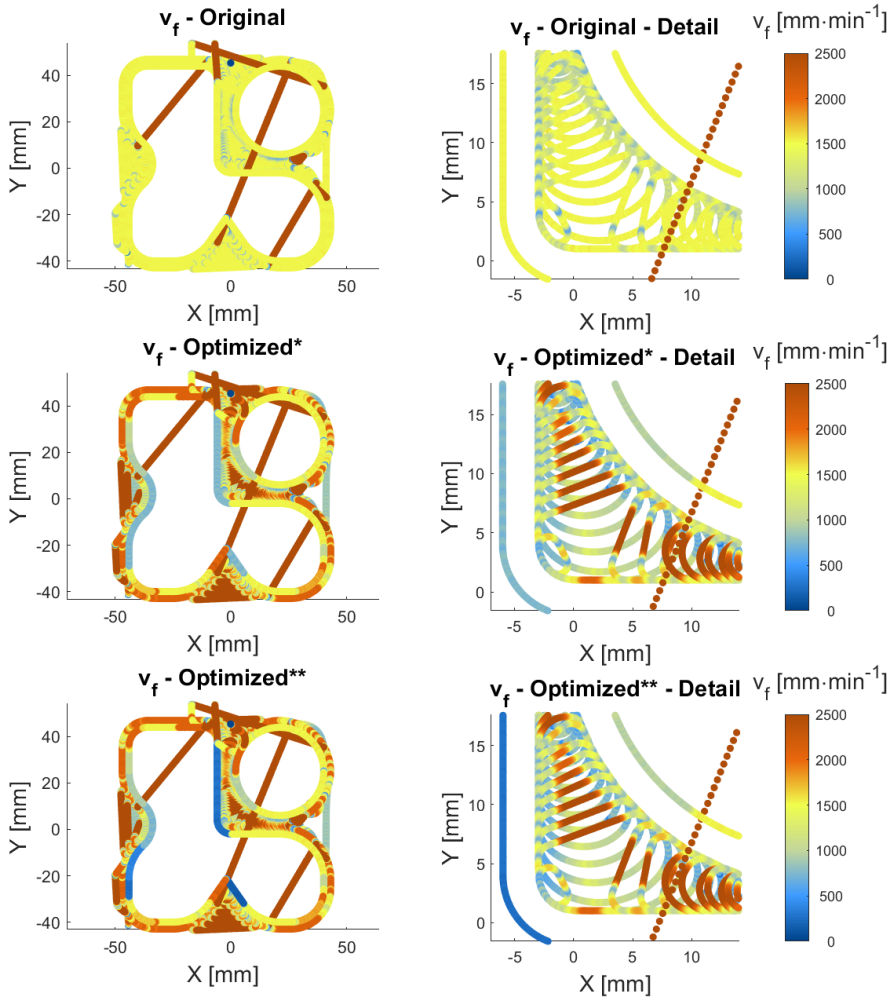

Figure 9.40: Adaptive milling - v_f

Original - original NC code
Optimized - optimized NC code (keep f_{zmin} function enabled)*
*Optimized** - optimized NC code (keep f_{zmin} function disabled)*

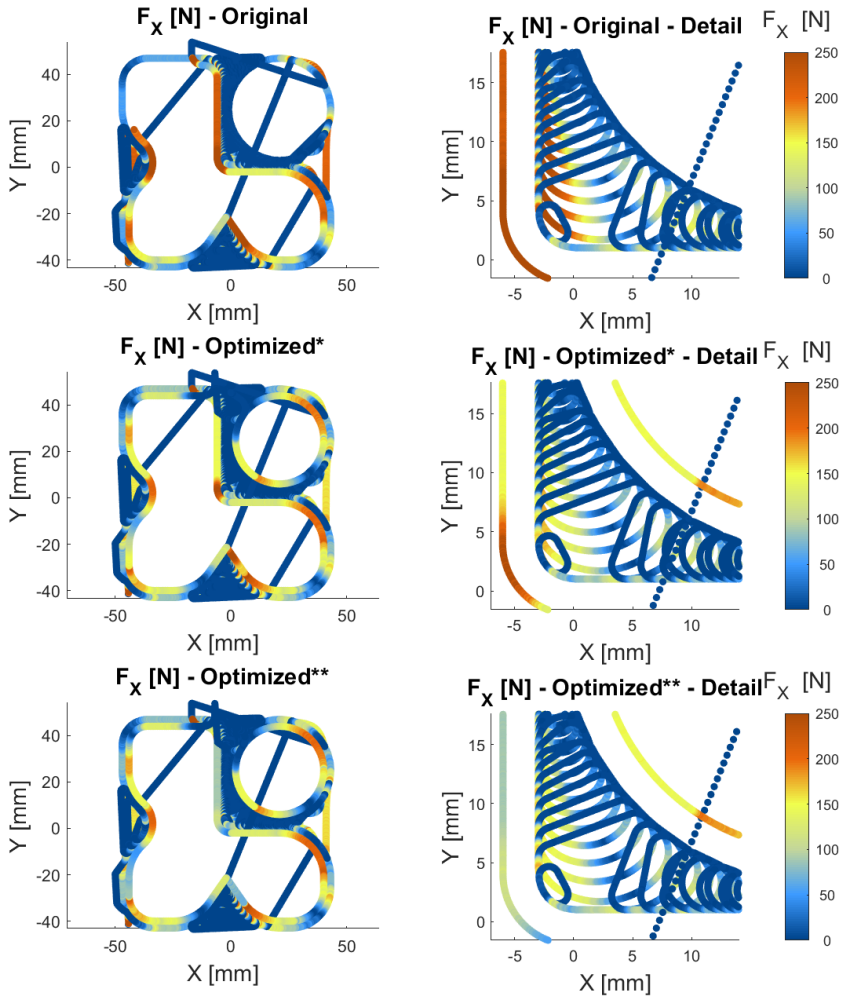

Figure 9.41: Adaptive milling - F_x

Original - original NC code
Optimized - optimized NC code (keep f_{zmin} function enabled)*
*Optimized** - optimized NC code (keep f_{zmin} function disabled)*

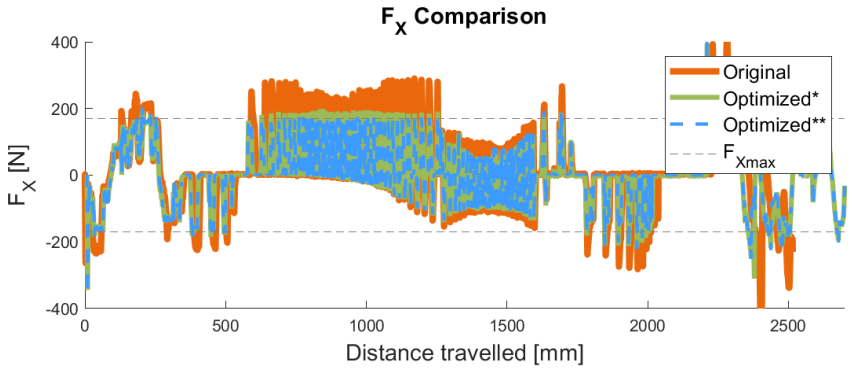

Figure 9.42: Adaptive milling - F_x comparison

Original - original NC code
Optimized - optimized NC code (keep f_{zmin} function enabled)*
*Optimized** - optimized NC code (keep f_{zmin} function disabled)*
dashed lines show the F_x force upper limits

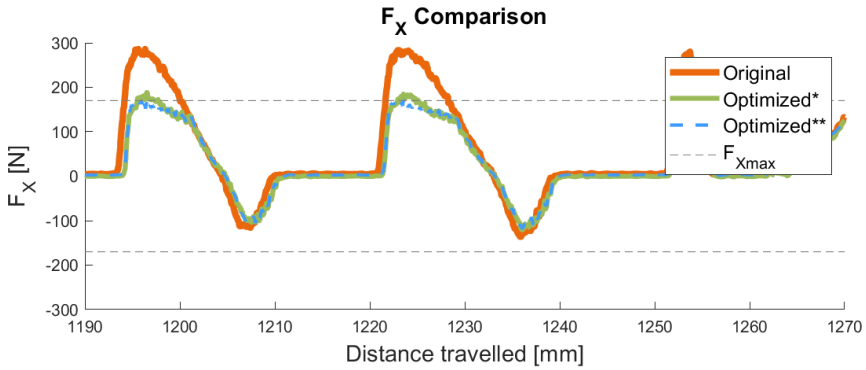

Figure 9.43: Adaptive milling - F_x comparison - detail

(the corresponding section of the toolpath is highlighted in Figure 9.28)
Original - original NC code
Optimized - optimized NC code (keep f_{zmin} function enabled)*
*Optimized** - optimized NC code (keep f_{zmin} function disabled)*
dashed lines show the F_x force upper limits

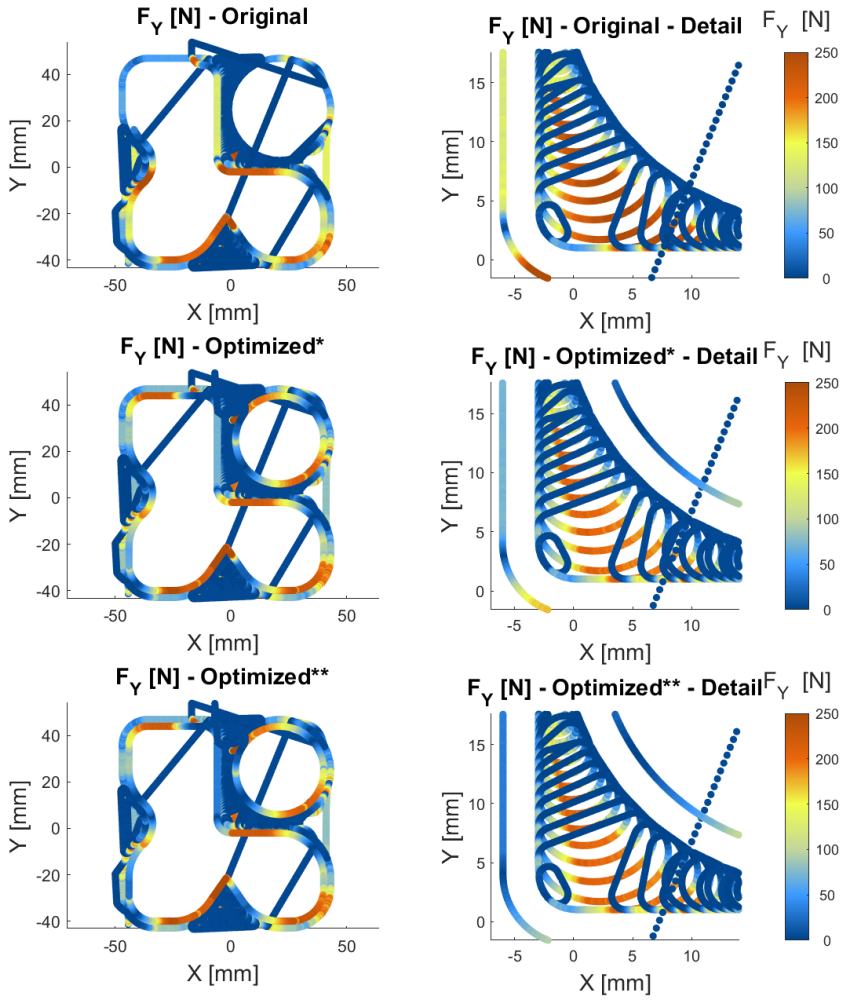

Figure 9.44: Adaptive milling - F_y

Original - original NC code
Optimized - optimized NC code (keep f_{zmin} function enabled)*
*Optimized** - optimized NC code (keep f_{zmin} function disabled)*

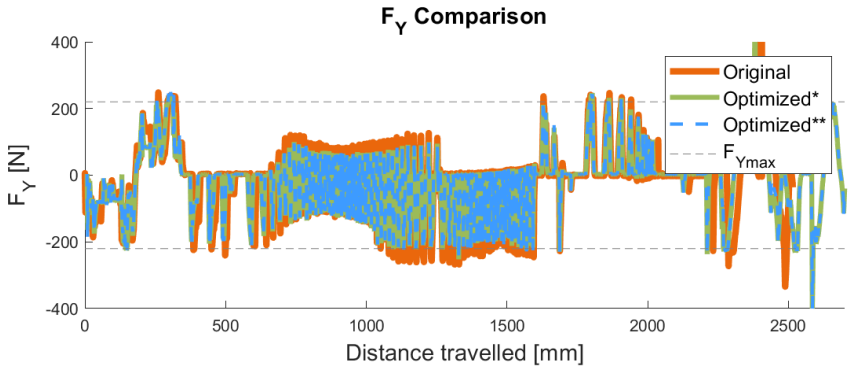

Figure 9.45: Adaptive milling - F_y comparison

Original - original NC code
Optimized - optimized NC code (keep f_{zmin} function enabled)*
*Optimized** - optimized NC code (keep f_{zmin} function disabled)*
dashed lines show the F_y force upper limits

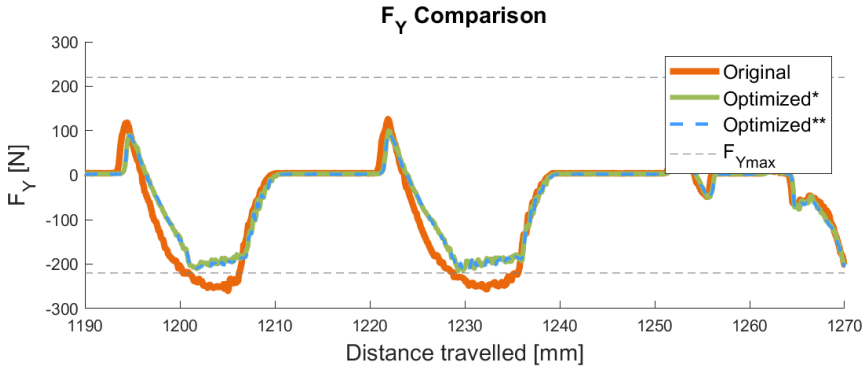

Figure 9.46: Adaptive milling - F_y comparison - detail

(the corresponding section of the toolpath is highlighted in Figure 9.28)
Original - original NC code
Optimized - optimized NC code (keep f_{zmin} function enabled)*
*Optimized** - optimized NC code (keep f_{zmin} function disabled)*
dashed lines show the F_y force upper limits

In all three cases of adaptive milling, the milling was stable, and there was no tool damage. Machining according to the original program took 133 seconds, according to the optimized program and keeping the minimum feed per tooth recommended by the tool manufacturer 140 seconds, and according to the program that did not have to meet this condition, the machining took 153 seconds.

9.3.3 Conclusions for Adaptive Milling

The second part of the experiment was milling using an adaptive strategy (trying to maintain a constant radial depth of cut a_e). This strategy requires a machine with high dynamics. Due to the dimensions of the workpiece and the programmed feed rates, the machine was not able to achieve the programmed feeds in some sections. This resulted in a reduction of cutting forces in these parts of the toolpath. However, given the initial motivation of trying to avoid overloading the pivot spindle head on large milling machines during roughing, it can be expected that the workpieces will be larger, the toolpaths will be longer, and the machine with lower even dynamic properties will be able to achieve the programmed feed rate. Even if the machine is unable to achieve the programmed feed rates, it will not affect the functionality of the optimization algorithm.

From the graphs comparing the forces (Figures 9.43 and 9.46), it can be seen that the reduction of the feed rate in the section machined by the adaptive milling strategy has sufficiently reduced the directional forces below their set limits.

The total machining time increased after optimization in both cases.

Chapter 10

Discussion

With the initial motivation to avoid overloading pivot spindle heads on large milling machines, a strategy for adjusting feed rates in NC code was proposed. The strategy was also verified by both simulations and experiments.

The optimization is based on the results of a virtual machining model which uses a linear mechanistic model of cutting forces. As the experiment showed, it is important to use an appropriate force model to achieve the desired results.

The simulation is based on programmed feed rates. These feeds may not always be achieved by the real machine (due to its structure, drives, etc.), but this does not threaten the functionality of the algorithm. If the simulation shows that the machine is overloaded at any point, the algorithm will reduce the feed rate so that overloading does not occur. However, if at the same location, the machine is unable to reach the programmed feed rate, and as a result, the forces are not exceeded, the optimized feed rate at that section will also be unachievable for the machine, and the machine will still move at the highest achievable feed at that section. This means that there is neither an overshoot in force nor an increase in machining time in the respective section before and after feed rate adjustment.

Another input to the optimization algorithm is the NC code, which is modified during the optimization process. The last required input is the setting of individual force limits and other user-defined parameters.

To verify the proposed strategy, an experiment was designed and conducted. The experiment was adapted to the time availability and the available equipment. A relatively small (180 x 180 x 10 mm) C45 carbon steel workpiece was machined with a 12mm 4-flute flat-end mill. To satisfy the initial motivation, it would be useful to verify the optimization strategy for large facing milling cutters and hard-to-machine materials. Large facing milling cutters

have a higher number of cutting edges and, since they are not monolithic but have carbide inserts, they have different geometrical properties of the cutting edges and thus different ratios of cutting and edge force components. Also, it would be valuable to choose a real workpiece for verification in which the initial motivation problem occurred.

Simulations and experiments confirmed the functionality of the proposed algorithm. Compared to most of the existing solutions that use only MRR for optimization, the proposed algorithm offers to adjust the feed rate in the NC code according to the directional loads. Limits are set for each direction individually. The algorithm allows adjustment of the feed rates according to the limits of the rotary axes. The proposed strategy approaches the optimization of the feed rates with the knowledge of the force model since the reduction of the feed rate does not result in a reduction of the cutting forces in the same proportion. As a result, compared to the conventional MRR-based method, the proposed strategy should provide an improved adjustment of the feed rates respecting the actual force loading of the tool. By building the strategy on a force model, the feed rate adjustment is direct and does not require multiple iterations.

However, the simulations revealed locations where a sufficient reduction in directional load could not be achieved by simply reducing the feed rate. Nevertheless, this is only valid in the simulations because one force model is used, which is valid only for a certain range of cutting conditions. If we set the feed rates relatively close to zero, there will be a sufficient reduction in cutting forces. On the other hand, with such a drastic reduction in feed rate, unstable machining was induced during the experiment, resulting in tool damage.

The proposed algorithm allows optimization under the condition of keeping the minimum feed per tooth recommended by the tool manufacturer. Experiments showed higher machining stability for such settings, but at the same time higher cutting forces and non-compliance with the prescribed force limits.

Adjusting the feed rates naturally affects the overall machining time. The algorithm offers an increase in feed rates where the tool is underloaded and a decrease in feed rates where the specified limits are exceeded. However, it is not possible to say in general how the adjustment of feed rates will change the overall machining time. It always depends on the specific strategy chosen and the limits set.

In the future, the algorithm could also be extended to adjust the spindle speed, which has an impact on productivity and machining stability. Another extension of the optimization algorithm could be to control the stability of the machining and to adjust the cutting conditions to avoid loss of stability. In

locations where a reduction in feed rate cannot be safely achieved by reducing the directional load, toolpaths could be adjusted to meet force limits.

Simulations and experiments have shown that the proposed strategy of adjusting the feed rate considering the machine and tool load works. The optimization was shown to have an effect not only on the force load but also on the machining stability. In the future, it would be appropriate to extend the algorithm with other functionalities mentioned above.

Chapter 11

Conclusions

This thesis deals with the optimization of feed rates in NC programs based on tool load. The goal was to design a strategy for optimizing the feed rate in NC programs according to the defined limits of the directional force load of the tool.

The first part of the thesis deals with the description of milling technology, its kinematics, the description of technological parameters, and the description of cutting forces. Furthermore, the thesis contains the basics of the cutting process dynamics, namely forced and self-excited vibrations, and machining stability. The next chapter is dedicated to the phenomenon of digital twins and specifically to two fundamental issues for building a virtual model of the machining process, such as the description of bodies in virtual space and methods for modeling cutting forces. The last chapter of the theoretical part of the thesis is a research of the current state of the art and existing approaches to feed rate optimization. The review describes not only scientific research activities but also existing commercial software. In the following practical part, the proposed strategy for modifying the feed rate in the NC code, its inputs, adjustable parameters, outputs, functionality, and algorithmization are presented. The assumptions on which the strategy is based are also explained. The chapter also includes a case study section where the functionality of the algorithm is demonstrated by simulation. The last but one part of the thesis is devoted to the experiment conducted to verify the algorithm. The design of the experiment, its realization, and its results are presented. The last section is devoted to the discussion of the proposed algorithm for feed rate adjustment in NC code, the findings acquired during the work on this thesis, and the results of the experiment.

After the research was done, a preprocessing strategy for adjusting feed rates in NC code was designed. The proposed strategy is based on a virtual machining model. For this, it was necessary to perform a force analysis of the

machining load. Furthermore, an algorithmization of the designed strategy was proposed. The proposed algorithm was then verified on the roughing strategy both by simulations and experimentally.

Unlike most other existing solutions, the presented strategy for feed rate control offers the capability to adjust the feed rate in the NC code based on directional loads, including the turning moments acting on the rotary axes of the machine. This capability aims to prevent tool and machine motion axis overloading, specifically concerning the rotary axes of the pivot spindle heads. This represents a significant innovation compared to known commercial approaches, motivated by real industrial applications.

In the future, it would be possible to extend the algorithm by controlling the machining stability. Another extension could be to modify the toolpaths in places where only reducing the feed rate will not cause a sufficient reduction in the force load.

Bibliography

[1] TOS VARNSDORF. Production programme [online]. 2023, [Accessed: 2023-11-10]. Available from: https://www.tosvarnsdorf.cz/en/wht-110-130

[2] MADHAV UNIVERSITY. Types of Milling Cutters Used in Machining Process [online]. 2018, [Accessed: 2023-08-27]. Available from: https://madhavuniversity.edu.in/types-of-milling-cutters.html

[3] MÁDL, Jan, KAFKA, Jindřich, VRABEC Martin, DVOŘÁK, Rudolf. *Technologie obrábění*. Nakladatelství ČVUT, second edition, 2007, ISBN 9788001037522.

[4] ISCAR LTD. ISCAR cutting tools - metal working tools - precision carbide metal working tools - metal cutting applications [online]. 2023, [Accessed: 2023-11-9]. Available from: https://www.iscar.com/index.aspx/countryid/1/lang/en

[5] MÁDL, Jan, BARCAL, Jaroslav. *Základy technologie II*. Česká technika - nakladatelství ČVUT, first edition, 2005, ISBN 80-01-02610-8.

[6] WAYKEN. Face Milling: Definition, Process, Differences, And Practical Tips - WayKen [online]. 2022-08-13, [Accessed: 2023-10-10]. Available from: https://waykenrm.com/blogs/what-is-face-milling/

[7] SANDVIK COROMAT. Down milling vs. up milling [online]. [Accessed: 2023-11-12]. Available from: https://www.sandvik.coromant.com/en-gb/knowledge/milling/down-milling-vs-up-milling

[8] MÁDL, Jan. *Teorie obrábění*. České vysoké učení technické v Praze, first edition, 1990.

[9] JUMALI, Muhammad Syafik, SUNDI, Syahrul Azwan, MUHAMAD, Mohd Razali. The Influence of Tool Geometry towards Cutting Performance in Machining Aluminium 7075. *MATEC Web of Conferences*

[online], volume 97, 2017-02, doi:10.1051/matecconf/20179701079, [Accessed: 2023-11-7]. Available from: https://www.matec-conferences.org/articles/matecconf/pdf/2017/11/matecconf_etic2017_01079.pdf

[10] TOOLNOTES. Cutting Parameters for Milling [online]. [Accessed: 2023-10-11]. Available from: http://toolnotes.com/home/machining/mills-101/cutting-parameters-for-milling/

[11] HARVEY PERFORMANCE COMPANY. Diving Into the Depth of Cut [online]. 2017-06-15, [Accessed: 2023-10-11]. Available from: https://www.harveyperformance.com/in-the-loupe/depth-of-cut/

[12] KŮRKA, Martin. Optimalizace NC kódu na základě zatížení nástroje a dynamických vlastností stroje [online]. Prague, 2020, [Accessed: 2023-04-15]. Master's thesis. Czech Technical University in Prague, Faculty of Mechanical Engineering. Available from: https://dspace.cvut.cz/handle/10467/99594

[13] JUNYING METAL MANUFACTURING CO. 5 Machining Strategies For Milling – Basic Advanced Milling Methods — Milling Machining Strategy [online]. 2021-04-27, [Accessed: 2023-10-24]. Available from: https://www.cnclathing.com/guide/machining-strategies-for-milling-basic-advanced-milling-methods-milling-machining-strategy

[14] SECO TOOLS. What are technological milling strategies and how can you use them at your advantage? [online]. 2022-12-19, [Accessed: 2023-11-12]. Available from: https://www.youtube.com/watch?app=desktop&v=Gj68iJnvD7c

[15] SANDVIK COROMANT UK. Milling [online]. [Accessed: 2023-11-12]. Available from: https://www.sandvik.coromant.com/en-gb/knowledge/milling

[16] YE, Ronan. What is Milling: Definition, Process & Operations [online]. 2023-07-10, [Accessed: 2023-11-12]. Available from: https://www.3erp.com/blog/milling/

[17] SANDVIK COROMANT UK. Shoulder milling [online]. [Accessed: 2023-11-12]. Available from: https://www.sandvik.coromant.com/en-gb/knowledge/milling/shoulder-milling

[18] SANDVIK COROMANT UK. Face milling [online]. [Accessed: 2023-11-12]. Available from: https://www.sandvik.coromant.com/en-gb/knowledge/milling/face-milling

[19] SANDVIK COROMANT UK. Groove or slot milling [online]. [Accessed: 2023-11-12]. Available from: https://www.sandvik.coromant.com/en-gb/knowledge/milling/groove-or-slot-milling

[20] SAPIENCE. Adaptive Milling – New Technological Enhancement for High Speed Machining [online]. 2020-09-17, [Accessed: 2023-11-12]. Available from: https://www.sapience-group.com/adaptive-milling-new-technological-enhancement-for-high-speed-machining/

[21] THOMPSON, Joe. High-speed Machining Defined [online]. 2023-02-13, [Accessed: 2023-11-10]. Available from: https://www.canadianmetalworking.com/canadianmetalworking/article/cuttingtools/high-speed--machining-defined

[22] KOLÁŘ, Petr, JANOTA, Miroslav, FALTA, Jiří, FOJTŮ, Petr, SULITKA, Matěj. Stabilita obrábění. PowerPoint slides. 2017, Prague: Czech Technical University in Prague, Faculty of Mechanical Engineering, Ú12135, [Accessed: 2023-10-15].

[23] FOJTŮ, Petr. Problematika samobuzeného kmitání. In: *Konference studentské tvůrčí činnosti - STČ 2009* [online]. 2009, [Accessed: 2023-10-15]. Available from: https://stc.fs.cvut.cz/history/2009/sbornik/Papers/pdf/FojtuPetr-304483.pdf

[24] LAŠOVÁ, Václava. *Základy stavby obráběcích strojů [online]*. Pilsen: University of West Bohemia, first edition, 2012, ISBN 978-80-261-0126-0, [Accessed: 2023-10-15]. Available from: https://dspace5.zcu.cz/bitstream/11025/16835/1/Zaklady_stavby.pdf

[25] JANOTA, Miroslav. *Měření a diagnostika výrobních storjů, P04: Stabilita obrábění (chatter)*. PowerPoint slides. 2023, Prague: Czech Technical University in Prague, Faculty of Mechanical Engineering, Ú12135, [Accessed: 2023-10-15].

[26] ULLRICH, Jakub. Multiparametrický model řezných sil pro virtuální simulace obrábění [online]. In *Diplomová práce*, Prague, 2023, [Accessed: 2023-10-12]. Master's thesis. Czech Technical University in Prague, Faculty of Mechanical Engineering. Available from: https://dspace.cvut.cz/handle/10467/111135

[27] ISO 23247-1, 2021. Automation systems and integration - Digital twin framework for manufacturing - Part 1: Overview and general principles. Technical report, International Standard Organisation, Geneva.

[28] KRITZINGER, Werner, KARNER, Matthias, TRAAR, Georg, HENJES, Jan, SIHN, Wilfried. Digital Twin in manufacturing: A categorical literature review and classification. *IFAC-PapersOnLine* [online], volume 51, no. 11, 2018: pp. 1016–1022, ISSN 2405-8963, doi:https://doi.org/10.1016/j.ifacol.2018.08.474, 16th IFAC Symposium on Information Control Problems in Manufacturing INCOM 2018. Available from: https://www.sciencedirect.com/science/article/pii/S2405896318316021

[29] SHAFTO, Mike, CONROY, Michael, DOYLE, Rich, GLAESSGEN, Ed, KEMP, Chris, LEMOIGNE, Jacqueline, WANG, Lui. Modeling, Simulation, Information Technology and Processing Roadmap [online]. 2010, [Accessed: 2023-10-20]. Available from: https://www.researchgate.net/publication/280310295_Modeling_Simulation_Information_Technology_and_Processing_Roadmap

[30] SULITKA, M. *Digitální dvojče stroje a procesu promonitorování stavu procesu*. PowerPoint slides. 2022, Prague: Czech Technical University in Prague, Faculty of Mechanical Engineering, Ú12135, [Accessed: 2023-10-15].

[31] SULITKA, Matěj. *Virtuální modelování a digitální dvojčata strojů a procesů*. PowerPoint slides. 2023, Prague: Czech Technical University in Prague, Faculty of Mechanical Engineering, Ú12135, [Accessed: 2023-10-15].

[32] KOKOTOVIĆ, Branko, VORKAPIĆ, Nikola. Feedrate optimization for 2.5D milling operations. *FME Transactions* [online], volume 47, no. 3, 2019: pp. 613–623, doi:10.5937/fmet1903613K, [Accessed: 2023-04-17]. Available from: https://www.researchgate.net/publication/336114664_Feedrate_Optimization_for_25D_Milling_Operations

[33] ALTINTAS, Yusuf, KERSTING, P., BIERMANN, D., BUDAK, Erhan, DAKENA, Berend, LAZOGLU, I. Virtual process systems for part machining operations. *CIRP Annals* [online], volume 63, no. 2, 2014-07-23: pp. 585–605, ISSN 0007-8506, doi:https://doi.org/10.1016/j.cirp.2014.05.007, [Accessed: 2023-08-15]. Available from: https://www.sciencedirect.com/science/article/pii/S0007850614001899

[34] JANG, Donggo, KIM, Kwangsoo, JUNG, Jungmin. Voxe-Based Virtual Multi-Axis Machining. *The International Journal of Advanced Manufacturing Technology [online]*, volume 2000, no. 16, 2000: pp. 709–713, doi: https://doi.org/10.1007/s001700070022, [Accessed: 2023-08-15]. Available from: https://link.springer.com/article/10.1007/s001700070022

[35] TUNC, L. Taner, SULITKA, Matěj, KOPAČKA, Ján. Integrated Simulation System for 5-axis Milling Cycles. *Procedia CIRP* [online], volume 31, 2015: pp. 64–69, ISSN 2212-8271, doi:https://doi.org/10.1016/j.procir.2015.03.057, 15th CIRP Conference on Modelling of Machining Operations (15th CMMO). [Accessed: 2023-08-17]. Available from: https://www.sciencedirect.com/science/article/pii/S2212827115002553

[36] ROY, Utpal, XU, Yaoxian. Computation of a geometric model of a machined part from its NC machining programs. *Computer-Aided*

Design [online], volume 31, no. 6, 1999-03-10: pp. 401–411, doi: https://doi.org/10.1016/S0010-4485(99)00039-1, [Accessed: 2023-08-16]. Available from: https://www.sciencedirect.com/science/article/pii/S0010448599000391?via%3Dihub

[37] ALTINTAS, Yusuf. *Manufacturing Automation - Metal Cutting Mechanics, Machine Tool Vibrations, And CNC Design*. Vancouver: Cambridge University Press, second edition, 2012, ISBN 978-1-107-00148-0.

[38] ASTAKHOV, Viktor, OUTEIRO, Jose C. M. *Metal Cutting Mechanics, Finite Element Modelling*. 2008, ISBN 978-1-84800-212-8, pp. 1–27, doi:10.1007/978-1-84800-213-5_1, [Accessed: 2023-08-20]. Available from: https://www.researchgate.net/publication/278697562_Metal_Cutting_Mechanics_Finite_Element_Modelling

[39] Sec. Geral Ministério da Economia catalog. http://catalogo.biblioteca.min-economia.pt/cgi-bin/koha/opac-search.pl?idx=au&q=par%20Coquilhat, [Accessed: 2023-11-08].

[40] Un général belge, grand-père de l'astronautique. https://www.esa.int/Space_in_Member_States/Belgium_-_Francais/Un_general_belge_grand-pere_de_l_astronautique, [Accessed: 2023-12-24].

[41] GERMAIN, Dimitri, FROMENTIN, Guillaume, POULACHON, Gérard, BISSEY-BRETON, Stéphanie. From large-scale to micro machining: a review of force prediction models. *Journal of Manufacturing Processes* [online], volume 15, 2013: pp. 389–401, doi:https://doi.org/10.1016/j.jmapro.2013.02.006, [Accessed: 2023-10-11]. Available from: https://www.sciencedirect.com/science/article/pii/S1526612513000297

[42] MARKOPOULOS, A. P. *Cutting Mechanics and Analytical Modeling*. London: Springer London, 2013, ISBN 978-1-4471-4330-7, pp. 11–27, doi:10.1007/978-1-4471-4330-7_2, [Accessed: 2023-10-26]. Available from: https://doi.org/10.1007/978-1-4471-4330-7_2

[43] KULJANIC, E., SORTINO, Marco. Some Approaches in Machining Research [online]. 06 2005, pp. 41–56, conference Advanced Manufacturing Systems and technology 2005, Udine. Available from: https://www.researchgate.net/publication/257444136_Some_Approaches_in_Machining_Research

[44] VAN LUTTERVELT, C. A., CHILDS, T. H. C., JAWAHIR, I. S., KLOCKE, F., VENUVINOD, P. K., ALTINTAS, Y., ARMAREGO, E., DORNFIELD, D., GRABEC, I., LEOPOLD, J., LINDSTROM, B., LUCCA, D., OBIKAWA, T., SHIRAKASHI, SATO, H. Present Situation and Future Trends in Modelling of Machining Operations Progress Report of the CIRP Working Group 'Modelling of Machining Operations'. *CIRP*

Annals [online], volume 47, no. 2, 1998: pp. 587–626, ISSN 0007-8506, doi:https://doi.org/10.1016/S0007-8506(07)63244-2, [Accessed: 2023-08-15]. Available from: https://www.sciencedirect.com/science/article/pii/S0007850607632442

[45] SULITKA, Matěj, SMOLÍK, Jan. *Zpráva o průběhu řešení WP01 v roce 2018*. 2018, Prague: Czech Technical University in Prague, Faculty of Mechanical Engineering, Ú12135, [Accessed: 2023-10-15].

[46] KURT, Mustafa, BAGCI, Eyup. Feedrate optimisation/scheduling on sculptured surface machining: a comprehensive review, applications and future directions. *International Journal of Advanced Manufacturing Technology* [online], volume 55, 08 2011: pp. 1037–1067, doi:10.1007/s00170-010-3131-3, [Accessed: 2023-04-25]. Available from: https://www.researchgate.net/publication/225225856_Feedrate_optimisationscheduling_on_sculptured_surface_machining_A_comprehensive_review_applications_and_future_directions

[47] SAHOO, Priyabrata, PATRA, Karali. Mechanistic modeling of cutting forces in microend-milling considering tool run out, minimum chip thickness and tooth overlapping effects. *Machining Science and Technology* [online], volume 13, 2019: pp. 407–430, ISSN 1091-0344, [Accessed: 2023-07-25]. Available from: https://www.researchgate.net/publication/328601976_Mechanistic_modeling_of_cutting_forces_in_microend-_milling_considering_tool_run_out_minimum_chip_thickness_and_tooth_overlapping_effects

[48] KOVALČÍK, Jaroslav. *Predikce silových parametrů řezného procesu při frézování [online]*. Dissertation thesis, Czech Technical University in Prague, Faculty of Mechanical Engineering, Prague, 2020-09-12, [Accessed: 2023-08-25]. Available from: https://dspace.cvut.cz/handle/10467/91031

[49] HORVÁTH, Richárd. A New Model for Fine Turning Forces. *Acta Polytechnica Hungarica* [online], volume 12, 01 2015: pp. 109–128, doi:10.12700/APH.12.7.2015.7.7, [Accessed: 2023-12-31]. Available from: https://www.researchgate.net/publication/290797543_A_New_Model_for_Fine_Turning_Forces

[50] AYKUT, Ş., GÖLCÜ, M., SEMIZ, S., ERGÜR, H. S. Modeling of cutting forces as function of cutting parameters for face milling of satellite 6 using an artificial neural network. *Journal of Materials Processing Technology* [online], volume 190, no. 1-3, 2007: pp. 199–203, doi:https://doi.org/10.1016/j.jmatprotec.2007.02.045, [Accessed: 2023-04-18]. Available from: https://www.sciencedirect.com/science/article/pii/S0924013607001872

[51] AN-MIN, Liu. Study of cutting forces and chatter in high speed milling. 2003, [Accessed: 2023-10-16]. Available from: https://lirias.kuleuven.be/bitstream/123456789/167744/1/doct%20Liu%20An%20Min.pdf

[52] KISTLER. *Measurement systems and sensors*. Online. 2023, [Accessed: 2023-11-6]. Available from: https://www.kistler.com/CZ/en/

[53] SULITKA, Matěj, KOLÁŘ, Petr, ZEMAN, Pavel, FALTA, Jiří, FOJTŮ, Petr. *Modelování řezných sil*. PowerPoint slides. 2017, Prague: Czech Technical University in Prague, Faculty of Mechanical Engineering, Ú12135, [Accessed: 2023-10-17].

[54] KISTLER. *Multicomponent Dynamometer [online]*. 2009, [Accessed: 2023-11-6]. Available from: http://www.helmar.com.pl/helmar/plik/9255b_nn3846.pdf

[55] KISTLER. *Rotating 4-Component Dynamometer RCD [online]*. 2004, [Accessed: 2023-11-6]. Available from: http://www.helmar.com.pl/helmar/plik/9123cxx11_nn3849.pdf

[56] KIM, Tae-Yong, WOO, Joongwon, SHIN, Dongwon, KIM, Jongwon. Indirect cutting force measurement in multi-axis simultaneous NC milling processes. *International Journal of Machine Tools and Manufacture* [online], volume 39, no. 11, 1999: pp. 1717–1731, ISSN 0890-6955, doi:https://doi.org/10.1016/S0890-6955(99)00027-9, [Accessed: 2023-11-6]. Available from: https://www.sciencedirect.com/science/article/pii/S0890695599000279

[57] KOREN, Yoram. Adaptive Control Systems for Machining. In: *The American Control Conference* [online]. 1988, doi: 10.23919/ACC.1988.4789896, [Accessed: 2023-09-29]. Available from: https://www.researchgate.net/publication/224388916_Adaptive_Control_Systems_for_Machining

[58] WANG, W. P. Solid modeling for optimizing metal removal of three-dimensional NC end milling. *Journal of Manufacturing Systems* [online], volume 7, no. 1, 1988: pp. 57–65, ISSN 0278-6125, doi:https://doi.org/10.1016/0278-6125(88)90033-7, [Accessed: 2023-08-16]. Available from: https://www.sciencedirect.com/science/article/pii/0278612588900337

[59] ALTAN, Taylan, SHATLA, Mahmoud, YEN, Yung-Chang, AKGERMAN, Nuri. High Performance Machining for Die/Mold Manufacturing — RD in Progress [online]. 01 1998, ISBN 978-1-4757-5690-6, pp. 293–314, doi:10.1007/978-0-387-35392-0_31, machining Impossible Shapes, IFIP TC5 WG5.3 International Conference on Sculptured Surface Machining (SSM98), Chrysler Technology Center, Michigan, USA, 1998-11-09.

[60] YAZAR, Zeki, KOCH, Karl Friedrich, MERRICK, Tom, ALTAN, Taylan. Feed rate optimization based on cutting force calculations in 3-axis milling of dies and molds with sculptured surfaces. *International Journal of Machine Tools and Manufacture* [online], volume 34, no. 3, 1994: pp. 365–377, ISSN 0890-6955, doi:https://doi.org/10.1016/0890-6955(94)90006-X, [Accessed: 2023-08-23]. Available from: https://www.sciencedirect.com/science/article/pii/089069559490006X

[61] SALAMI, R., SADEGHI, M., MOTAKEF, B. Feed rate optimization for 3-axis ball-end milling of sculptured surfaces. *International Journal of Machine Tools and Manufacture* [online], volume 47, 04 2007: pp. 760–767, doi:10.1016/j.ijmachtools.2006.09.011, [Accessed: 2023-08-22]. Available from: https://www.researchgate.net/publication/222760106_Feed_rate_optimization_for_3-axis_ball-end_milling_of_sculptured_surfaces

[62] XU, Ke, TANG, Kai. Five-axis tool path and feed rate optimization based on the cutting force–area quotient potential field. *The International Journal of Advanced Manufacturing Technology* [online], volume 75, 12 2014, doi:10.1007/s00170-014-6221-9, [Accessed: 2023-08-22]. Available from: https://www.researchgate.net/publication/268335260_Five-axis_tool_path_and_feed_rate_optimization_based_on_the_cutting_force-area_quotient_potential_field

[63] ZHONGXI, Zhang, MING, Luo, DINGHUA, Zhang, BAOHAI Wu. A force-measuring-based approach for feed rate optimization considering the stochasticity of machining allowance. *The International Journal of Advanced Manufacturing Technology* [online], volume 97, no. 5-8, 2018: pp. 2545–2556, doi:https://doi.org/10.1007/s00170-018-2127-2, [Accessed: 2023-08-28]. Available from: https://link.springer.com/article/10.1007/s00170-018-2127-2

[64] ERKORKMAZ, Kaan, LAYEGH, S. Ehsan, LAZOGLU, Ismail, ERDIM, Huseyin. Feedrate optimization for freeform milling considering constraints from the feed drive system and process mechanics. *CIRP Annals* [online], volume 62, no. 1, 2013: pp. 395–398, ISSN 0007-8506, doi:https://doi.org/10.1016/j.cirp.2013.03.084, [Accessed: 2023-08-23]. Available from: https://www.sciencedirect.com/science/article/pii/S0007850613000851

[65] BAHRATHI, Akilan, DONG, Jingyan. A Smooth Trajectory Generation Algorithm for Addressing Higher-Order Dynamic Constraints in Nanopositioning Systems. *Procedia Manufacturing* [online], volume 1, 2015: pp. 216–225, ISSN 2351-9789, doi:https://doi.org/10.1016/j.promfg.2015.09.006, 43rd North American Manufacturing Research

Conference, NAMRC 43, 8-12 June 2015, UNC Charlotte, North Carolina, United States. Available from: https://www.sciencedirect.com/science/article/pii/S2351978915010069

[66] LU, Lei, ZHANG, Jiong, FUH, Jerry Ying Hsi, HAN, Jiang, WANG, Hao. Time-optimal tool motion planning with tool-tip kinematic constraints for robotic machining of sculptured surfaces. *Robotics and Computer-Integrated Manufacturing* [online], volume 65, 2020: p. 101969, ISSN 0736-5845, doi:https://doi.org/10.1016/j.rcim.2020.101969, [Accessed: 2023-08-25]. Available from: https://www.sciencedirect.com/science/article/pii/S073658451930691X

[67] MUNDADA, N. S. K. R., Venkatesh. Optimization of Milling Operations Using Artificial Neural Networks (ANN) and Simulated Annealing Algorithm (SAA). *Materials Today: Proceedings* [online], volume 5, no. 2, Part 1, 2018: pp. 4971–4985, ISSN 2214-7853, doi:https://doi.org/10.1016/j.matpr.2017.12.075, 7th International Conference of Materials Processing and Characterization, March 17-19, 2017. Available from: https://www.sciencedirect.com/science/article/pii/S2214785317330547

[68] MAL. *Virtual machining & optimization solutions*. Online. 2022, [Accessed: 2023-09-03]. Available from: http://www.malinc.com

[69] CGTECH. *VERICUT USA*. Online. [Accessed: 2023-11-26]. Available from: https://www.cgtech.com

[70] NCGRAPHICS. *Feed-rate optimisation - NC graphics GmbH*. Online. [Accessed: 2023-10-15]. Available from: https://www.ncgraphics.de/cm/en/features/186-feed-rate-optimisation.html.

[71] ICAM TECHNOLOGIES. *SmartPACK. Automatically Optimize positioning tool-path and feed-rate*. Online. Apr. 2023, [Accessed: 2023-10-15]. Available from: https://icam.com/tool-path-optimization-software

[72] SULITKA, Matěj, KOPAČKA, Ján, FOJTŮ, Petr, MAŠEK, Petr. *Virtuální prototypování: Digitální modely, chytré funkce CNC systémů, pokročilé prostředky pro vyšší produktivitu a kvalitu výroby*. PowerPoint slides. 2018-03-01, Prague: Czech Technical University in Prague, Faculty of Mechanical Engineering, Ú12135, [Accessed: 2023-10-12].

[73] SULITKA, Matěj, FALTA, Jiří, FOJTŮ, Petr, PETRÁČEK, Petr, PETRÁŠOVÁ, Tereza, STEJSKAL, Michal, ŠVÉDA, Jiří. *SW nástroje pro návrh a optimalizaci řízení procesů a systémů*. PowerPoint slides. 2020-02-13, Prague: Czech Technical University in Prague, Faculty of Mechanical Engineering, Ú12135, [Accessed: 2023-10-12].

[74] THIRD WAVE SYSTEMS. *Production module – third wave systems*. Online. 2023, [Accessed: 2023-11-6]. Available from: https://thirdwavesys.com/machining-modeling/productionmodule/

[75] ROBORIS. *G-code optimization*. Online. https://www.roboris.it/en/eureka-chronos/, 2020, accessed: 2023-11-6.

[76] SEMACO. *NCSIMUL*. Online. 2021, [Accessed: 2023-11-6]. Available from: https://www.semaco.cz/software/produkty/ncsimul

[77] TECHNOLOGY-SUPPORT. *NCBrain.Cz*. Online. [Accessed: 2023-11-6]. Available from: https://www.ncbrain.cz

[78] SULITKA, Matěj, KOLÁŘ, Petr, ŠVÉDA, Jiří, SMOLÍK, Jan. Strategy for implementating predictive process-oriented machine tool digital twins. *MM Science Journal* [online], volume 2022, no. 3, 2022: pp. 5954–5961, doi:10.17973/MMSJ.2022_10_2022121, [Accessed: 2023-09-30]. Available from: https://www.mmscience.eu/journal/issues/october-2022/articles/strategy-for-implementating-predictive-process-oriented-machine-tool-digital-twins

[79] TAJMAC-ZPS. *HORIZONTAL MACHINING CENTRE H 630 [online]*. 2019, [Accessed: 2023-11-10]. Available from: https://www.tajmac-zps.cz/h630

[80] HOFFMANN-GROUP. *Hoffmann Group — Kvalitní nástroje na vysoké úrovni*. Online. 2023, [Accessed: 2023-12-5]. Available from: https://www.hoffmann-group.com/CZ/

Notation

A_1		first analytical force model parameter
A_2		second analytical force model parameter
A_D	[mm^2]	cut layer cross-section area or chip cross-section area
a_x	[$m \cdot s^{-2}$]	acceleration in the x-direction
a_y	[$m \cdot s^{-2}$]	acceleration in the y-direction
a_z	[$m \cdot s^{-2}$]	acceleration in the z-direction
a_e	[mm]	radial depth of cut
a_p	[mm]	axial depth of cut
$a_{p_{crit}}$	[mm]	critical axial depth of cut
b_D	[mm]	chip width
c		damping of the tool clamping
C_{ijk}		general notation of the multiparametric mechanistic force model coefficient
D	[mm]	tool diameter
D_S	[mm]	shank diameter
e_x	[$m \cdot s^{-3}$]	jerk in the x-direction

e_y	$[\mathrm{m} \cdot \mathrm{s}^{-3}]$	jerk in the y-direction
e_z	$[\mathrm{m} \cdot \mathrm{s}^{-3}]$	jerk in the z-direction
F	[N]	resultant cutting force
F_a	[N]	axial force
F_b	[N]	binormal force
F_c	[N]	cutting force
F_{cmax}	[N]	maximum cutting force component
F_{emax}	[N]	maximum edge force component
F_f	[N]	feed force
F_{fr}	[N]	friction force
F_i	[N]	general notation the directional force
F_{ib}	[N]	general notation of binormal force
F_{ic}	[N]	general notation the force cutting $(x - y - z)$ component
F_{ie}	[N]	general notation the force edge $(x - y - z)$ component
F_n	[N]	normal force
F_t	[N]	tangential force
F_{ijc}	[N]	general notation of the force cutting $(t - n - b)$ component
F_{ije}	[N]	general notation of the force edge $(t-n-b)$ component
F_{max}	[N]	maximum allowable force component
F_n	[N]	normal force
f_n	[mm]	feed rate per revolution
F_P	[N]	pressure force
F_p	[N]	passive force

F_r	[N]	radial force
f_{rapid}	[mm]	rapid feed rate
F_S	[N]	shear force
F_t	[N]	tangential force
F_X	[N]	force in the x-direction (in GCS)
F_x	[N]	force in the x-direction (in WCS)
F_{xmax}	[N]	upper x-force limit
F_{xmin}	[N]	lower x-force limit
F_Y	[N]	force in the x-direction (in GCS)
F_y	[N]	force in the y-direction (in WCS)
F_{ymax}	[N]	upper x-force limit
F_{ymin}	[N]	lower y-force limit
F_Z	[N]	force in the z-direction (in GCS)
F_z	[N]	force in the z-direction (in WCS)
f_z	[mm]	feed rate per tooth
F_{zmax}	[N]	upper x-force limit
F_{zmin}	[N]	lower z-force limit
f_{zmax}	[mm]	maximum feed rate per tooth
f_{zmin}	[mm]	minimum feed rate per tooth
h_D	[mm]	uncut chip thickness
h_m	[mm]	average chip thickness
i	[1]	index of the general notation of the force direction
I_i	[mm]	general notation of the first coordinate of the circle center

J_i	[mm]	general notation of the second coordinate of the circle center
j	[1]	index of the general notation of the force component
k	$[\mathrm{N} \cdot \mathrm{m}^{-1}]$	stiffness of the tool clamping
K	[1]	shear stress coefficient
k_1	$[\mathrm{N} \cdot \mathrm{m}^{-1}]$	first stiffness of the tool clamping
k_2	$[\mathrm{N} \cdot \mathrm{m}^{-1}]$	second stiffness of the tool clamping
k_c	$[\mathrm{N} \cdot \mathrm{mm}^{-2}]$	specific cutting resistance
k_{c11}	$[\mathrm{N} \cdot \mathrm{mm}^{-2}]$	nominal cutting resistance
K_{Fi}		general notation of pressure force coefficient
K_{ic}	$[\mathrm{N} \cdot \mathrm{mm}^{-2}]$	general notation of cutting coefficient
K_{ie}	$[\mathrm{N} \cdot \mathrm{mm}^{-1}]$	general notation of edge coefficient
K_{ij}		general notation of the mechanistic force model coefficient
K_{tc}	$[\mathrm{N} \cdot \mathrm{mm}^{-2}]$	specific cutting pressure
K_{fc}	$[\mathrm{N} \cdot \mathrm{mm}^{-2}]$	feed force constant
K_{Pi}	$[\mathrm{N} \cdot \mathrm{mm}^{-2}]$	general notation of pressure force coefficient
K_{fri}	$[\mathrm{N} \cdot \mathrm{mm}^{-1}]$	general notation of friction force coefficient
L	[mm]	overall tool length
L_a	[mm]	arm length (distance between the tool tip and the rotary axis)
L_c	[mm]	milling cutter flute length
m	[kg]	mass of the tool
M_A	$[\mathrm{N} \cdot \mathrm{m}]$	torque on the A-axis
M_{Amax}	$[\mathrm{N} \cdot \mathrm{m}]$	maximum allowable torque on the A-axis

n	$[\mathrm{min}^{-1}]$	spindle speed
P_0	[1]	parameter of the parametric curve - start
P_1	[1]	parameter of the parametric curve - end
R	[μm]	cutting edge radius
v_c	$[\mathrm{mm} \cdot \mathrm{min}^{-1}]$	cutting speed
v_f	$[\mathrm{mm} \cdot \mathrm{min}^{-1}]$	feed rate
v_{max}	$[\mathrm{mm} \cdot \mathrm{min}^{-1}]$	minimum feed rate
v_{fmax}	$[\mathrm{mm} \cdot \mathrm{min}^{-1}]$	maximum feed rate
v_{fopti}	$[\mathrm{mm} \cdot \mathrm{min}^{-1}]$	optimal feed rate
q_c		exponent describing the relation of the of chip thickness on the cutting coefficient
X_{Fi}		general notation of the exponent describing the relation of the force dependence on the axial depth of cut
X_i	[mm]	general notation of the X-coordinate
Y_{Fi}		general notation of the exponent describing the relation of the force dependence on the feed rate per tooth
Y_i	[mm]	general notation of the Y-coordinate
z	[1]	number of cutting edges
Z_{Fi}		general notation of the exponent describing the relation of the force dependence on the cutting speed
α	[°]	helix angle
α_a	[°]	axial relief angle
α_r	[°]	radial relief angle
β_a	[°]	friction angle
γ	[°]	rake angle

γ_a	$[^\circ]$	axial rake angle
γ_a	$[^\circ]$	axial rake angle
γ_r	$[^\circ]$	radial rake angle
κ_r	$[^\circ]$	cutting edge angle
λ	$[^\circ]$	helix angle
μ	$[^\circ]$	friction coefficient
ξ	$[^\circ]$	inclination angle of the Kienzle force model
σ	$[\mathrm{N} \cdot \mathrm{mm}^{-2}]$	normal stress
τ	$[\mathrm{N} \cdot \mathrm{mm}^{-2}]$	shear stress
ϕ	$[^\circ]$	instantaneous tool rotation
ϕ_c	$[^\circ]$	primary shear angle
ψ	$[^\circ]$	phase shift between the waves of the actual and the previous cut

List of Figures

List of Tables

List of Abbreviations

AI	artificial intelligence
ANN	artificial neural network
APT	automatically programmed tool
B-rep	boundary representation
CAD	computer aided design
CAE	computer aided engineering
CAM	computer aided manufacturing
CC	cutter contact [62]
CL	cutter location
CNC	computerized numerical control
CSG	constructive solid geometry
DAQ	data acquisition
Dexel	depth pixel
DoF	degree of freedom
ERC/NSM	name of the software referred to in [60]
f-c-p	feed - cutting - passive vector basis

f-t-r	feed - tangential - radial vector basis
FEA	finite element analysis
GCS	global coordinate system
HDC	high dynamic cutting
HFC	high feed cutting
HPC	high performance cutting
HSC	high speed cutting
ISO	International Organization for Standardization
MRR	material removal rate
NC	numerical control
NURBS	non-uniform rational B-splines
R&D	research and development
ROS	robot operating system
SAA	simulated annealing algorithm
TPS	thermal protection system
TCS	tool coordinate system
t-n-b	tangential - normal - binormal vector basis
Voxel	volumetric pixel
WCS	workpiece coordinate system
x-y-z	x - y - z direction vector basis

List of Software

MATLAB R2020b	feed rate control algorithm, simulation and experimental data processing
MillVis	virtual machining - force simulations
SolidWorks 2017	workpiece modeling, creation of schemes
HSMExpress 2018	tool path generating
SINUMERIK ONE Create MyVirtual Machine	virtual model of the machine - set-point position simulation
DynoWare	dynamometer data acquisition
SinuTrace	set-point data acquisition
Overleaf	writing
InkScape	creation of schemes
GIMP 2	creation of schemes

List of Appendices

Contents of the Attached CD

- `Code` ..... folder with source codes for MATLAB
  - `Experiment` ..... source codes for experiment processing
  - `FROpti` ..... source codes for the feed rate optimization
- `NCCode` ..... folder with NC codes used in the experiment
- `Thesis` ..... folder with source codes of the thesis in LaTeX format
- `Uhlir_DP_1836.pdf` ..... thesis in PDF
- `readme.txt` ..... contents of the attached CD

CZECH TECHNICAL UNIVERSITY IN PRAGUE

FACULTY OF MECHANICAL ENGINEERING

Department of Production Machines and Equipment

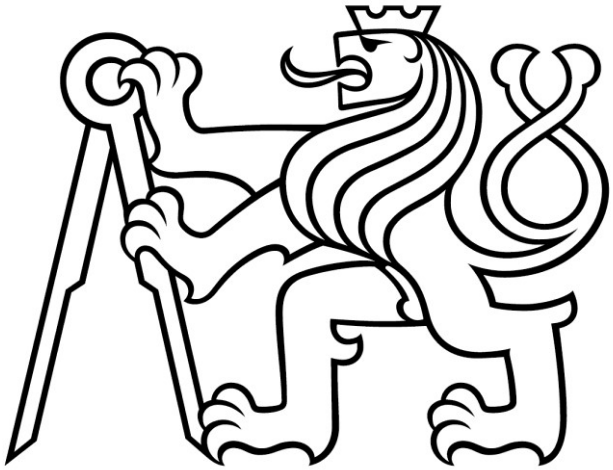

Master's thesis

Optimization of feed rates in NC programs based on tool load

APPENDICES

Bc. Jan Uhlíř

2023 1836

Appendix **A**

Optimization Algorithm Decision Tree

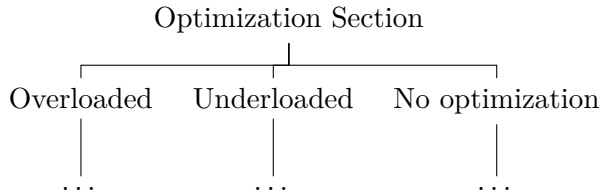

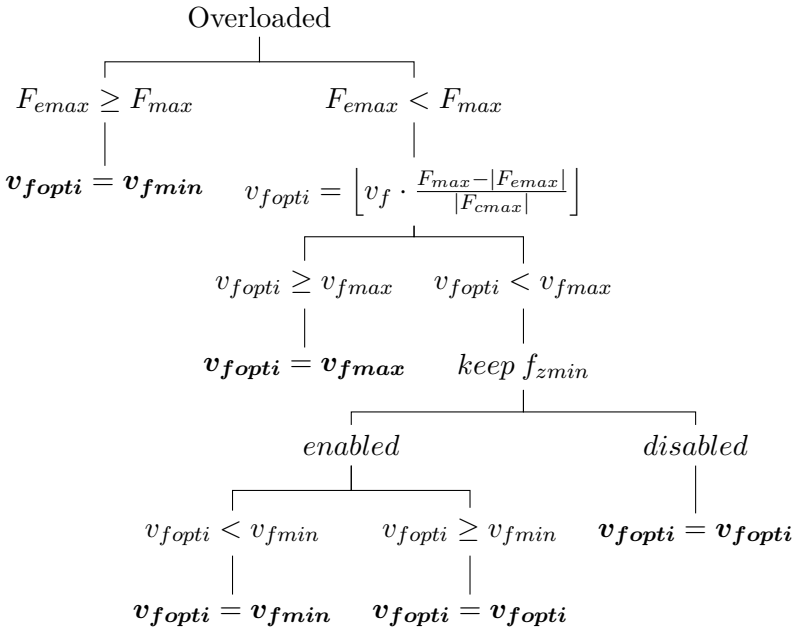

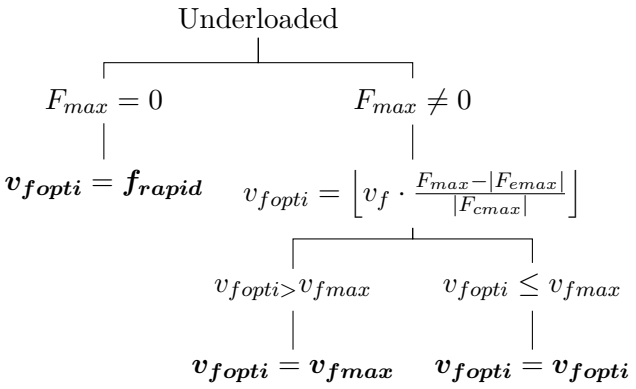
Underloaded
$F_{max} = 0$
$F_{max} \neq 0$
$\boldsymbol{v_{fopti} = f_{rapid}}$
$v_{fopti} = \left\lfloor v_f \cdot \frac{F_{max} - \lvert F_{emax} \rvert}{\lvert F_{cmax} \rvert} \right\rfloor$
$v_{fopti} > v_{fmax}$
$v_{fopti} \leq v_{fmax}$
$\boldsymbol{v_{fopti} = v_{fmax}}$
$\boldsymbol{v_{fopti} = v_{fopti}}$

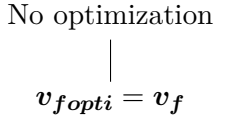
No optimization
$\boldsymbol{v_{fopti} = v_f}$

Appendix B

Experimental Workpiece

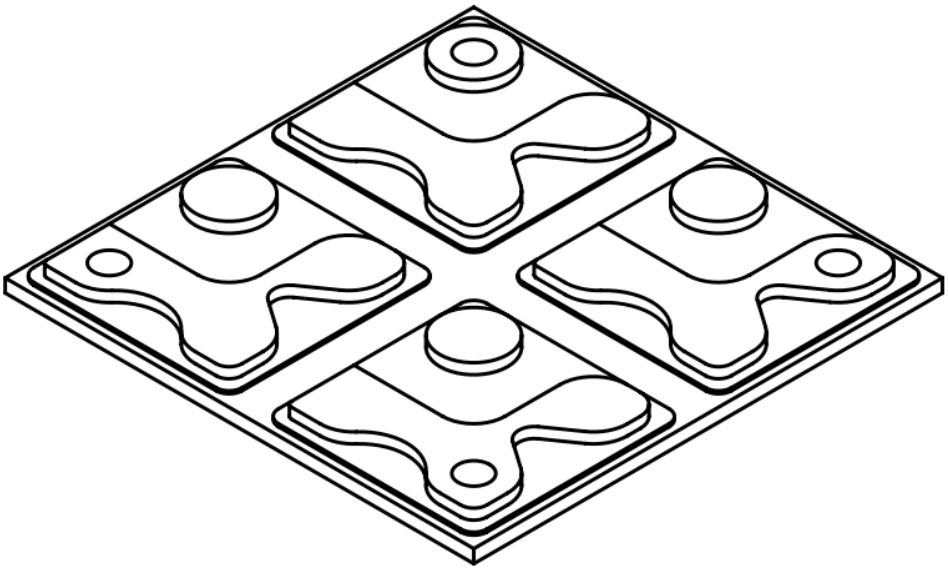

A3

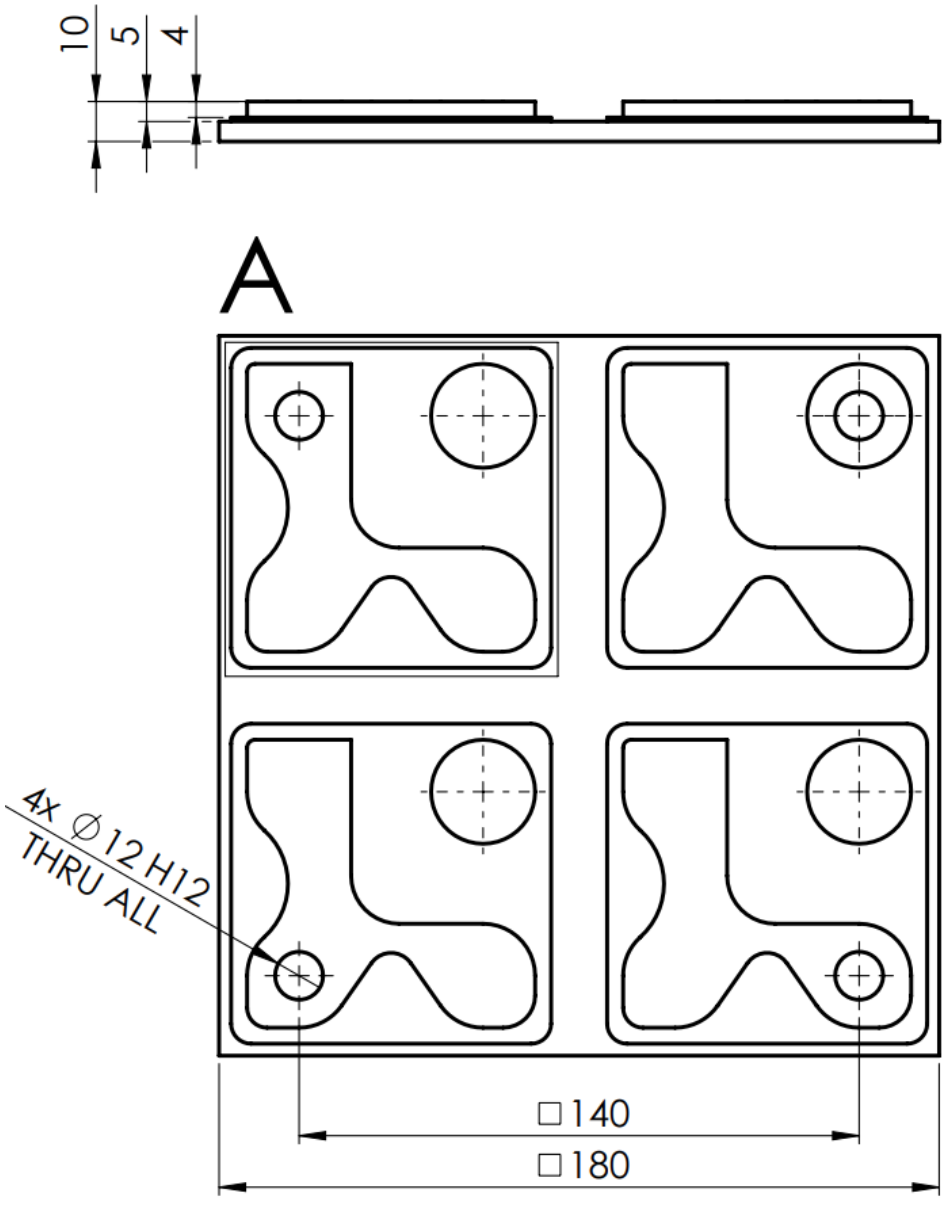
10
5
4
A
4x ∅12 H12
THRU ALL
□140
□180

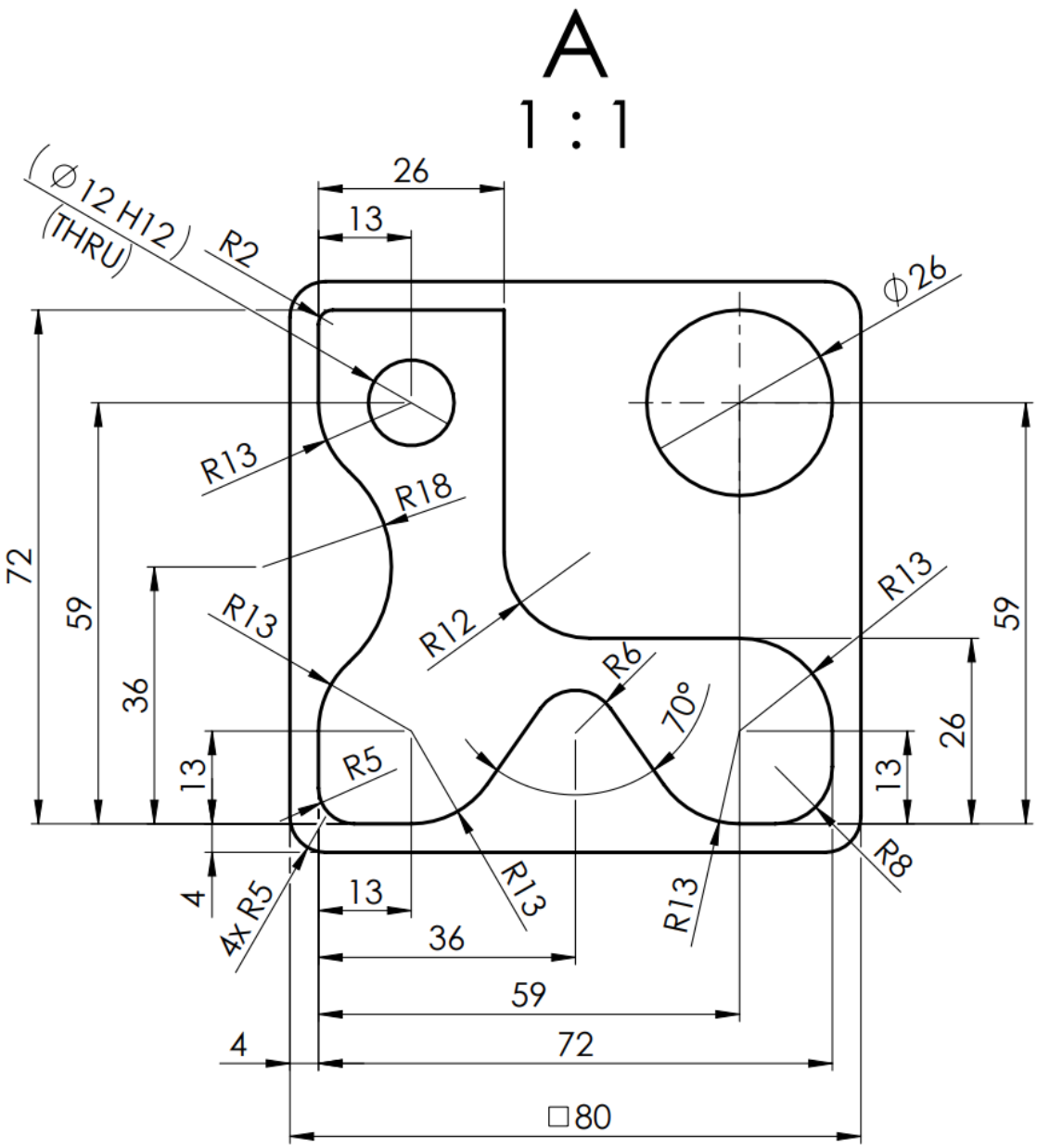
A
1 : 1
⌀12 H12
(THRU)
R2
26
13
⌀26
R13
R18
72
59
36
R13
R12
R6
70°
R13
59
26
13
R5
13
4
4x R5
13
R13
R13
R8
36
59
4
72
□80

Appendix C

Pressure-Friction Force Model for C45 Carbon Steel

This appendix provides the calculation of the cutting and edge coefficients of the mechanistic model used for adaptive machining (see Section 9.3.1) according to the pressure-friction multiparametric force model. The linear part of the model presented in [26] was used.

The pressure force F_P, friction force F_{fr}, and chip flow angle η are calculated according to the following equations:

$$\begin{aligned} F_P &= b_D \cdot (K_{P0} + K_{P1} \cdot h_D) \\ F_{fr} &= b_D \cdot (K_{fr0} + K_{fr1} \cdot h_D) \\ \eta &= 36 \cdot \lambda - 7.9 \cdot R \cdot \lambda \end{aligned} \tag{C.1}$$

$$\begin{aligned} K_{P0} &= 19 \cdot \tilde{R} - 11 \cdot \tilde{\lambda} + 19 \cdot \tilde{\lambda}^2 + 6.1 \cdot \tilde{v}_c + 8 \cdot \tilde{v}_c^2 + 28 \\ K_{P1} &= 13 \cdot \tilde{\lambda} - 130 \cdot \tilde{\gamma} + 11 \cdot \tilde{v}_c + 670 \end{aligned} \tag{C.2}$$

$$\begin{aligned} K_{fr0} &= 31 \cdot \tilde{R} - 15 \cdot \tilde{\lambda} + 33 \cdot \tilde{\lambda}^2 + 6.1 \cdot \tilde{v}_c + 38 \\ K_{fr1} &= -30 \cdot \tilde{\gamma} - 19 \cdot \tilde{\lambda} + 110 \cdot \tilde{v}_c + 550 \end{aligned} \tag{C.3}$$

where the input parameters are scaled according to Equation C.4.

$$\begin{aligned} \tilde{\gamma} &= \frac{\gamma - 4}{8} \\ \tilde{v}_c &= \frac{v_c - 165}{85} \\ \tilde{\lambda} &= \frac{\lambda}{45} \\ \tilde{R} &= \frac{R - 50}{40} \end{aligned} \tag{C.4}$$

where $R\,[\mu\mathrm{m}]$ is the cutting edge radius, $\lambda\,[^\circ]$ is helix angle, $v_c\,[\mathrm{m}\cdot\mathrm{min}^{-1}]$ is cutting speed, $\gamma\,[^\circ]$ is rake angle, and $h_D\,[\mathrm{mm}]$ is cut layer thickness. Rake angle γ is calculated from axial rake angle γ_a and radial rake angle γ_r by the following equation:

$$\gamma = \arctan\left(\frac{\tan(\gamma_r - 90^\circ)}{\cos(\gamma_a)}\right) + 90 \tag{C.5}$$

$$\begin{aligned} F_t &= \cos(\lambda)\cdot\cos(\gamma)\cdot F_P + (\cos(\eta)\cdot\cos(\lambda)\cdot\sin(\gamma) + \sin(\eta)\cdot\sin(\lambda))\cdot F_{fr} \\ F_n &= -\sin(\gamma)\cdot F_P + \cos(\eta)\cdot\cos(\gamma)\cdot F_{fr} \\ F_b &= -\sin(\lambda)\cdot\cos(\gamma)\cdot F_P + (-\cos(\eta)\cdot\sin(\lambda)\cdot\sin(\gamma) + \sin(\eta)\cdot\cos(\lambda))\cdot F_{fr} \end{aligned} \tag{C.6}$$

$$\begin{aligned} K_{tc} &= \cos(\lambda)\cdot\cos(\gamma)\cdot K_{P1} + (\cos(\eta)\cdot\cos(\lambda)\cdot\sin(\gamma) + \sin(\eta)\cdot\sin(\lambda))\cdot K_{fr1} \\ K_{te} &= \cos(\lambda)\cdot\cos(\gamma)\cdot K_{P0} + (\cos(\eta)\cdot\cos(\lambda)\cdot\sin(\gamma) + \sin(\eta)\cdot\sin(\lambda))\cdot K_{fr0} \\ K_{nc} &= -\sin(\gamma)\cdot K_{P1} + \cos(\eta)\cdot\cos(\gamma)\cdot K_{fr1} \\ K_{ne} &= -\sin(\gamma)\cdot K_{P0} + \cos(\eta)\cdot\cos(\gamma)\cdot K_{fr0} \\ K_{bc} &= -\sin(\lambda)\cdot\cos(\gamma)\cdot K_{P1} + (-\cos(\eta)\cdot\sin(\lambda)\cdot\sin(\gamma) + \sin(\eta)\cdot\cos(\lambda))\cdot K_{fr1} \\ K_{be} &= -\sin(\lambda)\cdot\cos(\gamma)\cdot K_{P0} + (-\cos(\eta)\cdot\sin(\lambda)\cdot\sin(\gamma) + \sin(\eta)\cdot\cos(\lambda))\cdot K_{fr0} \end{aligned} \tag{C.7}$$